

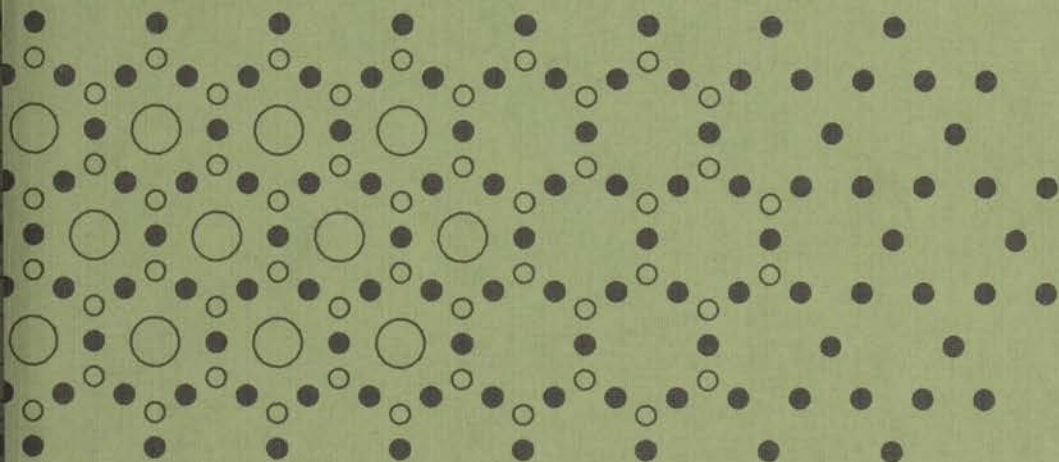
MAGNETIC ORDER IN COMPOUNDS

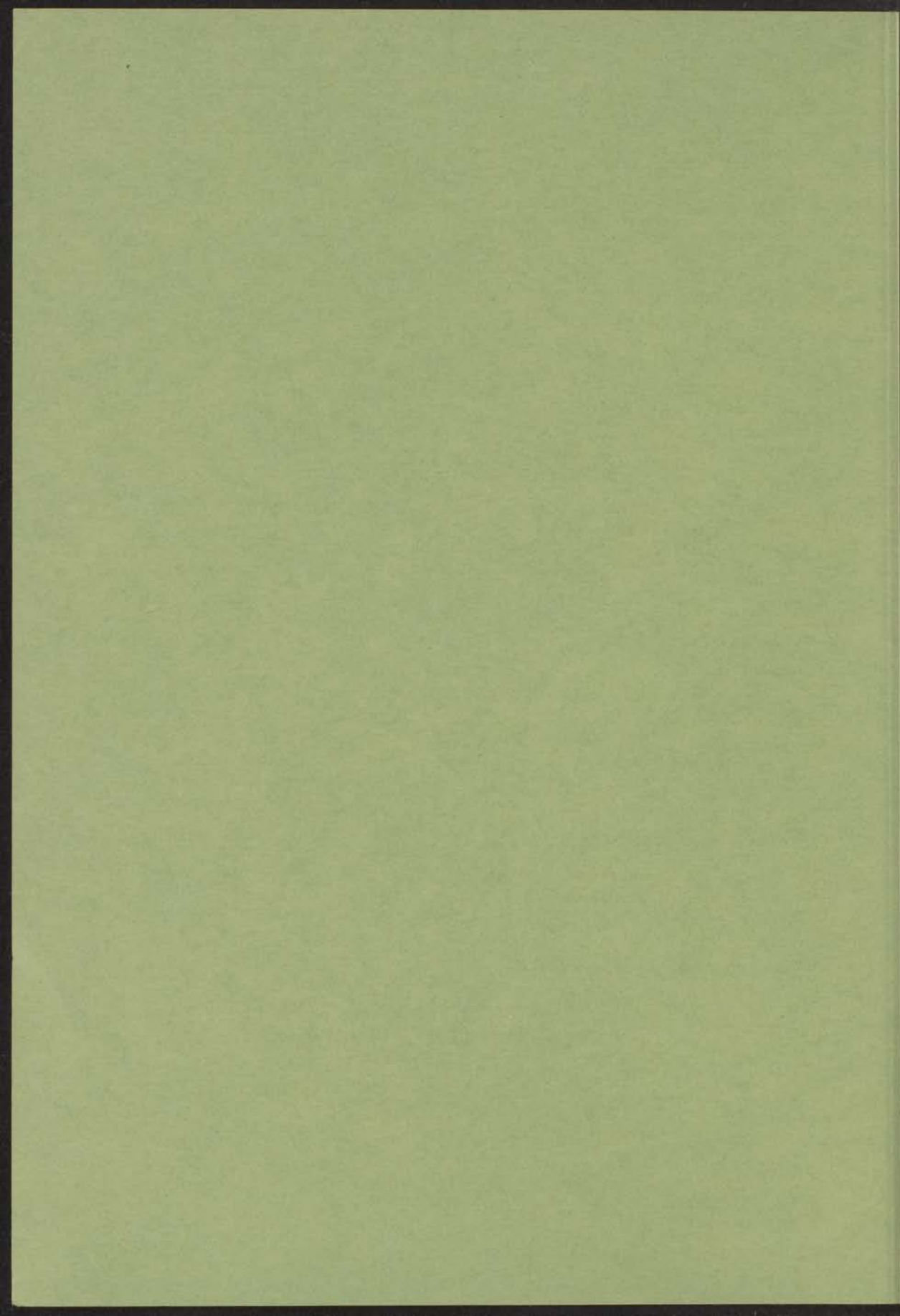
BETWEEN

THORIUM AND IRON

INSTITUUT-LORENZ
voor theoretische natuurkunde
Nieuwsteeg 18-Leiden-Nederland

J.B.A.A. ELEMANS





23 SEP. 1975

MAGNETIC ORDER IN COMPOUNDS BETWEEN
THORIUM AND IRON

PROEFSCHRIFT

TER VERKRIJGING VAN DE GRAAD VAN DOCTOR IN
DE WISKUNDE EN NATUURWETENSCHAPPEN AAN DE
RIJKSUNIVERSITEIT TE LEIDEN, OP GEZAG VAN DE
RECTOR MAGNIFICUS DR. A.E. COHEN, HOGLERAAR
IN DE FACULTEIT DER LETTEREN, VOLGENS BESLUIT
VAN HET COLLEGE VAN DEKANEN TE VERDEDIGEN OP
WOENSDAG 10 SEPTEMBER 1975 TE KLOKKE 16.15 UUR.

DOOR

JACQUELINE ELEMANS
GEBOREN TE LEIDEN IN 1943

INSTITUUT-LORENTZ
voor theoretische natuurkunde
Nieuwsteeg 18-Leiden-Nederland

kast dissertaties

PROMOTOREN:

J. van den Handel

J.A. Goedkoop

COREFERENTEN:

B.O. Loopstra

G.J. Nieuwenhuys

STELLINGEN

1. De aanname van baan-baankoppeling naast spin-spin koppeling leidt mogelijk tot een verklaring van de waargenomen magnetische ordening in Th-Fe legeringen.

L.L. Hirst, Z. Physik 244, 230 (1971).

2. Het door Narasimhan et al. gebruikte model ter berekening van het verzuigingsmoment in $Dy(Fe,Ni)_3$, $Ho(Fe,Ni)_3$ etc. is aan grote twijfel onderhevig.

K.S.V.L. Narasimhan, R.A. Butera, and R.S. Craig, J. Appl. Phys. 44, 879 (1973).

3. Bij de interpretatie van de waargenomen verandering in de elektrische en magnetische eigenschappen van $PrCo_2$ en $NdCo_2$ na verhitting van deze verbindingen in vacuüm hebben Titcomb et al. onvoldoende rekening gehouden met de faserelaties in de betreffende lanthanide-cobalt systemen.

C. Titcomb, R.S. Craig, W.E. Wallace and V.U.S. Rao, Physics Letters 39A, 157 (1972).

4. De conclusie van Brodsky dat uraan in UCu_5 tweewaardig zou zijn berust op een eenzijdige interpretatie van zijn susceptibiliteitsmetingen.

M.B. Brodsky, AIP Conference proceedings, Magnetism and Magnetic Materials 18, 357 (1973).

5. Het is wenselijk de toepasbaarheid van de theorie van de "multiplier representations" op de beschrijving van magnetische ordening in kristallen nader te analyseren.

6. De verbinding $CaU_2O_6F_2$ is, anders dan beschreven door Fonteneau et al., waarschijnlijk isostructureel met $\beta-U_3O_8$.

G. Fonteneau, H. L'Helgoualch and J. Lucas, Inorg. Nucl. Chem. Letters 11, 207 (1975).
B.O. Loopstra, Acta Cryst. B26, 656 (1970).

7. Een groepentheoretisch formalisme analoog aan dat van Maradudin en Vosko voor de beschrijving van symmetrie-eigenschappen van fononen is mogelijk een nuttig hulpmiddel bij het bepalen van de structuur van gemoduleerde kristallen.

A.A. Maradudin and S.H. Vosko, Reviews of Modern Physics 40, 1 (1968).

8. De conclusie van Arend et al. dat een (dimensionaliteits) overgang van twee- naar driedimensionaal magnetisch gedrag is af te leiden uit de door hen gemeten susceptibiliteit van $(\text{CH}_3\text{NH}_3)_2\text{CuCl}_4$ nabij de Curietemperatuur, wordt niet door hun experiment gerechtvaardigd.
- H. Arend, J. Schoenes, and P. Wachter,
Phys. Stat. Sol. (b) 69, 105 (1975).
9. Omdat enerzijds er discrepanties bestaan tussen metingen met verschillende akoustische thermometers en anderzijds één van deze metingen tot een afwijkende waarde voor de gasconstante leidt, is het gewenst de bepaling van de gasconstante met de klassieke methoden te herhalen en tevens nader onderzoek te verrichten naar bronnen van systematische fouten in de akoustische thermometer.
- H.H. Plumb and G. Cataland, Metrologia 4, 127 (1966).
T.J. Quinn, T.R.D. Chandler and A.R. Colclough,
Procès Verbaux du Comité Consultatif de Thermométrie
(Sèvres, France) 1974, document 27.
A.R. Colclough, Metrologia 9, 75 (1973).
10. Het moet mogelijk zijn om m.b.v. adiabatische demagnetisatie in het roterend coördinatenstelsel van de electronenspins een magnetische ordening te induceren in $\text{Gd}_2(\text{SO}_4)_3 \cdot 8\text{H}_2\text{O}$.
- M. Goldman, M. Chapellier, Vu Hoang Chau, and A. Abragam,
Phys. Rev. B10, 226 (1974).
A.J. van Duyneveldt, persoonlijke mededeling.
11. Hoewel Gunzburg's beoordelingsschaal een nuttig hulpmiddel is om de mate van zelfredzaamheid van een geestelijk gehandicapte te bepalen, is het uitsluitend gebruik hiervan bij het samenstellen van leefgroepen in een inrichting ontoereikend.
12. Het adagium "Mijn spelen is leren, mijn leren is spelen" kan gerealiseerd worden door een aanzienlijke ruimte op de lesroosters van basis- en voortgezet onderwijs vrij te maken voor muziekbeoefening.

Jacqueline Elemans

10 september 1975.

Faint, illegible text at the top of the page, possibly a header or introductory paragraph.

Main body of faint, illegible text, appearing to be several paragraphs of a document.

Section of faint, illegible text, possibly a sub-section or a specific paragraph.

Section of faint, illegible text, continuing the main body of the document.

Final section of faint, illegible text at the bottom of the page, possibly a conclusion or footer.

TABLE OF CONTENTS

| | <u>Page</u> |
|---|-------------|
| I. THE DETERMINATION OF CRYSTAL AND MAGNETIC STRUCTURES | 5 |
| 1.1 The ideas | 5 |
| 1.2 The instrument | 9 |
| 1.3 Data reduction | 16 |
| II. INTERMETALLIC COMPOUNDS WITH LANTHANIDES | 20 |
| 2.1 Crystal structures | 20 |
| 2.2 Exchange interactions | 23 |
| 2.3 Results obtained by other workers | 27 |
| 2.4 The scope of the present investigation | 31 |
| 2.5 The samples | 35 |
| III. CRYSTAL AND MAGNETIC STRUCTURE OF INTERMETALLIC COMPOUNDS OF THE TYPE $\text{Th}(\text{Co}_x\text{Fe}_{1-x})_5$ | 36 |
| 3.1 Introduction | 36 |
| 3.2 Experimental | 37 |
| 3.3 Structure determination | 37 |
| 3.4 Structure refinements | 38 |
| 3.4.1 the crystal structure | 38 |
| 3.4.2 ferromagnetic part of the magnetic structure | 39 |
| 3.4.3 antiferromagnetic part of the magnetic structure | 41 |
| 3.5 Discussion | |
| IV. MAGNETIC ORDER IN THE PSEUDO-BINARY SYSTEM $\text{Th}(\text{Fe}_{1-x}\text{Ni}_x)_5$ | 45 |
| 4.1 Introduction | 45 |
| 4.2 Experimental | 47 |
| 4.2.1 experimental procedures | 47 |
| 4.2.2 magnetic measurements | 47 |
| 4.2.3 crystal structure | 48 |
| 4.2.4 magnetic order | 49 |
| 4.3 Discussion | 51 |
| V. MAGNETIC ORDER AND MAGNETIC HISTORY EFFECTS IN $\text{Th}(\text{Co}_x\text{Ni}_{1-x})_5$ | 54 |
| 5.1 Introduction | 54 |
| 5.2 Experimental procedure | 55 |
| 5.3 Results of magnetic measurements | 55 |

| | <u>Page</u> |
|--|-------------|
| 5.4 Analysis of neutron diffraction data | 57 |
| 5.5 Discussion | 59 |
| VI. INVESTIGATIONS OF R_2M_{17} COMPOUNDS | 64 |
| 6.1 On the interpretation of Mössbauer-effect and diffraction measurements on rare earth-iron compounds of the type R_2Fe_{17} . | 64 |
| 6.1.1 introduction | 64 |
| 6.1.2 evidence for off-stoichiometry | 65 |
| 6.1.3 evidence for stoichiometric composition: metallographic examination | 69 |
| 6.1.4 alternative interpretation of results of diffraction experiments | 75 |
| 6.1.5 discussion | 76 |
| 6.2 The magnetic structure of Tm_2Fe_{17} | 79 |
| VII. MAGNETIC ORDER IN $ThFe_3$ AND Th_2Fe_7 | 81 |
| 7.1 Introduction | 81 |
| 7.2 $ThFe_3$ | 83 |
| 7.2.1 ferromagnetic temperature regions | 83 |
| 7.2.2 intermediate temperature range | 85 |
| 7.3 Th_2Fe_7 | 85 |
| 7.4 Discussion | 87 |
| VIII. SYMMARY AND CONCLUSIONS | 88 |
| 8.1 Introduction | 88 |
| 8.2 Crystal structure of the ThM_5 pseudo-binary compounds | 88 |
| 8.2.1 symmetry and atomic coordinate | 88 |
| 8.2.2 site occupancies in the pseudo-binary systems | 89 |
| 8.3 Magnetic order in ThM_5 compounds | 93 |
| 8.3.1 summary of previous results | 93 |
| 8.3.2 reinterpretation of the diffracted intensities in $Th(Fe,Ni)_5$ | 94 |
| 8.3.3 the canted structure of $ThFe_5$ | 95 |
| 8.4 Magnetic structures of the Th-Fe compounds | 97 |
| LIST OF REFERENCES | 99 |
| SAMENVATTING | 103 |
| NAWOORD | 105 |

I. THE DETERMINATION OF CRYSTAL AND MAGNETIC STRUCTURES

Since one may build a modest library of books on crystallography, X-ray diffraction and thermal neutron scattering it is rather impossible to achieve completeness or originality within the scope of one introductory chapter in a thesis. However, one may not assume that solid state physicists are thoroughly familiar with the field of crystal structure analysis. Therefore it is envisaged to outline this very useful branch of science, especially the technique of thermal neutron scattering by powder samples, in so far as is necessary to understand the results obtained. It is hoped that the power and the limitations of the method will be demonstrated in the reports of the investigations contained in the present work.

There is a natural way of partitioning the material to be presented. First we shall concentrate on the ideas involved; then an account will be given of the experimental setup, and lastly the focus will be on the processing of the results of the measurement.

1.1 The ideas

Diffraction is defined as the coherent and elastic scattering of a wave. Coherence means that there is a phase relation between the incident and the scattered wave; elastic scattering indicates that there is momentum transfer but no energy transfer between the wave and the scatterer.

Neglecting the diffraction by liquids, gases and amorphous solids, interesting though they are, we shall limit ourselves to scattering by crystalline solids.

For the present purpose we may take a crystal to be an infinite assembly of atoms showing translational symmetry in three dimensions. It is then possible to choose primitive translation vectors \vec{a} , \vec{b} and \vec{c} such that the crystal is invariant for a translation over any linear combination of

integral multiples of these vectors. By considering all the atoms in the crystal one may prove that the momentum transfer in the diffraction process, $\vec{h}\vec{\kappa}$, is discrete and can be written as

$$\vec{\kappa} = 2\pi \vec{\tau}$$

in which $\vec{\tau}$ is a vector of the reciprocal lattice:

$$\vec{\tau} = h \vec{a}^* + k \vec{b}^* + l \vec{c}^*$$

with integral h, k, l . The basis vectors of reciprocal space, \vec{a}^*, \vec{b}^* and \vec{c}^* are defined by 9 relations such as $\vec{a} \cdot \vec{a}^* = 1$ and $\vec{a} \cdot \vec{b}^* = 0$. These defining equations link the real "direct" space and the reciprocal, momentum space of the crystal.

When we express $\vec{\kappa}$ in the deflection angle 2θ and the wavelength λ , and relate $\vec{\tau}$ to an interplanar spacing d , the familiar Bragg law results: $|\vec{\kappa}| = 4\pi \sin \theta / \lambda$; $d = |\vec{\tau}|^{-1}$; $\lambda = 2d(hkl) \sin \theta(hkl)$. Therefore, the direction of a Bragg-reflection or diffraction peak is determined by the vectors $\vec{a}^*, \vec{b}^*, \vec{c}^*$ and the numbers h, k, l .

One may further show that the intensity of a reflection is determined by h, k, l and the contents of the unit cell defined by \vec{a}, \vec{b} and \vec{c} . Consider N point scatterers ("atoms") in the unit cell, the j th atom having the average position $\vec{r}_j = x_j \vec{a} + y_j \vec{b} + z_j \vec{c}$, and scattering a wavelet with amplitude b_j . Their combined effect is then a wave with amplitude

$$F(\vec{\kappa}) = \sum_j b_j \exp i \vec{\kappa} \cdot \vec{r}_j$$

The function $F(\vec{\kappa})$ is recognized as a Fourier transform. This becomes even clearer when we formally define a "continuous" scattering density distribution function as a sum of delta-functions [†]:

$$b(\vec{r}) = \sum_j b_j \delta(\vec{r} - \vec{r}_j)$$

and write $F(\vec{\kappa})$ as

$$F(\vec{\kappa}) = \int_{\text{cell}} b(\vec{r}) \exp i \vec{\kappa} \cdot \vec{r} d\vec{r}$$

[†]) The Dirac delta-function is defined by the expressions $\delta(x) = 0$ for $x \neq 0$, $\delta(x) = \infty$ for $x = 0$, and $\int_{-\infty}^{+\infty} \delta(x) dx = 1$. It has the property $\int_{-\infty}^{+\infty} f(x) \delta(a-x) dx = f(a)$ and can be Fourier-transformed as $\delta(x) = \frac{1}{2\pi} \int_{-\infty}^{+\infty} e^{-ikx} dx$. The three-dimensional $\delta(\vec{r})$ is defined as $\delta(\vec{r}) = \delta(x) \delta(y) \delta(z)$.

Crystallographers call $F(\vec{\kappa})$ the structure factor and write it as

$$F(hkl) = \sum_j b_j \exp 2\pi i (hx_j + ky_j + lz_j).$$

Omitting at present several factors, continuous in θ , arising from the geometry of the experiment, the scattered intensity is proportional to the square of the amplitude:

$$I(hkl) \sim |F(hkl)|^2$$

This poses the central problem in a crystal structure determination: the information available by experiment contains the magnitude of the structure factor F , not its complex phase angle. This prohibits us to perform the inverse Fourier transformation yielding the scattering density:

$$b(\vec{r}) = \frac{1}{(2\pi)^3} \sum_{\vec{\kappa}} F(\vec{\kappa}) \exp -i \vec{\kappa} \cdot \vec{r}$$

or, equivalently,

$$b(\vec{r}) = \frac{1}{(2\pi)^3} \sum_{h,k,l} F(hkl) \exp -2\pi i (hx + ky + lz)$$

In order to find $b(\vec{r})$ we must guess the phase of F by approximately solving the structure, for which several techniques are available.

Now having outlined an abstract formalism describing scattering of a "wave" by a "crystal", the next step is to specify the nature of the wave, the crystal and the interaction process.

First, the wave.

This is not the place to discuss the wave properties of the neutron. We limit ourselves to noting that thermal neutrons emerging from a reactor show an essentially maxwellian velocity distribution, the maximum of which corresponds to a wavelength λ of about 1.8 \AA . This is the right order of magnitude for crystal structure analysis.

Second, the scattering potential.

Except gravitation, two types of force are known to which neutrons are sensitive. Of course, the first of these is the nuclear force acting between hadrons, and the second is the electromagnetic force acting on the neutron spin.

Third, the crystal.

Due to nuclear interaction the neutron beam will be subject to scattering by the nuclei. In this case the assumption of point scatterers is valid, because the size of the nucleus is very small compared to the neutron wavelength.

Since no detailed theory of nuclear interaction is available at present there is no way to calculate the scattering lengths b for the isotopes. Values of b have been determined by experiment; they are of the order of 10^{-12} cm and can be positive, negative and complex.

In the case of magnetic scattering a number of things change. The electromagnetic force is active between the magnetic moment γ of the neutron spin and the magnetic moment μ of the atoms in the crystal.

Since the spatial extent of electron wave functions is of the same order of magnitude as the neutron wavelength, magnetic atoms cannot be described as point scatterers. This is accounted for by the introduction of the magnetic form factor $f(\vec{\kappa})$, the Fourier transform of the electron wave functions centred at the nucleus. These have been calculated and tabulated for 3d metals and lanthanides, [26] and [45].

Moreover, since the magnetic moment $\vec{\mu}$ is a vector quantity the Fourier transform of the magnetic scattering density is also a vector quantity:

$$\vec{F}_M(\vec{\kappa}) = b_M \sum_j \vec{\mu}_j f_j(\vec{\kappa}) \exp i \vec{\kappa} \cdot \vec{r}_j$$

where b_M is the scattering length of a magnetic moment of 1 Bohr magneton; the calculated value is

$$b_M \equiv \frac{e^2}{2mc^2} \gamma = 0.2695 \times 10^{-12} \text{ cm.}$$

Lastly, the magnetic interaction is not isotropic: the scattered intensity depends on the polarization of the neutron spin and on the direction of $\vec{\kappa}$ with respect to \vec{F}_M . For unpolarized neutrons the scattered intensity can be written as:

$$I_M(\vec{\kappa}) \sim |\vec{F}_M(\vec{\kappa})|^2 - \frac{|\vec{\kappa} \cdot \vec{F}_M(\vec{\kappa})|^2}{|\vec{\kappa}|^2}$$

This implies that only the component of \vec{F}_M perpendicular to $\vec{\kappa}$ contributes to the magnetic scattering. This is a most useful property since it enables one to determine the direction of the magnetic moments with respect to the crystal axes \vec{a} , \vec{b} and \vec{c} . In a powder experiment certain limits are set by the symmetry of the magnetic structure. In a cubic magnetic symmetry the magnitude only of $\vec{\mu}$ can be determined in a powder experiment; in a uniaxial (tetragonal, hexagonal or trigonal) magnetic symmetry the components parallel and perpendicular to the unique axis can be determined.

It remains to be noted that for unpolarized neutrons there is no coherence, i.e. no interference, between magnetic and nuclear scattering: the intensities are simply additive. This is usually a handicap in the investigation of a ferromagnet, for which nuclear and magnetic scattering peaks coincide.

It will be clear that this presentation is rather crude and far from complete. In a sophisticated derivation of scattering cross sections one

should apply a formal quantum mechanical theory of scattering [1]. Furthermore, symmetry properties other than translational are ignored, whereas in fact the establishment of symmetry relations between atoms in the unit cell, if they exist, is an essential step in any crystal or magnetic structure analysis [2].

Moreover, a number of important processes occurring in real crystals were completely neglected [3]. The most important of these for a diffraction experiment are thermal vibrations and absorption.

Due to thermal motion the j th atom appears to the neutron as located at an instantaneous position \vec{r}' differing from its mean value \vec{r} by a vector \vec{u}_j . As a result an additional phase factor $\exp i \vec{\kappa} \cdot \vec{u}_j$ is introduced in the structure factor expression that is increasingly important at higher scattering angles. For an evaluation of the total effect the individual phase differences must be averaged over the crystal, and this leads to the Debye-Waller factor. In its simplest form equal mean square displacements are assumed for all atoms, from which one derives a factor in the intensity equal to $\exp -\frac{1}{3} \langle \vec{u}^2 \rangle \kappa^2$, usually written as $\exp -2B \sin^2 \theta / \lambda^2$. If the measurements are extended to sufficiently high values of $\vec{\kappa}$, one may determine the differences in $\langle \vec{u}^2 \rangle$ for different atoms, or even anisotropic values.

The influence of absorption on the measured intensity is not so easily evaluated in a general case. Absorption effects are very sensitive to the geometrical shape of the specimen and its orientation, since the mean path of a neutron in the sample is the relevant quantity. In the case of a cylindrical specimen shape, as is usually employed, the results of numerical calculations have been tabulated; however, experience shows that, when no absorption correction is carried out the parameters for the thermal motion are decreased with respect to their expected values, whereas the structure parameters are not affected by the neglect of absorption effects.

1.2 The instrument

The type of instrument commonly used for single crystal and powder diffraction, when no energy or polarization analysis is carried out, is a two-axis spectrometer using a constant beam of monochromatized neutrons. It is designated two-axis since the neutrons are deflected twice, once by the monochromator and once by the sample prior to being detected in the counting system.

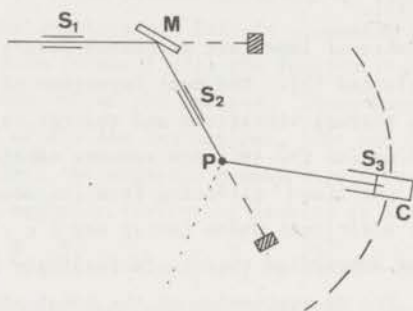


Fig. 1 Schematic drawing of a powder diffractometer.

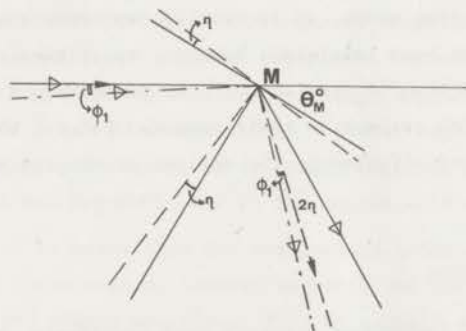


Fig. 2a The monochromatization process.

For single crystal work a mechanism is required to orient the crystal in any desired position, in order to bring any scattering vector in the horizontal plane where the neutrons can be counted. For a powder specimen no such mechanism is required, since all crystal orientations are available. As a consequence the two-axis powder diffractometer is the simplest type of neutron spectrometer, measuring scattered intensity as a function of scattering angle only.

In order to formulate criteria for a good spectrometer it is necessary to understand its "optical" properties. A complete treatment, though for a slightly idealized case, was given by Caglioti et al. in a number of papers that appeared around 1958. Their analysis of the powder diffractometer [4] was the starting point for the design of the spectrometer at the HFR at Petten and for the method of analysis described in section 3.

A schematic drawing of the instrument is presented in fig. 1.

Apart from other radiation, a beam of thermalized neutrons emerges from the reactor through a slit system S_1 . It is diffracted by the monochromator crystal M. The scattered neutrons are taken off at an angle $2\theta_M$ defined by slit system S_2 , which results in a beam with a narrow wavelength band. The sample P is bathed in the once deflected beam, and the scattered neutrons are detected by a counter moving on an arc centred at the sample position. In front of the detector a third slit system S_3 is placed.

The slit systems have finite apertures and the monochromator has a finite mosaic structure. In order to find the peak shape and luminosity, we must follow the path of neutrons that deviate in initial direction and in wavelength from the so-called central ray. In doing so we shall restrict ourselves to the plane in which the scattering takes place, i.e. we assume perfect vertical collimation.

The monochromatization process is shown in fig. 2a.

A neutron passing S_1 at an angle ϕ_1 with respect to the mean direction, and with a wavelength $\lambda = \lambda_0 + \Delta\lambda$, will select a crystal mosaic block at an angle η with respect to the mean of the distribution, such that $\lambda = 2 d_M \sin(\theta_M^0 + \eta + \phi_1)$. It will be scattered in the direction $2\theta_M = 2\theta_M^0 + 2\eta + \phi_1$.

The incoming direction of the neutron is described by the parameter ϕ_1 ; the wavelength shift $\Delta\lambda$ is related to $\Delta\theta_M \equiv \eta + \phi_1 = \delta$ by the expression

$$\Delta\lambda = 2 d_M \cos \theta_M^0 \times \delta,$$

as is evident by differentiation of Bragg's law.

The scattering by the specimen is illustrated in fig. 2b.

The neutron with initial parameters (ϕ_1, δ) now travels at an angle $\phi_2 = 2\theta_M - 2\theta_M^0 = 2\eta + \phi_1$ with respect to S_2 . The Bragg angle at the sample will be $\theta_P = \theta_P^0 + \zeta$, with ζ to be determined, so that for the geometry shown in fig. 2b the neutron will be scattered in the direction $2\theta_P^0 + 2\zeta - \phi_2$. The minus sign is a direct consequence of the geometry chosen; if the twice reflected beam would be chosen according to the dotted line in fig. 1. the + sign would be appropriate. This is the well-known focussing property of the so-called parallel geometry.

The parameter ζ is related to the neutron wavelength and must therefore be related to δ ; the relation is:

$$\Delta\lambda = 2 d_M \cos \theta_M^0 \times \delta = 2 d_P \cos \theta_P^0 \times \zeta$$

whence

$$\zeta = \frac{d_M \cos \theta_M^0}{d_P \cos \theta_P^0} \times \delta = \frac{\text{tg } \theta_P^0}{\text{tg } \theta_M^0} \times \delta \equiv p \times \delta$$

where $p = \text{tg } \theta_P^0 / \text{tg } \theta_M^0$

As stated, the neutron travels in the direction $2\theta_P^0 + 2\zeta - \phi_2 \equiv 2\theta_P^0 + \phi_3$ with $\phi_3 = 2\zeta - \phi_2$; if the counter is at the position $2\theta_P^0 + \rho$ the neutron travels at an angle $\phi_3 - \rho$ with respect to S_3 .

In order to calculate the peak shape and integrated intensity as a function of ϕ_1 , δ and p we must introduce the probability that a neutron traveling at an angle ϕ_i with respect to S_i will be transmitted, and the probability for the mosaic angle η of the monochromator to be available. In the ideal case all orientations are equally probable in the powder.

As is shown by experiment, the transmission function of a Soller slit S_i may be described to a good approximation by a gaussian:

$$P_i(\phi_i) \sim \exp - \phi_i^2 / \alpha_i^2$$

where α_i is a measure of the aperture of S_i ; moreover the distribution function of mosaic blocks may be approximated by a gaussian:

$$P_M(\eta) \sim \exp - \eta^2 / \beta^2$$

where β is related to the mosaic spread of the monochromator. The distribution

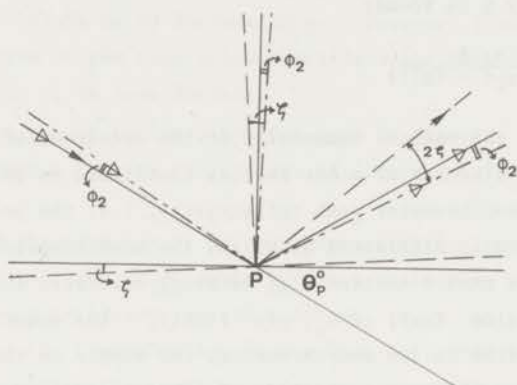


Fig. 2b Scattering by the sample.

function for the whole spectrometer is then found as the product of the individual transmission functions:

$$P(\phi_1, \delta, p, \rho) \sim \exp - \left[\phi_1^2 / \alpha_1^2 + \eta^2 / \beta^2 + \phi_2^2 / \alpha_2^2 + (\phi_3 - \rho)^2 / \alpha_3^2 \right]$$

Integration over ϕ_1 and δ yields the peak shape $I(\rho)$; a final integration over ρ yields the integrated intensity, i.e. luminosity, as a function of p .

Carrying out the integrations Caglioti et al found the peak shape $I(\rho)$ to be a gaussian function with peak width W

$$I(\rho) \sim \exp - \rho^2 / W^2;$$

the proportionality factor being a function of the α_i , β and p but not of ρ . The peak width W is determined by

$$W^2 = A p^2 + B p + C$$

where A , B and C are functions of the α_i and β :

$$A = 4 \frac{\alpha_1^2 \alpha_2^2 + \alpha_1^2 \beta^2 + \alpha_2^2 \beta^2}{\alpha_1^2 + \alpha_2^2 + 4\beta^2}$$

$$B = -4 \frac{\alpha_1^2 \alpha_2^2 + 2\alpha_2^2 \beta^2}{\alpha_1^2 + \alpha_2^2 + 4\beta^2}$$

$$C = \alpha_3^2 + \frac{\alpha_1^2 \alpha_2^2 + 4\alpha_2^2 \beta^2}{\alpha_1^2 + \alpha_2^2 + 4\beta^2}$$

For the luminosity L is found:

$$L = \frac{\alpha_1 \alpha_2 \alpha_3 \beta}{(\alpha_1^2 + \alpha_2^2 + 4\beta^2)^{\frac{1}{2}}}$$

L might be called the optical luminosity of the spectrometer. In the actual countrate a number of other factors contribute as well. The first of these is the monochromator peak reflectivity, i.e. the probability that an incident neutron is diffracted at all by the monochromator. Then there is the probability that a neutron will be Bragg-scattered at all in the particular reflection (hkl) at θ_0 , viz. $F(hkl)$, the quantity to be measured. Absorption in the monochromator, the sample or the surrounding air will reduce the countrate, and a further reduction will occur due to a non-100% efficiency of the counting system.

Moreover, the crystallites are arranged at random; calculation of the fraction oriented such that neutrons diffracted by them will reach the counter, leads to the Lorentz factor $1/\sin \theta \sin 2\theta$.

Finally, the influence of vertical divergence. Since for a spherical sample the paths of diffracted neutrons form a cone, the segment of the cone intercepted by the counter surface bears a direct relation to the countrate. For low angles this will lead to a marked asymmetry of the peak; however, in first approximation this does not lead to a change in the Lorentz factor. In cylindrical samples the diffraction cone is convoluted with the sample height, which at low θ leads to a broadened but more symmetric peak.

Caglioti et al. give numerous examples of particular combinations of α_i 's and β , illustrating the effect of variation of one or more parameters. One may draw the following general conclusions:

a) resolution is not a sensitive function of the monochromator's mosaic spread, whereas L increases with increasing β , so that β should be made as large as possible. Since monochromators are usually far too perfect crystals this has led to many investigations with respect to the performance of monochromator crystal materials.

b) over the range of p covered in actual experiments the resolution is not a sensitive function of α_2 . In fact the crude natural collimation of about 1° provided by the ratio of sample diameter to its distance from the monochromator is quite sufficient. For this reason most powder

spectrometers operate without an explicit slit system S_2 .

c) since the luminosity is linear in α_3 , perhaps the easiest way of increasing the countrate is by increasing α_3 . However, since α_3 appears in the constant term of the resolution function W the loss in resolution, particularly at low p , is considerable.

d) resolution should be improved very much by choosing a large θ_M , resulting in a lower p for the reflections of interest. This will be discussed below.

Lastly, from the geometry of the monochromatization process it is evident that the crystal, set at an angle θ_M for a reflection hkl at wavelength λ_0 is also in reflection position for nh , nk , nl at wavelength λ_0/n . In order to reduce λ/n contamination in the once deflected beam powder spectrometers are usually designed to operate at a wavelength near 1 \AA .

When the spectrometer at the High Flux Reactor at Petten was designed it was considered revolutionary, being based on a new interpretation of the work by Caglioti et al.

Loopstra showed [5] that the proper way to gain resolution is by increasing θ_M , at constant d_M , thereby operating at a relatively long wavelength. In doing so one moves over the maximum in the wavelength distribution, such that there are fewer neutrons of the selected wavelength λ_0 and more of the unwanted $\lambda_0/2$ available in the beam coming from the reactor. Thus, the use of an appropriate filter is essential. Pyrolytic graphite is suitable, more than other filter materials, since it has a transparency window in the region $2.3 < \lambda < 2.9 \text{ \AA}$ *).

Moreover, it is possible to make up for the decrease in primary flux by a number of cooperating factors such as increased reflectivity of the specimen at longer λ , better efficiency of the counter, and positive use of vertical divergence through a short distance between specimen and counter.

*) The material consists of hexagonal crystallites that have their c axis aligned in a normal mosaic distribution, but whose a and b axes are oriented at random in the plane $\perp \vec{c}$. When the neutrons are incident $\parallel \vec{c}$ they will be (Bragg)scattered except when their wavelength does not match a Bragg-angle.

The validity of this approach has been proved by the performance of the spectrometer at Petten during its years of operation. In its normal configuration, operating at $\lambda = 2.57 \text{ \AA}$ obtained from a Cu (111) crystal at $2\theta_M = 76^\circ$, with a total thickness of 10 cm pyrolytic graphite as a $\lambda/2$ filter, and 30' slits S_1 and S_3 , it compares favourably with other spectrometers. Its resolution and peak to background ratio are very good while maintaining a comparable countrate (per unit of central thermal flux in the reactor core), resulting in a standard measurement time of two days for a 10 cm^3 sample.

1.3 Data reduction

In section 1 of this chapter it was noted that the result of a measurement consists of the magnitudes of Fourier coefficients of the scattering density in the unit cell, and that the art of structure analysis consists in reconstructing the phase angles of these Fourier coefficients. This analysis is not always straight-forward.

In fig. 3 some results are shown. For three different compounds the measured diagram is given by the dots, representing the actual counts assembled as a function of scattering angle 2θ (the experimental unit of angle, dmc, is such that $10^4 \text{ dmc} \equiv 360^\circ$). The drawn line in each diagram represents the result of the calculations to be described.

If nothing is known at all about the crystal structure of the compound, the first step is to try and find the unit cell, i.e. the vectors \vec{a}^* , \vec{b}^* and \vec{c}^* such that each peak in the diagram can be represented by three integer numbers hkl with $|\vec{\kappa}| = 4\pi \sin \theta/\lambda = |h\vec{a}^* + k\vec{b}^* + l\vec{c}^*|$.

The second step is the determination, if possible, of the full symmetry of the crystal structure [2]. The distinction between mirror planes and rotation axes, or the establishment of a centre of symmetry is only possible by statistical analysis. However, glide planes and screw axes manifest themselves through systematic extinction of certain types of reflections. In a minority of cases a unique allocation of the space group is possible by determination of the reflection conditions, notably when screw axes and/or glide planes are present. When no reflection conditions are found one knows that screw axes and glide planes are absent, but one has no information about the

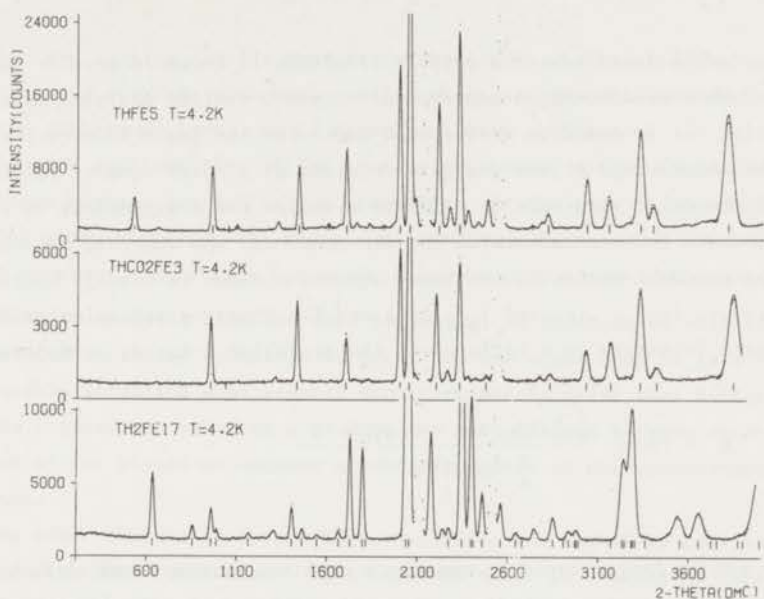


Fig. 3. Examples of powder diffraction diagrams.

existence of rotation axes and mirror planes. In this latter case one has to keep the possible combinations of these in mind until the very end of the investigation.

When the unit cell is known one may determine how many formula units it contains by calculating the resultant density. The condition that this number is integral and compatible with the symmetry found, together with some idea about the actual density, is usually sufficient. Then one may attempt a shrewd guess at the structure, or proceed by more sophisticated techniques, to arrive at a structure model. It would go too far to attempt to give a detailed description of these techniques, since they depend on having a large number of structure factor magnitudes available, and in a powder diffraction experiment they can hardly be used. Most of them make use of the fact that relations must exist between structure factors, since their number is far greater than the number of parameters, i.e. the atomic coordinates. For instance, the phase of a reflection (nh, nk, nl) is determined as soon as the phase of (hkl) is specified. Moreover, it occurs only very rarely that the analysis described so far has not been carried out prior or parallel to the neutron diffraction experiment, by an X-ray single crystal investigation.

So in the usual case the crystal structure is known in more or less detail. When determining a magnetic structure a similar analysis must be carried out in order to arrive at a model for the magnetic structure.

The final stage of the analysis consists of a least squares refinement of the trial structure in order to minimize the disagreement between the structure factors calculated for the model and the observed values.

The residual misfit in the least squares minimum is usually evaluated as follows: if $I_{\text{obs}}(\kappa)$ and $I_{\text{calc}}(\kappa)$ are the observed and calculated integrated intensity in a reflection, the so-called R-factor is defined as

$$R = 100 \times \frac{\sum_{\kappa} | I_{\text{obs}}(\kappa) - I_{\text{calc}}(\kappa) |}{\sum_{\kappa} I_{\text{obs}}(\kappa)}$$

Here we can no longer avoid to mention a problem, circumvented so far, inherent in the powder method: overlap of neighbouring reflections. Until now we tacitly assumed that all structure factor magnitudes were measured independently, as can be done in a single crystal investigation. In a powder investigation this can only very seldom be realized. Since the scattered intensity is determined as a function of the magnitude of $\vec{\kappa}$ the number of reflections in a κ -interval increases with increasing $|\vec{\kappa}|$, so that overlap of neighbouring reflections must occur inevitably for some value of $|\vec{\kappa}|$, whatever the resolution is.

However, there is a solution to this difficulty: it was demonstrated in section 2 that the peak shape is gaussian, with a known functional form of the half width. At every measured point we may therefore calculate the contribution of each reflection adding to the total count at that point, and use the point by point measured intensities, rather than integrated intensities, in the least squares refinement, thereby making full use of the information available. This method of analysis [6], as opposed to estimating the area under a diffraction peak, is called profile analysis.

The limitation of this method is set by the determination of the background count, which must be subtracted before the refinements are carried out.

Part of the background count may be described by analytic functions, namely the incoherent and inelastic scattering, if known. However, the count due to neutrons swarming in the reactor hall, or possibly other radiation picked up by the counter, and any contribution from sample holder,

cryostat and cooling liquids must be determined by analysis of the actual countrate. In diagrams with much overlap there are insufficient regions where the background level can be determined with confidence.

The wide applicability of the profile refinement method revives the old dilemma between resolution and intensity. In the case of high resolution, but poor intensity, the individual structure factors are known with limited accuracy. This is a favourable situation in a case where one needs to perform an analysis from the very beginning, in order to be able to "play around" with the structure factors. On the other hand it is a very unfavourable situation when several structure models exist that differ in relative intensities only, as e.g. when one must discern between rotation axes and mirror planes or between a centrosymmetric or non-centrosymmetric structure.

The other extreme is a very high countrate, and therefore good accuracy, obtained with poor resolution. If a reliable model is available, this can be refined very well; if on the other hand the model proves to be incorrect one does not have the means to search for a better one.

Both extreme cases are clearly to be avoided, and the optimum experimental conditions must be sought somewhere between the two. It would be useful to develop criteria, if possible, from which one may derive the required countrate and resolution for a particular investigation.

II. INTERMETALLIC COMPOUNDS WITH LANTHANIDES

2.1. Crystal structures

Alloys and (ordered) compounds of lanthanides (R) and other metals (M) have been extensively studied over the past twenty years. This is reflected by Taylor's review article [7] and Wallace's book [8] on compounds of rare earths with other metals.

Since chemical properties do not vary over the range of lanthanides, except phenomena related to a change of valence in Ce, Yb and sometimes Eu, a specific compound is formed usually with all R. Moreover, a particular structure type occurs usually with more than one specific M. The most common example of this is possibly found in the AB_2 Laves phases which occur for quite a number of intermetallic systems, including RM_2 compounds. Lastly, families of structures exist that can be thought of as derived from one common basic structure. These features enable one to study metallic interactions between well-localized and more diffuse magnetic moments under widely varying, but related, conditions.

The present work is concerned with a family of compounds between on one hand Y, Th and lanthanides proper and on the other hand the 3d transition metals Fe, Co, Ni. The parent structure has the composition RM_5 and is known as the $CaCu_5$ structure. Its symmetry is hexagonal, space group $P6/mmm$, with atomic positions

$$\begin{aligned} R & \text{ at } 1(a) \ 000 \text{ with point symmetry } 6/mmm \\ M_1 & \text{ at } 2(c) \ \pm(\frac{1}{3}, \frac{2}{3}, 0) \text{ with point symmetry } \bar{6}m2 \\ M_2 & \text{ at } 3(g) \ 0\frac{1}{2}\frac{1}{2}, \frac{1}{2}0\frac{1}{2}, \frac{1}{2}\frac{1}{2}0, \text{ with point symmetry } mmm, \end{aligned}$$

in a unit cell of dimensions $a = b = 5.0 \text{ \AA}$, $c = 4.0 \text{ \AA}$

This structure is visualized in fig. 4.

The shortest interatomic distances are:

$$M_1 - M_2 = M_2 - M_2 = 2.5 \text{ \AA}$$

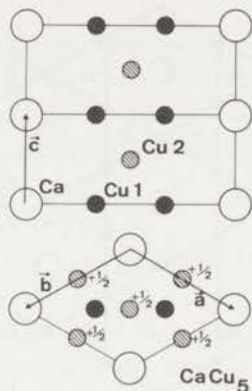


Fig. 4. The CaCu_5 crystal structure exhibited by RM_5 compounds. The R atom occupies the Ca site, M is found on the Cu sites. The upper part of the figure gives a *section* through the crystal perpendicular to the a-b plane; this method of presentation is adopted in all related figures. The lower part gives a *projection* on the a-b plane.

$$\begin{aligned} \text{R} - \text{M}_1 &= \text{M}_1 - \text{M}_1 \approx 3.0 \text{ \AA} \\ \text{R} - \text{M}_2 &= 3.3 \text{ \AA} \end{aligned}$$

The atoms are arranged in two different kinds of layers separated by $\frac{1}{2}c \approx 2.0 \text{ \AA}$. One layer, at $z = 0$, consists of hexagons of M_1 , the centres of which are occupied by R atoms. The other layer at $z = \frac{1}{2}$ contains the M_2 atoms arranged on what is known as a kagome net, such that the R and M_1 in adjacent layers fit in the large and small holes respectively, cf. fig. 5. Each M_2 atom has four nearest neighbours of its own kind, in addition to two M_1 and two R atoms in each adjacent layer, totalling $8\text{M} + 4\text{R}$. Second nearest neighbours are other M_2 atoms.

An M_1 atom has, apart from 3 R atoms, M_2 atoms as its nearest neighbours, three in each neighbouring layer. The three M_1 in the same layer are second neighbours. The two different M sites are therefore not merely crystallographically inequivalent, but are also located in physically very different environments.

From this basic structure type one may derive other structures by systematic substitutions.

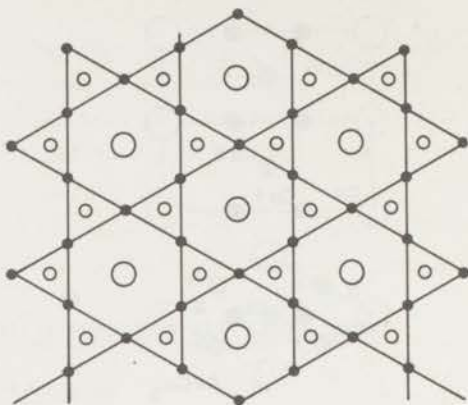
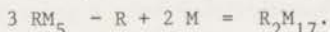


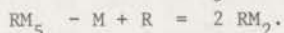
Fig. 5. Extended projection of CaCu_5 crystal structure. Black circles connected by solid lines give the M_2 kagome arrangement at $z = \frac{1}{2}$; large and small open circles represent Th and M_1 at $z = 0$.

The first of these substitution schemes yields an M-rich compound by the replacement of $1/3$ of the R atoms by a pair of M:



In addition to a truly random replacement two regular substitution schemes are realized, shown in fig. 6a, of hexagonal or rhombohedral symmetry. Many R can form both structure types. As a consequence disorder is possible in these compounds. Since this is discussed in detail in chapter VI we limit ourselves here to note that similar mechanisms might be active in other compounds forming both hexagonal and rhombohedral structures.

The other substitution schemes known lead to M-poorer compounds, all being based on the replacement of some M_1 by R. In the RM_2 compounds (fig. 6b) this is done in every RM_5 unit:

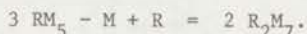


These are the Laves phases already mentioned. The M_2 atoms now have one M_1 and three R neighbours on either side, as well as the four M_2 as before; for the M_1 atoms the nearest neighbour configuration is unchanged. In RM_3 compounds (fig. 6c) the substitution is effected in every second block:



The M_1 site now splits in two inequivalent sites, one of RM_5 and one of RM_2 type; the M_2 site does not split crystallographically but has an RM_5 type layer at one side and one of RM_2 type at the other side.

Finally, in R_2M_7 compounds (fig. 6d) the substitution occurs in every third block:



Again the M_1 site is split; now also M_2 splits in one of RM_5 type and two of RM_3 type.

For the existence of phases based on a further extension of this scheme evidence is scarce [9]. This suggests an estimate of the range of interatomic forces in these crystals: beyond approximately $3 \times 4 = 12 \text{ \AA}$ there is little, if any, correlation between substitutions, and in fact beyond 8 \AA correlations appear to diminish.

Whereas the Laves phases are very common the same is not true for the other members of the family. In R-M systems they are rarely found for other M than Fe, Co or Ni, and even so not all structures are found for all possible combinations: notable absences are RFe_5 and R_2Fe_7 other than for $R = \text{Th}$; hexagonal RM_3 appears to be stable for $M = \text{Ni}$ only, and RFe_2 similarly for the heavy lanthanides.

2.2 Exchange interactions

One, typically metallic, exchange mechanism is indirect coupling via itinerant electrons. The basic idea is the following: assume a localized moment at the origin in a Fermi sea; exchange between the localized ("f") and itinerant ("s") electrons polarizes the latter. In a first order perturbation calculation a uniform polarization results; in second order an oscillating polarization is found. A second localized moment at position \vec{R} is sensitive to the local polarization through the same exchange interaction with the itinerant electrons, and thereby is indirectly coupled to the magnetic moment at the origin. The strength of this coupling depends quadratically on the f-s exchange constant and the itinerant electron density at the Fermi surface, but also on the magnitude and sense of the local polarization.

This theory, known as RKKY after Rudermann, Kittel, Kasuya and Yosida, was originally developed for the interpretation of NMR experiments, then extended to the use for dilute magnetic alloys and applied with some success

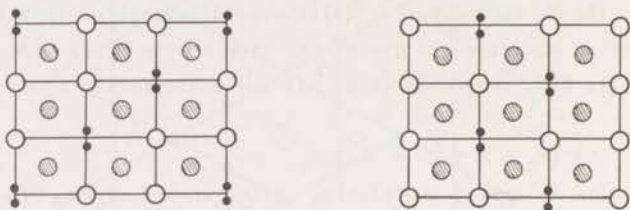


Fig. 6a, R_2M_{17}



Fig. 6b, RM_2

Figs. 6a - 6d. Stacking sequence and substitution schemes.
 Both hexagonal and rhombohedral stacking are shown.
 6a: R_2M_{17} ; 6b: RM_2 ; 6c: RM_3 ; 6d: R_2M_7 .
 The symbols used are those of fig. 4.

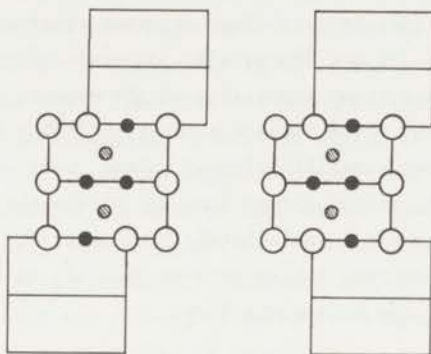


Fig. 6c, RM_3

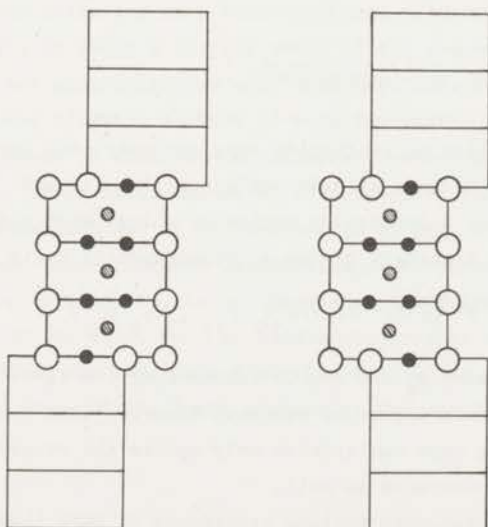


Fig. 6d, R_2M_7

to alloys and compounds between lanthanides and simple metals.

Though the basic idea is very clear an exact treatment in real cases is extremely difficult if not impossible. An exact calculation of the exchange constant V is already impossible at the moment; usually $V(\vec{R}, \vec{r}) = V_0 \delta(\vec{R} - \vec{r})$ is assumed, which implies a constant $V(\vec{q}) = V$ in momentum space. With the further simplification of plane wave itinerant electrons and an exactly localized moment \vec{S} at the origin the resulting second order spin polarization can be calculated. The next step is the derivation of the indirect exchange hamiltonian between spins \vec{S}_i at \vec{R}_i and \vec{S}_j at \vec{R}_j . This is found to be of the Heisenberg form:

$$H = \sum_{ij} H_{ij}$$

$$H_{ij} = -J(\vec{R}_{ij}) \vec{S}_i \cdot \vec{S}_j$$

with the exchange parameter

$$J(\vec{R}_{ij}) \sim c^2 V^2 F_{ij}(2 k_f R_{ij})$$

In this expression c is the itinerant electron concentration at the Fermi surface, V the constant exchange parameter in q -space, k_f the radius of the Fermi sphere and

$$F_{ij}(x) = \frac{\sin x - x \cos x}{x^4}$$

When this theory is applied to lanthanide ions one must take into account that \vec{S} is not conserved because of spin-orbit coupling and must be replaced by $(g-1) \vec{J}$ [7]; then, for a particular series of alloys with the same $E_{F_{ij}}(x)$ molecular field treatment yields a (paramagnetic) Curie temperature

$$\theta_p \sim c^2 V^2 (g-1)^2 J(J+1) \sum_{ij} F_{ij}(2 k_f R_{ij}).$$

The proportionality between θ_p and the De Gennes function $(g-1)^2 J(J+1)$ has been shown to hold in a number of systems; however, this proves the validity of a Heisenberg type hamiltonian only unless the proper c - and F dependence of J are demonstrated as well.

Freeman [10] discusses more refined treatments of RKKY theory, including the consequences of a non-spherical Fermi surface, correlation and exchange effects, non-constant $V(q)$ and interband mixing, but he concludes that the present state of theory and experiment is insufficient to decide on the form and magnitude of these effects. There is little doubt that

RKKY exchange is a fundamental mechanism in magnetic metals and alloys, especially for lanthanides with their well-localized 4f-shell. The situation is not so clear if the theory is to be applied to 3d-metals as s-d exchange, since the d-electrons are not strictly localized.

The theory of d-d exchange in transition metals is connected to that of the formation of localized magnetic moments and long-range magnetic order. By a shift of the spin-up band with respect to the spin-down band exchange energy can be gained but kinetic energy is lost, from which the well-known Stoner stability criterion follows (cf. textbooks on metals). This should not concern us here, since neutron form factors for metallic 3d electrons show that in fact they are essentially localized.

Friedel [11] discusses the behaviour of electrons in a d-band in tight binding approximation and shows how, in second order approximation, a mechanism similar to RKKY theory applies to d-d exchange. He proceeds to show how ferromagnetic and antiferromagnetic structures may arise as a function of d-electron concentration, Fermi radius or susceptibility. However, he also points out that for large magnetic moments perturbation theory is not applicable and that couplings between more than two moments must be taken into account.

We may draw attention to a band-structure calculation by Duff and Das for Fe [12], in which a correct value of the magnetic moment and good electron and spin densities were obtained, starting from almost first principles, using slightly diffuse 3d wave functions. It was estimated that there is about 5% admixture of itinerant behaviour in otherwise atomic d-functions. This small amount of itinerancy is thought to be essential for the establishment of ferromagnetism in Fe. Whereas this shows that a realistic band-structure calculation, incorporating localized moments, is possible for Fe, to our knowledge a similar calculation was not yet reported for Ni or Co. No band-structures at all are known for the compounds that are the subject of this thesis, so we have no information about the shape of the Fermi surface or the magnitudes of band widths and splittings.

2.3 Results obtained by other workers

Because of their high coercivity, anisotropy, induction and Curie temperature the R-Co compounds have technical importance as possible permanent magnet materials. Therefore these compounds have been thoroughly

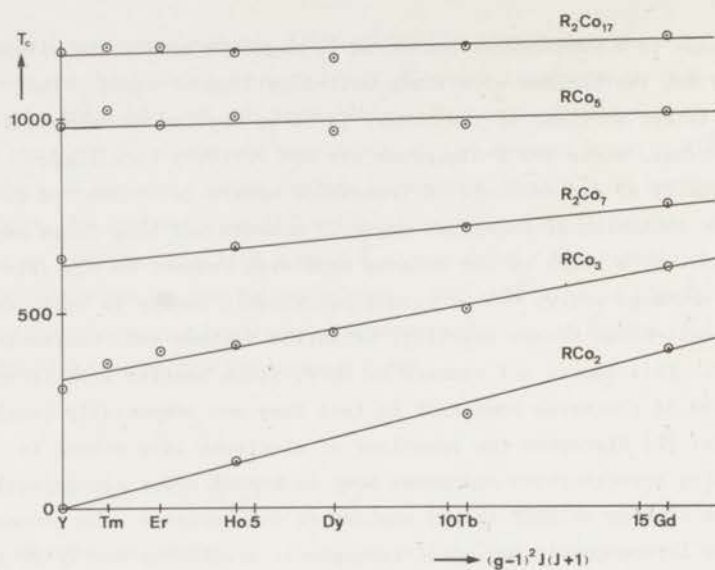


Fig. 7a Curie-temperatures as function of $(g-1)^2 J(J+1)$ for heavy R-Co compounds.

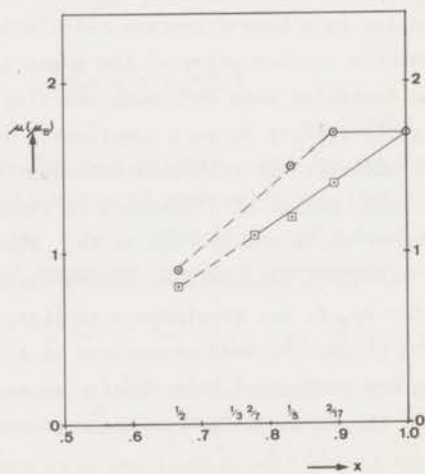


Fig. 7b Average Co-moment in $R_{1-x}Co_x$;

circles: heavy R;

squares: light R.

investigated. It has been found as a general rule that compounds with a light R, where \vec{S} and \vec{J} are antiparallel, are ferromagnets and that compounds with a heavy R, with parallel \vec{S} and \vec{J} , are ferrimagnets ([8], p. 152). This means that the spins of R and Co are always antiparallel, which is hardly compatible with RKKY theory ([8], p. 176). Crystal fields together with an internal field due to the Co moments determine the direction of easy magnetization [13], which usually but not always is found to be the c-axis.

In fig. 7a the Curie-temperatures T_c of a number of heavy-lanthanide-Co compounds are shown as a function of $(g-1)^2 J(J+1)$, the DeGennes function of the lanthanide ion. For light R there is more scatter in T_c : Pr and Nd compounds usually have a lower T_c than expected, which is probably due to crystal field effects. In fig. 7a indeed a term linear in the DeGennes function is found. It is tempting to attribute this to indirect exchange between R and Co, and to ascribe the constant term to direct and indirect exchange interaction between Co atoms.

The average magnetic moment per Co atom in RCo_x compounds is given in fig. 7b. It is seen that the moment is generally lower for light R. For RCo_3 the sublattice magnetization is not known; when one tries to split the measured moment per unit cell in a full-ion R part and the remainder as Co, highly improbable values for the Co moment result, indicating that the R moment must be reduced by crystal fields.

In figs. 8 and 9 results are presented in the same fashion for R-Ni and R-Fe compounds. These systems were not investigated as extensively as the Co-compounds. In the older literature Ni is reported to be non-magnetic, but later workers found an appreciable Ni-moment in R_2Ni_{17} compounds and a small value in RNi_2 and RNi_3 . In RNi_5 no magnetic moment is found on the Ni atoms [13]. In the R-Fe system the R_2Fe_{17} compounds have been investigated. The ferro- or ferrimagnetic coupling scheme found for Co compounds is valid for R_2Fe_{17} compounds as well. Their anisotropy is usually planar, with the exception of Tm_2Fe_{17} below 72 K (Cf. VI, 6.2). A very interesting feature of the R_2Fe_{17} compounds with non-magnetic R is the occurrence of helical magnetic order [15], [21]. This is thought to originate in an antiferromagnetic exchange interaction among the substituted Fe (cf. fig. 6a) which have very short nearest neighbour distances ($< 2.5 \text{ \AA}$). As soon as a magnetic moment develops on the R site the helical configuration is disturbed and the structure becomes collinear.

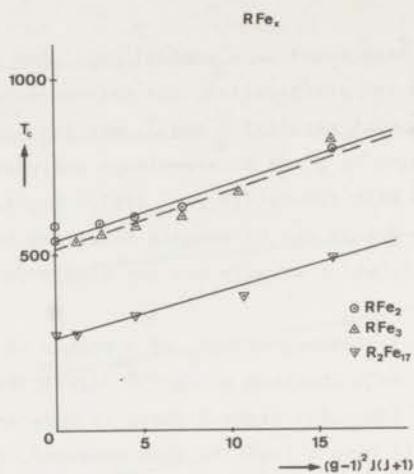


Fig. 8a Curie temperatures as function of $(g-1)^2 J(J+1)$ for heavy R-Fe compounds.

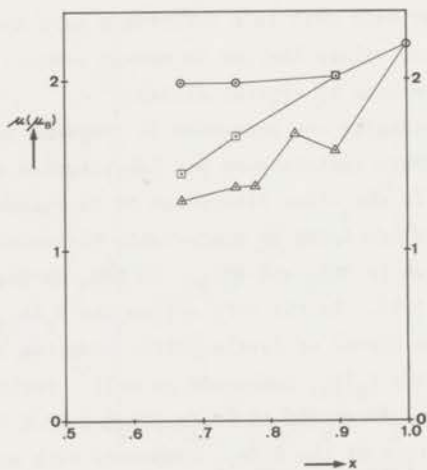


Fig. 8b Average moment in $R_{1-x}Fe_x$.
 circles: heavy R;
 squares: light R.
 triangles: Th.

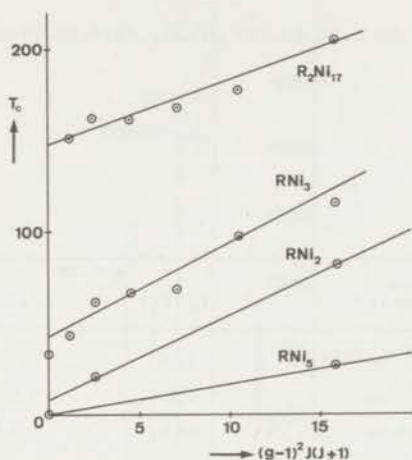


Fig. 9. Curie temperatures as function of $(g-1)^2 J(J+1)$ for heavy R-Ni compounds.

2.4 The scope of the present investigation

So far only lanthanides proper and Y, which behaves as a non-magnetic heavy R, have been mentioned. Since the conduction electron concentration is one of the parameters involved it is a natural extension to investigate Th compounds as well, since Th also behaves as a non-magnetic heavy R but contributes four conduction electrons to the Fermi sea. In table 1 a survey is given of the known compounds of Th with Fe, Co and Ni that are derived from the $CaCu_5$ structure.

The diffraction experiments described encompass all compounds that show long-range magnetic order. The work started with an investigation of the pseudo-binary system $Th(Co, Fe)_5$ in order to facilitate the interpretation of Mössbauer experiments on these compounds. The results stimulated a further investigation of magnetic order in compounds between Th and Fe, Co, Ni.

This first analysis of $Th(Co, Fe)_5$ is reported in chapter III; in chapters IV and V the results obtained for $Th(Ni, Fe)_5$ and $Th(Co, Ni)_5$ are given.

Table 1. Compounds of Th with Fe, Co or Ni, derived from the CaCu_5 structure.

compounds with Fe

| | Symmetry | T_c (K) | μ /atom |
|---------------------------------|---------------|-----------|-------------|
| ThFe_3 | $R \bar{3} m$ | 425 | 1.37 |
| $\alpha\text{-Th}_2\text{Fe}_7$ | $P6_3/mmc$ | 570 | 1.37 |
| ThFe_5 | $P6/mmm$ | 680 | 1.88 |
| $\text{Th}_2\text{Fe}_{17}$ | $R \bar{3} m$ | 295 | 1.76 |

compounds with Co

| | | | |
|-----------------------------|---------------|--------------|------|
| Th_2Co_7 | $P6_3/mmc$ | paramagnetic | |
| ThCo_5 | $P6/mmm$ | 415 | 0.94 |
| $\text{Th}_2\text{Co}_{17}$ | $R \bar{3} m$ | 1035 | 1.42 |

compounds with Ni

| | | | |
|-----------------------------|------------|--------------|--|
| ThNi_5 | $P6/mmm$ | paramagnetic | |
| $\text{Th}_2\text{Ni}_{17}$ | $P6_3/mmc$ | paramagnetic | |

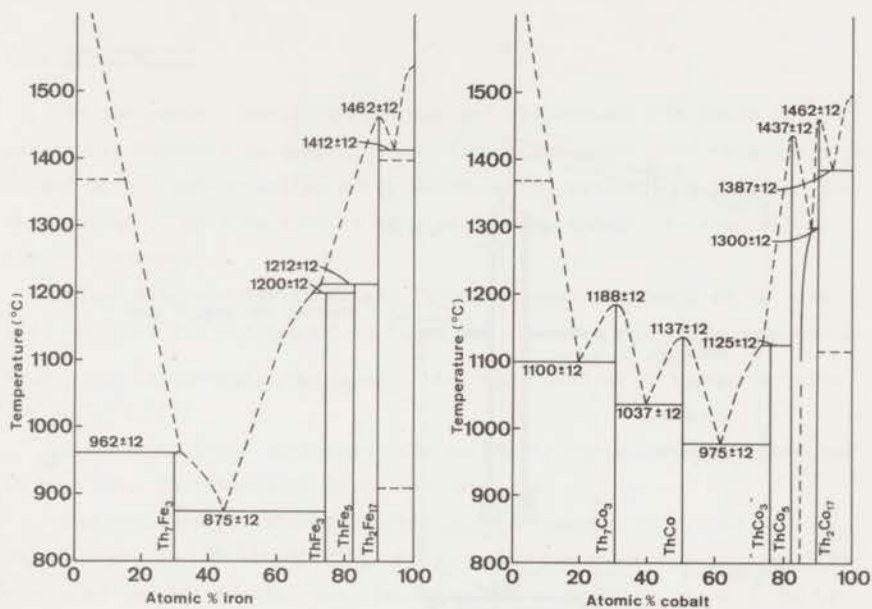


Fig. 10. Phase diagrams of $\text{Th}_{100-x} - \text{Fe}_x$ and $\text{Th}_{100-x} - \text{Co}_x$ (right) taken from ref. 16, cf. text for later revisions.

R_2M_{17} compounds are the subject matter of chapter VI. It is not limited to Th-compounds but has a more general stand point, discussing disorder in hexagonal R_2M_{17} compounds and supporting the discussion with experimental evidence.

$\text{Th}_2\text{Fe}_{17}$ and $\text{Th}_2\text{Co}_{17}$ are plain ferromagnets with planar anisotropy; no further discussion will be given of the diffraction experiment on these two compounds since the analysis was straight-forward and yielded immediate results.

Magnetic order in ThFe_3 and Th_2Fe_7 will be discussed in chapter VII.

Finally, chapter VIII is devoted to a critical evaluation of the results in relation to other experiments.

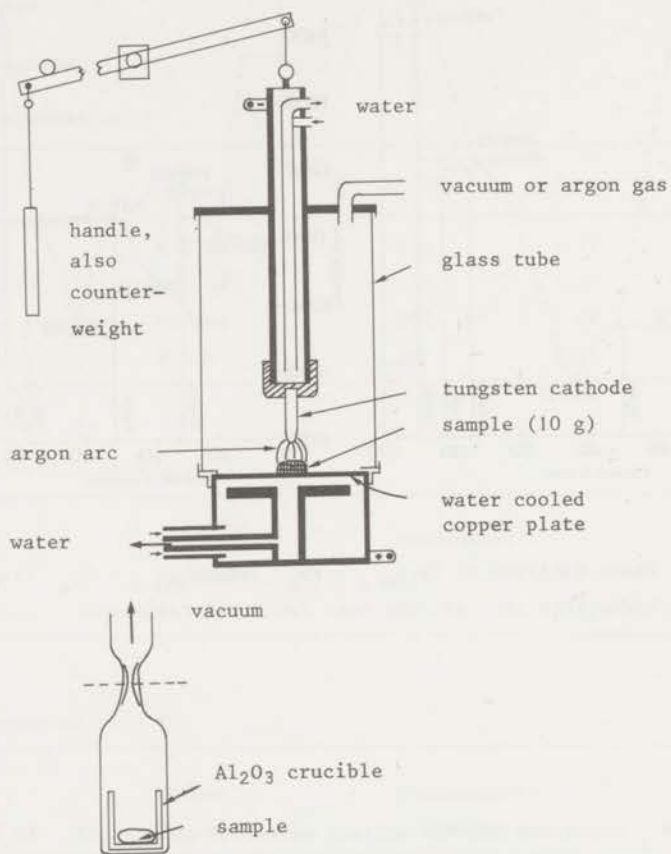


Fig. 11. Arc-melting apparatus and annealing configuration (courtesy of K.H.J. Buschow).

2.5 The samples

In the papers reproduced in chapters III through VII there is no particular emphasis on sample preparation. Therefore this chapter is concluded with a more detailed description of the procedure followed. The information in this section is made available through the courtesy of K.H.J. Buschow.

Phase diagrams for Th-Fe and Th-Co systems were reported in 1966 [16] and they are reproduced in fig. 10. In later years the compound Th_2Fe_7 was discovered. Moreover, ThFe_5 was found to be unstable below $T = 1000^\circ\text{C}$ [17].

A drawing of the equipment used in sample preparation is presented in fig. 11. The procedure is as follows:

The proper amounts of the constituent elements are placed on the copper plate in the arc-melting apparatus, after which the equipment is evacuated and filled with purified Ar gas to a pressure of 10-20 cm Hg. An electric arc is lit between the tungsten cathode and the metal pieces lying on the water-cooled copper plate. In order to ensure chemical homogeneity the button is turned over and remelted about four times. After the melting process the button is annealed, particularly if the compound has a peritectic melting point, in order to remove phases adjacent in the phase diagram. The alloy button is placed in a sintered Al_2O_3 crucible which in turn is sealed in a silica tube. The tube is evacuated for one or two hours whilst gently heated in order to remove all traces of adsorbed oxygen or water vapour, and then sealed. The sealed tube is placed in a resistance furnace and kept at the temperature during the time as indicated in the experimental section in each chapter.

III. CRYSTAL AND MAGNETIC STRUCTURE OF INTERMETALLIC COMPOUNDS OF THE
TYPE $\text{Th}(\text{Co}_x\text{Fe}_{1-x})_5$ ⁺

3.1 Introduction

The enormous number of rare earth 3d transitional metal compounds has received much attention in recent years and with the exception of only few of these compounds their magnetic properties have been determined [7]. In view of the presence of electrons of 4f as well as of 3d character these compounds give rise to rather complicated magnetic interactions, which are far from completely understood at the moment. This holds in particular for the 3d electron magnetism where the magnetic moments' origin and their coupling as well as the relative amount of localization involved are still open questions.

In order to contribute to a better understanding of these matters we have performed a neutron diffraction study of several CaCu_5 type compounds of thorium with Fe and Co of which part of the results were already reported in a previous note. The element Th was chosen because complications due to interactions involving unpaired 4f electrons are absent and because the series of solid solutions RCo_5 - RFe_5 , with $R = \text{Th}$ comprises the full range of iron concentrations, whereas for $R = \text{La}, \text{Y}$ or Lu a compound of the type RFe_5 does not exist.

⁺) J.B.A.A. Elemans, Kamerlingh Onnes Laboratory, Leiden, the Netherlands
K.H.J. Buschow, Philips Research Laboratories, Eindhoven, the Netherlands
Appeared in phys. stat. sol. (a) 24, 393 (1974).

3.2 Experimental

Samples of ThFe_5 , ThCoFe_4 , ThCo_2Fe_3 , ThCo_3Fe_2 , ThCo_5 and also of ThFe_3 and Th_2Fe_7 were prepared by arc melting followed by vacuum annealing at temperatures between 1150 and 1050 °C. The compound ThFe_5 was quenched after vacuum annealing at 1150 °C in order to prevent its decomposition into Th_2Fe_7 and $\text{Th}_2\text{Fe}_{17}$ at temperatures lower than about 1000 °C. Neutron diffraction diagrams were taken at the High Flux Reactor (HFR) at Petten (N-H) at room temperature and at liquid helium temperature under standard conditions with a wavelength $\lambda = 2.57 \text{ \AA}$, $\sin \theta/\lambda < 0.4 \text{ \AA}^{-1}$.

Impurities visible in the diagrams were identified as ThO_2 and, for $\text{Th}(\text{Co}_x\text{Fe}_{1-x})_5$ with small x values, as mainly $\text{Th}_2(\text{Co}_y\text{Fe}_{1-y})_7$. The ThO_2 peaks are few in number and well isolated and can therefore be ignored. However, the crystal structures of ThFe_3 and Th_2Fe_7 are closely related to that of ThFe_5 and consequently give rise to reflections in the vicinity of ThFe_5 peaks. Therefore diagrams of Th_2Fe_7 and ThFe_3 were also recorded. In addition to the diagrams taken with a wavelength equal to 2.57 \AA we examined the compound ThFe_5 at room temperature with $\lambda = 1.0 \text{ \AA}$, $\sin \theta/\lambda < 0.95 \text{ \AA}^{-1}$.

3.3 Structure determination

From the general appearance of the diagrams the CaCu_5 type structure was confirmed. For all compounds of the series $\text{Th}(\text{Co}_x\text{Fe}_{1-x})_5$ Th is found on 1(a), (000), and Fe and Co are distributed at random over 2(c), $(\frac{1}{3}, \frac{2}{3}, 0)$ and 3(g), $(\frac{1}{2}, 0, \frac{1}{2})$ in the space group P 6/mmm.

The main features of the magnetic structures become apparent upon inspection of the diagrams. For $x \geq 0.4$, i.e. on the Co-rich side, all magnetic intensities fall on top of the nuclear peaks. As the nuclear peak (001) is very small, a negligible total (nuclear plus magnetic) intensity of this reflection indicates a direction of the moments very nearly parallel to the c-axis.

For $x < 0.4$, i.e. on the Fe-rich side, the situation is more complex. In ThCoFe_4 the (001) reflection is clearly observed, showing that there is a considerable component perpendicular to the c-axis. In ThFe_5 the (001) is again not observed. Moreover, in ThCoFe_4 as well as in ThFe_5 some additional reflections are found that are readily indexed on the assumption

of a unit cell with a doubled c-axis. From the presence of reflections $(00\frac{1}{2})$ and $(00\frac{3}{2})$ an antiferromagnetic moment in the a-b plane is derived. The intensity of these antiferromagnetic reflections depends on both temperature and Co-concentration.

Comparison with the diagrams obtained with $\text{Th}_2\text{Fe}_{17}$, Th_2Fe_7 or ThFe_3 shows that the origin of these reflections is not due to the presence of other Th-Fe phases.

3.4 Structure refinements

3.4.1 The crystal structure.

Recently questions were raised with respect to the space group of the CaCu_5 type structure [18]. Therefore considerable attention was given to possible deviations from the ideal $P6/mmm$ structure preserving at least trigonal symmetry. It was checked whether such deviations are necessary in order to explain the observed intensities in the ThFe_5 diagram obtained with $\lambda = 1.0 \text{ \AA}$. Consideration of the subgroups of $P6/mmm$ leads to several types of possible deformations.

For instance the symmetry relation between the 2(c) sites $(\frac{1}{3}, \frac{2}{3}, 0)$ and $(\frac{2}{3}, \frac{1}{3}, 0)$ may be lost. This type of distortion implies a displacement of the Fe atoms at the (g) site according to the special position $(x, 2x, \frac{1}{2})$ or $(x, 2x, z)$, and in this case the surroundings of the positions $(\frac{1}{3}, \frac{2}{3}, 0)$ and $(\frac{2}{3}, \frac{1}{3}, 0)$ become different. This is highly improbable and therefore left out of consideration.

All other deformations of the ideal structure were refined, but the displacements calculated vanish or are hardly significant.

If one accepts the ideal coordinates then the only variables in the crystal structure are the relative site occupancies of the transition elements. These were refined while constraining the composition. Within the accuracy obtained the resulting values were independent of temperature and of the magnetic structure assumed. They are shown in fig.12.

Fe is preferentially located on the (g) site $(\frac{1}{2}, 0, \frac{1}{2})$, Co dominating the (c) site $(\frac{1}{3}, \frac{2}{3}, 0)$, which does not agree with the interpretation of x-ray and Mössbauer effect data obtained on these compounds [19].

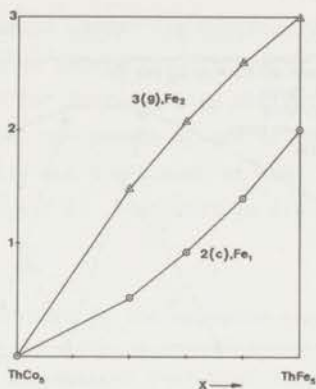


Fig. 12. Fe site occupancy for the two positions 2(c) and 3(g) as a function of Fe concentration.

3.4.2 Ferromagnetic part of the magnetic structure.

Initially strict ferromagnetism, i.e. equal moments oriented parallel for all transition metal atoms, was assumed. For each compound the components parallel and perpendicular to the *c*-axis were refined, both independently and simultaneously. The conclusions reached already by simple inspection of the diagrams were confirmed: in ThCoFe_4 the moment is perpendicular to the *c*-axis within experimental error, in ThCo_2Fe_3 an angle of 35° is found between the moment and the *c*-axis, while for the remainder of compounds investigated the ferromagnetic moment is parallel to the *c*-axis.

In a next stage we have analysed the data with respect to departures from this average structure.

One evident simplification in the gross model is the assumption of equal moments for Fe and Co. The simplest case to test this assumption is ThCo_3Fe_2 , because this compound has its moment parallel to the *c*-axis. A correlation of -99% between the moments calculated for Fe and Co independently shows that the measured intensities do not contain sufficient information with regard to the difference in moment on both atomic species. Another simplification is removed by allowing the moments on the two crystallographic sites to be unequal. For ThCo_5 the final moments differ from the average value by less than twice the standard deviation and the R factor

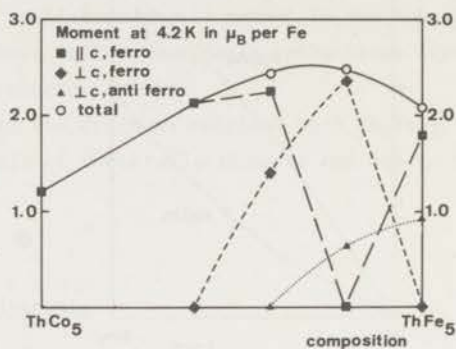


Fig. 13. Components of the magnetic moments at 4.2 K in μ_B per atom.

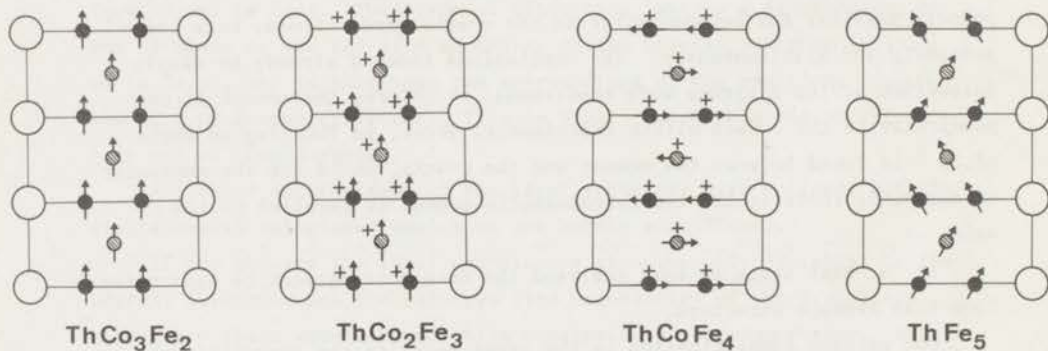


Fig. 14. Magnetic structures in the system $\text{Th}(\text{Co}_x\text{Fe}_{1-x})_5$. The ferromagnetic and antiferromagnetic components perpendicular to the c-axis are arbitrarily drawn normal to and in the plane of the paper, respectively. The normal component is indicated by a + sign.

hardly decreases. However, except for ThCoFe_4 , where the moment is in the ab plane, one finds an increasing difference in moment accompanied by decreasing R factors for increasing Fe content. For ThFe_5 the R factor drops from 10% to 5%, the moment at the (c) position becomes virtually zero or slightly negative and the moment at the (g) position reaches the value of $3.7 \mu_B/\text{atom}$ at 4.2 K. This will be discussed below.

3.4.3 Antiferromagnetic part of the magnetic structure

Antiferromagnetic reflections have been observed in ThFe_5 and ThCoFe_4 . They are most strongly developed in ThFe_5 at 4.2 K, so that the model found for this case was adopted for the other diagrams as well. In order to explain a relatively large intensity of the $(00\frac{1}{2})$ reflection one must assume that the moments within a layer of constant z coordinate are parallel.

Parallel or antiparallel coupling of neighbouring layers ($z = 0$, $z = \frac{1}{2}$) are equivalent through the transformation $\vec{c} \rightarrow -\vec{c}$.

The data are too limited to give reliable results when the antiferromagnetic components on the two sites are refined independently. Therefore, three models were tried, viz. zero moment for either one of the two sites and equal moments on both. Slightly better results were obtained assuming equal moments.

3.5 Discussion

Without going into great detail we want to comment on the ThFe_3 and Th_2Fe_7 diagrams. The diffraction pattern for ThFe_3 shows considerable complexity.

Th_2Fe_7 is reported to crystallize in the space group $P 6_3/mmc$ and to be ferromagnetic with a Curie temperature of 570 K [20]. In the neutron diagrams of this compound the reflections (001) and (003), prohibited by the space group, were clearly observed. We conclude that either the space group is wrong or the magnetic structure of Th_2Fe_7 also exhibits an antiferromagnetic component (cf. chapter VII).

The accuracy obtained in the analysis of the data of the $\text{Th}(\text{Co}_x\text{Fe}_{1-x})_5$ compounds is largely determined by the amount of impurities present, to

Table 2. Results of the refinements. Numbers in parentheses are standard deviations in units of the last decimal.

| sample | T(K) | R(%) | a(Å) | c(Å) | n(Fe ₁) (%) | $\mu_{//c}^{fm}$ (μ_B) | $\mu_{\perp c}^{fm}$ (μ_B) | $\mu_{\perp c}^{afm}$ (μ_B) | μ_{tot} (μ_B) | μ_{tot} (μ_B) | *) |
|-----------------------------------|------|------|-----------|-----------|----------------------------|---------------------------------|-------------------------------------|--------------------------------------|----------------------------|----------------------------|----|
| ThFe ₅ | 300 | 10 | 5.1113(4) | 4.0522(4) | 100(-) | 1.73(9) | -- | 0.42(4) | 1.78(9) | | |
| | 4.2 | 8 | 5.1027(4) | 4.0423(4) | 100(-) | 1.84(7) | -- | 0.93(2) | 2.07(7) | 1.88 | |
| ThCoFe ₄ | 300 | 3 | 5.1090(2) | 4.0453(2) | 69.6(4) | -- | 2.16(5) | -- | 2.16(5) | | |
| | 4.2 | 4 | 5.1032(2) | 4.0381(2) | 70.0(4) | -- | 2.38(5) | 0.64(2) | 2.47(5) | 1.82 | |
| ThCo ₂ Fe ₃ | 300 | 3 | 5.0809(3) | 4.0494(2) | 44.9(5) | 1.75(7) | 1.15(16) | -- | 2.10(5) | | |
| | 4.2 | 4 | 5.0728(2) | 4.0480(2) | 44.8(5) | 1.96(7) | 1.42(14) | -- | 2.43(5) | 1.86 | |
| ThCo ₃ Fe ₂ | 300 | 3 | 5.0519(2) | 4.0410(2) | 24.1(3) | 1.88(2) | -- | -- | 1.88(2) | | |
| | 4.2 | 6 | 5.0426(5) | 4.0370(6) | 22.9(8) | 2.13(6) | -- | -- | 2.13(6) | 1.68 | |
| ThCo ₅ | 300 | 5 | 4.9990(4) | 4.0015(3) | 0(-) | 1.16(3) | -- | -- | 1.16(3) | | |
| | 4.2 | 10 | 4.9850(6) | 3.9899(6) | 0(-) | 1.10(4) | -- | -- | 1.10(4) | 0.94 | |

*) Data of bulk magnetic measurements, taken from ref. 19.

the extent of introducing spurious details in the structure. So a magnetic structure of ThFe_5 in which one of the two sites carries all of the magnetic moment ($3.7 \mu_B$), can most certainly be excluded in view of the Mössbauer data available for this compound [19]. Whatever the interpretation of the Mössbauer spectrum might be, an iron moment of $3.7 \mu_B$ would imply an enormous hyperfine field, being about twice as high as the value actually observed.

The increasing difference in moment at the two sites (c) and (g) with increasing Fe content is probably to be interpreted as being caused by systematic errors in increasing importance. This is not so surprising since the compound ThFe_5 crystallizes with great difficulty and as a matter of fact is metastable at room temperature. As the final interpretation of our data we therefore wish to confine us to the "crude" model of equal moments at both sites.

The numerical results are collected in table 2; the magnetic moments at 4.2 K are also presented in fig.13 and the structures are visualized in fig. 14.

For comparison we have listed in table 2 the saturation moments obtained at 4.2 K by magnetic bulk measurements on polycrystalline material [19]. There exists fair agreement with the neutron diffraction data for ThFe_5 . For the compounds containing also Co the agreement is less satisfactory. It is possible that the somewhat lower values of the magnetic measurements find their origin in the presence of crystalline anisotropy in these compounds. The neutron diffraction data are furthermore seen to give rise to a maximum in the composition dependence of the total moment. Similar maxima in series of pseudobinary rare-earth-cobalt-iron compounds were reported before and have been ascribed to a filling of the 3d band in which both half bands appear unsaturated ([7], [19]).

The most striking feature of the magnetic properties of the compounds investigated is the presence of antiferromagnetic components in the iron-rich compounds. In the large family of intermetallic compounds of 3d transition metals and lanthanides, yttrium or thorium examples of antiferromagnetic components have only been reported for a few of the members of the R_2Fe_{17} series [21]. Phenomenologically there seems to be a relation between the occurrence of antiferromagnetic interactions in the R_2Fe_{17} compounds and a short unit cell dimension in the c-direction as the latter renders the nearest neighbour distance between the pairs of Fe atoms, typical of this structure type, extremely short.

The present compounds have a homogeneity region at elevated temperatures in which similar pairs of transition metal atoms can exist as those occurring in the structure of the R_2Fe_{17} compounds, cf $SmCo_5$ [22]. To exclude the possibility that the presence of antiferromagnetic components observed in the present compounds is triggered by the occurrence of such iron pairs we have carefully avoided the transition metal rich part of the homogeneity region by using a slight excess (1%) of thorium. In addition, in order to estimate the effect of the presence of Fe pairs we have deliberately prepared samples deficient in thorium such as for instance $Th[Co_{0.2}Fe_{0.8}]_{5.3}$. Neutron diffraction performed on this sample showed that there is a tendency of the antiferromagnetic moment component to decrease rather than to increase.

There are too many variable parameters involved (lattice constants a and c , conduction electron concentration, relative exchange of the 3d band etc.) to trace the origin of the antiferromagnetic contributions. Future work to elucidate their nature will comprise investigation of the pseudo-binary series $Th(Ni_xFe_{1-x})_5$.

Figure 12 indicates that a relatively strong preference exists for the Fe atoms in $Th(Co_xFe_{1-x})_5$ to occupy the crystallographic (g) position. This is in agreement with the results obtained by Laforest and Shah [23], but appears to deviate from the results obtained by Mössbauer effect measurements [19]. Moreover, the relation between cell constants and composition is more complicated than proposed there.

Finally we wish to discuss some questions with regard to magnetic symmetry. In $ThFe_5$ and $ThCoFe_4$ two spin components show different magnetic lattices. This can formally be described by doubling the cell and reducing the number of symmetry elements, thereby removing the translation symmetry $x, y, \frac{1}{2} + z$. There are several ways to do this, and careful analysis leaves four possible space groups. If we impose the conditions that the two formula units per doubled cell are coupled by symmetry and that 3 spin components are possible the only surviving space group is $Cmc2_1$ (nr 36 of the International Tables) with magnetic space group Cc' . The screw axis replaces the originally primitive translation symmetry $x, y, \frac{1}{2} + z$; the mirror plane retained is the originally diagonal mirror plane; the c glide plane contains a hexagonal axis. The crystal symmetry is now orthorhombic and one may ask whether a deformation of the crystal structure according to space group $Cmc2_1$ is realized. In the present diagrams there is, however, no evidence for such a deformation.

IV. MAGNETIC ORDER IN THE PSEUDO-BINARY SYSTEM $\text{Th}(\text{Fe}_{1-x}\text{Ni}_x)_5$ ^{†)}

4.1 Introduction

In chapter III [24] we reported on the crystal and magnetic structures of compounds of the series $\text{Th}(\text{Fe}_{1-x}\text{Co}_x)_5$. It was found that only part of these compounds are true ferromagnets. For the compounds with $x = 1$ and $x = 0.8$ also antiferromagnetic components are present leading to a doubling of the magnetic unit cell. In the present study we report on investigations of compounds of the series $\text{Th}(\text{Fe}_{1-x}\text{Ni}_x)_5$ where the Fe atoms are gradually replaced by Ni atoms. This comes close to magnetic dilution since the Ni atoms do not carry a magnetic moment in ThNi_5 . It will be shown that also in the present series most of the compounds are not true ferromagnets but give rise to an antiferromagnetic component. We will furthermore present evidence that in $\text{Th}(\text{Fe}_{1-x}\text{Ni}_x)_5$ the magnetic moments follow closely a localized description. Results of neutron diffraction and magnetic measurements of the series $\text{Th}(\text{Co}_{1-x}\text{Ni}_x)_5$ will be presented in chapter V [25].

^{†)} J.B.A.A. Elemans, Kamerlingh Onnes Laboratory, Leiden, the Netherlands
K.H.J. Buschow, Philips Research Laboratories, Eindhoven, the Netherlands
H.W. Zandbergen, Gorlaeus Laboratory, Leiden, the Netherlands
J.P. de Jong, Gorlaeus Laboratory, Leiden, the Netherlands.

to appear in phys. stat. sol. (a), 30 (1975).

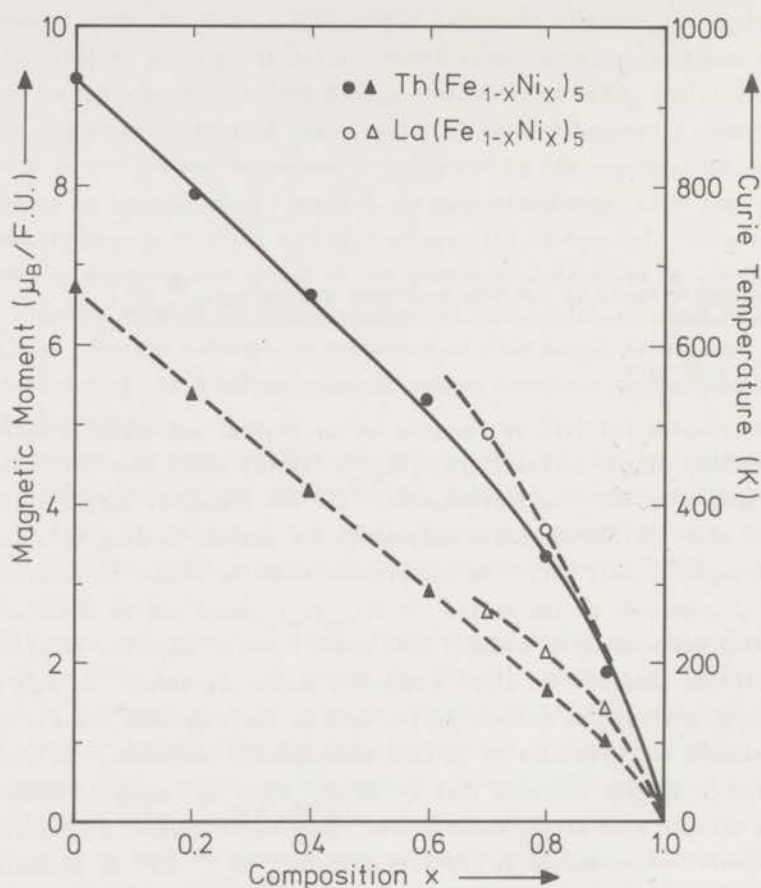


Fig.15. Composition dependence of the magnetic moment per formula unit (open and full circles) and composition dependence of the Curie temperature (open and full triangles) of the compounds $\text{Th}(\text{Fe}_{1-x}\text{Ni}_x)_5$ and $\text{La}(\text{Fe}_{1-x}\text{Ni}_x)_5$. The full line through the data points of $\text{Th}(\text{Fe}_{1-x}\text{Ni}_x)_5$ represents the results of model calculations (see text).

4.2 Experimental

4.2.1 Experimental procedures

The samples $\text{Th}(\text{Fe}_{1-x}\text{Ni}_x)_5$ and $\text{La}(\text{Fe}_{1-x}\text{Ni}_x)_5$ were prepared by arc melting followed by vacuum annealing as described in section 2.5. Neutron powder diffraction diagrams were recorded for several compounds of the first series at the High Flux Reactor (HFR) at Petten, using the conventional $\lambda = 2.57 \text{ \AA}$ with 30' collimation. Data were collected at room temperature (designated as 300 K) and at 4.2 K, in the angular range $\sin \theta/\lambda < 0.4 \text{ \AA}^{-1}$. Impurity lines present could be identified as due to ThO_2 , but the presence of transition metal oxides is also suspected. No absorption correction was applied. In the subsequent analysis scattering lengths were taken as $b(\text{Th}) = 1.033$, $b(\text{Fe}) = 0.951$ and $b(\text{Ni}) = 1.03$, all in units of 10^{-12} cm . Magnetic form factors for Fe^{2+} and Ni^{2+} were taken from Freeman and Watson [26]. Structure refinements were carried out using Rietveld's profile programme [6].

The magnetic measurements were performed on powdered materials using the Faraday method. The saturation moments were determined from magnetic isotherms recorded at 4.2 K. For field strengths higher than 10 kOe the magnetization was found to be saturated for all compounds but one. The ultimate measuring field strength was 30 kOe. The Curie temperatures were derived from magnetization (σ) versus temperature data obtained with low field strength (1-3 kOe) by plotting σ^2 versus T.

It was checked by x-ray diffraction that the samples were of a single phase. In the series $\text{La}(\text{Fe}_{1-x}\text{Ni}_x)_5$ single phase CaCu_5 type compounds could only be obtained for concentrations $x \geq 0.70$.

4.2.2 Magnetic measurements

The results of the magnetic measurements are summarized in fig. 15. Since the CaCu_5 structure for $\text{La}(\text{Fe}_{1-x}\text{Ni}_x)_5$ breaks down for Ni concentrations smaller than $x = 0.7$ only a limited number of experimental values is available for this series. For $\text{LaFe}_{0.5}\text{Ni}_{4.5}$ the magnetization at 4.2 K was found not yet to be saturated in a field of 30 kOe so that it is not possible to determine the saturation moment. In so far as a comparison of the magnetic properties of the compounds $\text{Th}(\text{Fe}_{1-x}\text{Ni}_x)_5$ with

those of $\text{La}(\text{Fe}_{1-x}\text{Ni}_x)_5$ is possible one can say that the saturation moments as well as the Curie temperatures are slightly higher for the latter series. Data for the magnetic properties of the series $\text{Th}(\text{Fe}_{1-x}\text{Ni}_x)_5$ were reported already before [19]. Unfortunately a small error in the molecular weight was involved in calculating the saturation moments from the corresponding isotherms at 4.2 K. The present values are therefore slightly lower for the Ni-rich compounds than those given previously.

4.2.3 Crystal structure

For all samples investigated the CaCu_5 structure is evident. The space group is $P6/mmm$, Th being located at 1(a) 000, Fe and Ni at 2(c) $1/3\ 2/3\ 0$ and 3(g) $1/2\ 0\ 1/2$.

As the scattering lengths of the constituent atoms are very nearly equal it is not possible to obtain information on the site occupations of Fe and Ni. However, this also implies that differences between observed and calculated intensities cannot be interpreted in terms of deviations from a random distribution. Special attention was therefore given to the room temperature diagrams of ThFeNi_4 ($x = 0.8$), which is paramagnetic at that temperature, and ThFe_2Ni_3 ($x = 0.6$) with $T_c = 290$ K, so that magnetic long range order scattering is negligible compared to the nuclear intensity. For ThFeNi_4 the ideal $P6/mmm$ structure can be refined to an R factor, based on integrated intensities, of 7%. The agreement between observed and calculated intensities of reflections with $l \neq 0$ is not quite satisfactory, since the deviations, though small, are systematic for all the compounds in the series $\text{Th}(\text{Fe},\text{Ni})_5$ and tend to increase with l . From the signs of the differences it is immediately clear that preferred orientation in the sample cannot be the cause, and therefore one may consider deviations from $P6/mmm$ symmetry.

It is possible to reduce R to 3.5% by refining in $P\bar{3}m1$ while correcting for preferred orientation. In this space group the 2(c) position has coordinates $\pm (1/3, 2/3, z)$ with a resulting $z(1) = 0.029$ in units of c . The solution found is stable against omission of the (102) reflection, which is rather badly reproduced by the ideal structure.

The same analysis applies to ThFe_2Ni_3 , where a final R of 5% is reached in $P\bar{3}m1$. Not all discrepancies are removed; however, deformations to $P3m1$, $P321$, $P6mm$, or to the space groups encountered in

RCO_5 hydrides [27], viz. $Cmmm$, $Imm2$ or $Ccca$ did not lead to significant improvement. All refinements were therefore carried out in $P\bar{3}m1$, comparing with results in $P6/mmm$ in all cases.

4.2.4 Magnetic order

When compared with the nuclear scattering cross-sections the magnetic scattering by moments of the order of $1 \mu_B$ must be small. Therefore the analysis of the magnetic structures is greatly hampered by the small but clearly visible misfit of the nuclear scattering.

The compounds investigated show ferromagnetic ordering, although each of their neutron diffraction diagrams shows details in the magnetic scattering that cannot be accounted for in a ferromagnetic model. The first feature encountered is a doubling of the crystallographic c -axis, as in ThFe_5 [24], for $x = 0.1$ and 0.2 (see fig. 16a). The component responsible for magnetic scattering in $(00\frac{1}{2})$ and other reflections with odd half integer l (which must be in the a - b plane) will be designated as antiferromagnetic. The second feature is the observation of a relatively strong intensity of the reflection (001) for compounds of the intermediate composition range. Normally when only nuclear scattering is important the intensity of the (001) reflection is weak. Since the

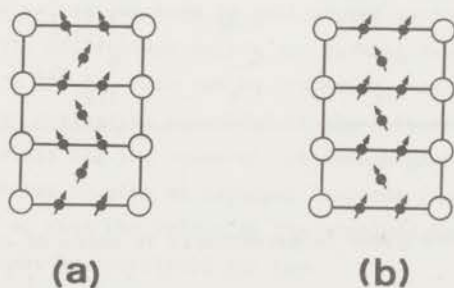


Fig. 16. Schematic representation of the magnetic structures occurring in the $\text{Th}(\text{Fe}_{1-x}\text{Ni}_x)_5$ system: (a) structure observed for compounds with $x \leq 0.2$; (b) structure observed for the compounds with $x = 0.4$ and 0.6 .

Table 3. Results for $\text{Th}(\text{Fe}_{1-x}\text{Ni}_x)_5$ at 300 K

| x | 0.1 | 0.2 | 0.4 | 0.6 | 0.8 |
|--|-----------|-----------|-----------|-----------|-----------|
| a(Å) | 5.0902(5) | 5.0662(4) | 5.0402(5) | 5.0052(3) | 4.9789(3) |
| c(Å) | 4.0682(3) | 4.0751(3) | 4.0681(3) | 4.0582(2) | 4.0336(2) |
| μ_{total} | 1.3(1) | 1.1(1) | 1.4(1) | - | - |
| $\mu_{\text{ferrom.}}^{\text{c}}$ | 1.3(1) | 1.1(1) | 1.3(1) | - | - |
| $\mu_{\text{antiferrom.}}^{\text{ab}}$ | - | - | - | - | - |
| $\mu_{\text{ferrim.}}^{\text{ab}}$ | - | 0.4(1) | 0.5(1) | - | - |
| z(l) (fract) | | 0.033(2) | 0.021(2) | 0.024(2) | 0.029(2) |
| R (%) | 8 | 4 | 6 | 5 | 4 |

Table 4. Results for $\text{Th}(\text{Fe}_{1-x}\text{Ni}_x)_5$ at 4.2 K

| x | 0.1 | 0.2 | 0.4 | 0.6 | 0.8 |
|---|-----------|-----------|-----------|-----------|-----------|
| a(Å) | 5.0821(5) | 5.0564(5) | 5.0303(3) | 4.9972(3) | 4.9680(3) |
| c(Å) | 4.0622(3) | 4.0711(4) | 4.0677(3) | 4.0560(2) | 4.0262(2) |
| $\mu_{\text{total}} (\mu_{\text{b}}/\text{at})$ | 1.7(1) | 1.6(1) | 1.7(1) | 1.4(1) | 1.1(1) |
| $\mu_{\text{ferrom.}}^{\text{c}}$ | 1.5(1) | 1.4(1) | 1.5(1) | 1.3(1) | 1.1(1) |
| $\mu_{\text{antiferrom.}}^{\text{ab}}$ | 0.8(1) | 0.5(1) | - | - | - |
| $\mu_{\text{ferrim.}}^{\text{ab}}$ | - | 0.5(1) | 0.8(1) | 0.7(1) | - |
| R (%) | 7 | 6 | 6 | 6 | 5 |
| $\mu_{\text{bulk}} (\mu_{\text{B}})$ | - | 1.6 | 1.4 | 1.2 | 0.7 |

Standard deviations are given in parentheses in units of the last decimal.

atoms in the $z = 0$ and $z = \frac{1}{2}$ plane scatter in antiphase it is evident that an (unphysically) large ferromagnetic moment would be required to account for the observed intensity. Only one fifth of that moment's magnitude would be sufficient in a ferrimagnetic structure (see fig. 16b) where the (c) and (g) positions (with occupation ratio 2:3, respectively) carry antiparallel moments.

Finally there is the main ferromagnetic component to be determined. It is found that this is not readily done on the basis of diffraction results alone, since moments constrained either to be parallel to the c-axis or to be in the a-b plane lead to refinements of equal quality. However, the magnitude of the calculated moment differs for the two models, which allows a choice to be made by comparison with the results of the magnetization measurements. Since the moments calculated for planar anisotropy are always far too high compared with the bulk magnetization results, while the moments calculated for axial anisotropy are only slightly higher, we conclude that the ferromagnetic component in the magnetic structure is parallel to the c-axis.

The results of the refinements are collected in tables 3 and 4 together with bulk magnetization values.

4.3 Discussion

When one compares the magnetic moments derived from the present experiment with the values obtained by bulk magnetization measurements it is seen that the diffraction values are several tenths of a Bohr magneton higher for $x \geq 0.4$. This can be traced to a slight misfit in the calculated nuclear scattering intensity of the reflection (100), which is mainly responsible for the value of the ferromagnetic component. This can be estimated to give an apparent increase in magnetic moment by $0.2 - 0.3 \mu_B$, so that the values of the standard deviations of the magnetic moment must be considered too low.

In the discussion of the concentration dependence of the magnetic moments (see below) we will use therefore only the moments derived from the magnetization measurements.

We mentioned already that the antiferromagnetic component in the compounds with $x = 0.1$ and 0.2 is similar to that observed in ThFe_5 [24]. The striking conclusion of the present investigation is the existence

of a canted orientation of the $z = 0$ and $z = \frac{1}{2}$ sublattice magnetization for compounds with $0.2 \leq x \leq 0.6$. It hinges on the interpretation of the reflection (001) as being primarily magnetic. This is a necessary consequence of the CaCu_5 structure type having layers of atoms stacked at a distance of $\frac{1}{2}c$. In order to be able to derive a calculated nuclear intensity of the same magnitude as observed it is necessary to move the 3(g) site off the $z = \frac{1}{2}$ plane. This is most readily done in space group $P6mm$, and with less ease in $Im2m$ and $Ccca$, but the results of the calculations of the corresponding nuclear intensities are at the most comparable in R factor, if not worse. We therefore see no reason to lower the symmetry further than $P\bar{3}m1$. It is even to be doubted whether there are real deviations from the ideal structure, since there remain systematic differences between observed and calculated intensities possibly due to oxides, and the improvement is not significant for low x values.

Finally we wish to comment on the concentration dependence of the magnetic properties of the compounds $\text{Th}(\text{Fe}_{1-x}\text{Ni}_x)_5$ and $\text{La}(\text{Fe}_{1-x}\text{Ni}_x)_5$. The compounds ThNi_5 and LaNi_5 are Pauli paramagnets with a more or less temperature independent susceptibility equal to 1.9×10^{-3} and 5.0×10^{-3} emu/mole, respectively. These relatively high values indicate that in these compounds one has a high density of states which probably is the result of a still unsaturated 3d band in which exchange splitting into subbands of different spin directions is absent. The magnetic moments observed by magnetization measurements for the compounds ThFeNi_4 and LaFeNi_4 are $3.3 \mu_B$ and $3.7 \mu_B$ per formula unit, respectively. These values are too high to be exclusively ascribed to the Fe moments. It is more likely that there is also a small moment on the Ni atoms due to the exchange splitting of the Ni 3d electrons caused by the polarizing influence of the neighbouring Fe atoms.

It is seen in fig. 15 that the moments in the La compounds are only slightly higher than those of the Th series. This is surprising since the higher valence electron concentration of Th usually leads to a marked decrease in transition metal moment: The saturation moment of e.g. LaCo_5 equals $1.5 \mu_B/\text{Co}$ compared to $0.9 \mu_B/\text{Co}$ in the case of ThCo_5 . An even more striking example are the compounds La_2Co_7 and Th_2Co_7 [7, 17]. In the former one has a saturation moment of about $1 \mu_B/\text{Co}$ whereas the latter compound is paramagnetic. The low sensitivity of the saturation magnetization in LaFeNi_4 towards a higher itinerant electron

concentration (ThFeNi₄) seems to indicate that these compounds can be regarded as so-called weak ferromagnets where one has an unsaturation of the spin up as well as of the spin down 3d subbands and where a more complete filling of the 3d band does not lead to a large change in saturation moment. It is also interesting to compare the saturation moment of ThFeNi₄ (3.3 μ_B/F.U) with that of ThCo₂Ni₃, as these compounds have the same number of 3d electrons. ThCo₂Ni₃ has a saturation moment (if any) of about 0.3 μ_B/F.U. It seems therefore as if the 3d electrons of Ni and Fe do not share a common 3d band so that the magnetic properties of the compounds Th(Fe_{1-x}Ni_x)₅ can probably better be described in terms of a localized model. If we assume that for all concentrations the Fe atoms have a moment of 1.88 μ_B and that all Ni atoms which have at least one Fe atom as neighbour carry a moment of 0.4 μ_B it is possible to represent the concentration dependence of the magnetic moment by

$$M = \{1.88(1-x) + 0.4x (1-P)\}\mu_B \quad (1)$$

The quantity P in this expression represents the probability of a Ni atom with exclusively Ni atom nearest neighbours. We have calculated P by means of

$$P(n, N, x) = \frac{N!}{n!(N-n)!} x^n (1-x)^{N-n} \quad (2)$$

where N is the maximum number of nearest Ni neighbours possible and n the actual number of Ni nearest neighbours. (For the present purpose n=N and P(N, N, x) ≡ x^N). The 3(g) and 2(g) site have N equal to 8 and 9, respectively. Since the 3(g) site occurs with the largest fraction we have used N=8 in eq. (2). The results of the calculations are shown by the full line in fig.15 which gives M as derived by eq. (1). The agreement with experiment is obvious. In keeping with a localized description is also the more or less linear decrease of the Curie temperature with x.

V. MAGNETIC ORDER AND MAGNETIC HISTORY EFFECTS IN $\text{Th}(\text{Co}_x\text{Ni}_{1-x})_5$ ⁺

5.1 Introduction

In the present chapter the results are described of a diffraction investigation of the pseudo-binary system $\text{Th}(\text{Co},\text{Ni})_5$. This investigation was prompted by the observation of antiferromagnetism in $\text{Th}(\text{Fe},\text{Co})_5$: as reported in ref. 24 cell doubling occurs in $\text{Th}(\text{Fe}_x\text{Co}_{1-x})_5$ for $x \geq 0.8$, in addition to a ferromagnetic component for which the magnetic and crystallographic unit cells are identical. Since the origin of the antiferromagnetic component is at present unknown we decided to investigate the pseudo-binary systems $\text{Th}(\text{Fe},\text{Ni})_5$ and $\text{Th}(\text{Co},\text{Ni})_5$ as well. The results for $\text{Th}(\text{Fe},\text{Ni})_5$ are given in chapter IV [28]. Further interest in the magnetic properties of the $\text{Th}(\text{Co},\text{Ni})_5$ compounds stems from the recent observation of pronounced thermomagnetic history effects in several members of this series [29]. Several possible explanations were proposed, and the present study was also undertaken in order to decide between these explanations.

For ThCo_2Ni_3 and ThCo_3Ni_2 neutron diffraction results were reported by Atoji et al. [18]. However, they were not able to observe magnetic scattering directly and inferred the direction of the magnetic moment from diffraction on powders, the grains of which were oriented by a strong magnetic field. Here a direct observation of the magnetic structures for the concentration range $0.5 \leq x \leq 1$ is reported.

In ref. 25, from which this chapter is derived, compressibilities and Curie temperatures as a function of pressure are reported for the same concentration range, and magnetization curves are given for the full range of concentrations. These measurements, which are not a part of this work, will be summarized in section 5.3.

⁺) Adapted from: K.H.J. Buschow, M. Brouha and J.B.A.A. Elemans, to appear in phys. stat. sol. (a), 30 1975.

5.2 Experimental procedure

The samples of $\text{Th}(\text{Co}_x\text{Ni}_{1-x})_5$ were prepared by arc melting, using Co, Ni and Th of 99.9% purity. Vacuum annealing of the samples was performed at 1100°C for about 3 days, after which the samples were quenched. X-ray diffraction showed that after this procedure no other metallic phases than of CaCu_5 type were present in the samples.

Neutron diffraction data were collected at the High Flux Reactor (HFR) at Petten. Elastic neutron scattering diagrams were obtained at room temperature and at 4.2 K in the angular region $\sin\theta/\lambda < 0.4 \text{ \AA}^{-1}$ using $\lambda = 2.57 \text{ \AA}$. In the analysis of the scattered intensities the scattering lengths of Th, Co and Ni were taken as 1.033, 0.250 and 1.03×10^{-12} cm respectively. Form factors for Co^{2+} and Ni^{2+} were taken from Freeman and Watson [26]. For the least squares refinement Rietveld's profile programme [6] was used.

5.3 Results of magnetic measurements ⁺⁾

$\text{Th}(\text{Co}_x\text{Ni}_{1-x})_5$ compounds exhibit peculiar magnetization curves. When a sample has been subjected to a high external magnetic field, a ferromagnetic behaviour is found for the magnetization, σ , as function of the applied field, H , at constant temperature. In virgin samples on the other hand the magnetization increases very slowly at first, until at an applied field H_f the magnetization jumps to the ferromagnetic value. This process is irreversible: the compound remains in a magnetized state when the field is decreased.

When measurements are made in a constant external field as a function of rising temperature, the transition from an unmagnetized to a magnetized state occurs in a virgin sample at a temperature T_f . This transition is steeper (T_f better defined) as the applied field is higher, and an empirical relation $H_f \times T_f \approx \text{constant}$ appears to hold. Similar behaviour is found for samples cooled in a magnetic field, cf. fig. 17. This behaviour is now thought to be caused by a very high anisotropy as compared to the strength of exchange, leading to narrow domain walls [30]. In that case magnetic moments can only be parallel or antiparallel to the direction of easy magnetization. If a domain is initially magnetized antiparallel to the applied field it

⁺⁾ Described in full in ref. 25.

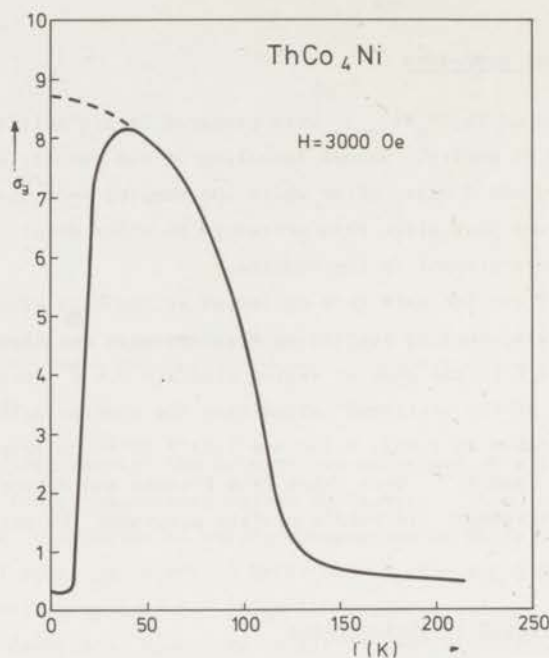


Fig. 17. Temperature dependence of the magnetization of ThCo_4Ni obtained at $H = 3 \text{ kOe}$ without field cooling and premagnetization (full curve). The broken curve was recorded after field cooling ($\sim 5 \text{ kOe}$).

will remain so if the field is low. When the applied field is strong enough to overcome the total molecular field [30] the magnetization direction of the domain reverses, and will remain reversed upon reduction of the field. This reversal of domains must be activated by temperature, as is apparent from the interdependence of H_f and T_f . This describes only one aspect of the behaviour of these compounds. A second feature, more relevant to the subject matter of this thesis, is related to the magnetic order.

As illustrated in fig. 18, the magnetization curves in the ferromagnetic state are indeed those of an ordinary ferromagnet for samples with $x \geq 0.8$. It is then fairly easy to determine T_c by an extrapolation of σ^2 as a function of T . This is not true for compounds with $x < 0.8$. Here the magnetization curves show very long tails, to such an extent that the Brillouin function is not clearly recognized. In this case the $\sigma^2(T)$ extrapolation may not be expected to yield accurate values for T_c .

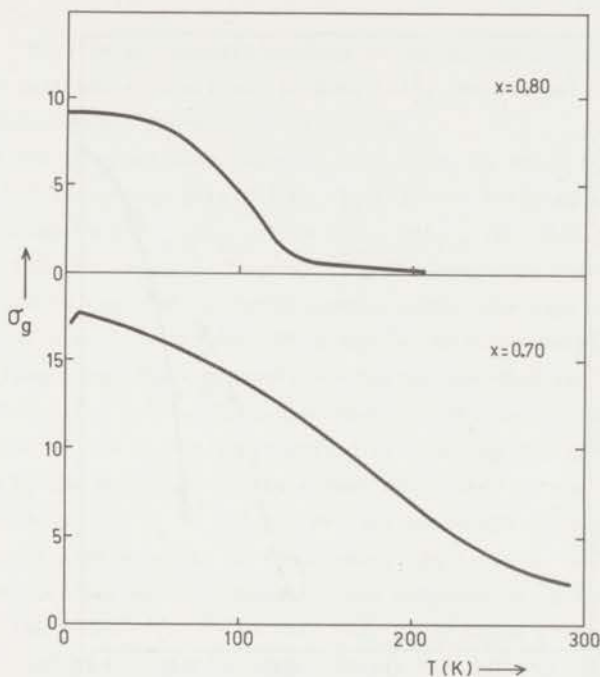


Fig. 18. Temperature dependence of the magnetization of several $\text{Th}(\text{Co}_x \text{Ni}_{1-x})_5$ compounds obtained with a field strength of 3 kOe.

An independent estimate of T_c was obtained from measurements of the initial permeability, as reported in ref. 25. The Curie temperatures resulting from both procedures are shown in fig. 19. It is seen that the value of T_c is a very sensitive function of composition near $x = 0.8$. Therefore, the purpose of the diffraction experiment was to investigate the nature of the magnetic order in virgin samples of $\text{Th}(\text{Co},\text{Ni})_5$.

5.4 Analysis of neutron diffraction data

From the general appearance of the diagrams the CaCu_5 structure is evident. This structure type has $P6/mmm$ symmetry, with the following atomic positions: Th in 1(a), 000, (Co, Ni)₁ in 2(c), $\pm(\frac{1}{3}, \frac{2}{3}, 0)$ and (Co, Ni)₂ in 3(g), $\frac{1}{2}0\frac{1}{2}$, $0\frac{1}{2}\frac{1}{2}$ and $\frac{1}{2}\frac{1}{2}\frac{1}{2}$. We did not question the validity of the assignment as we did in ref. 24 and 28, but refined site occupancies for Co and Ni

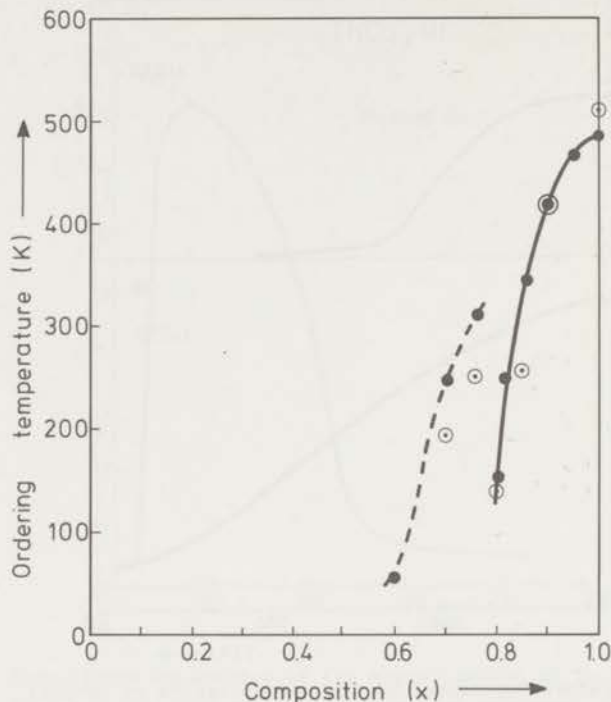


Fig. 19. Composition dependence of the Curie temperature of $\text{Th}(\text{Co}_x\text{Ni}_{1-x})_5$ compounds. Closed and open circles represent values obtained by σ^2 (T) extrapolation and permeability measurement, respectively.

while constraining the total composition.

The magnetic intensities are small compared to the nuclear scattering. This is to be expected: the magnitude of the Co moment in ThCo_5 is $1.1 \mu_B$; dilution with Ni still decreases the overall magnetization since Ni does not contribute significantly to the magnetic moment. Considerable care was therefore required when interpreting the experimental results. In fact only the (100) reflection shows clear magnetic effects that allow the construction of structure models. However, once a model is assumed the overall fit of the calculated profile enables one to check its validity.

It proved not possible to differentiate between models in which only Co atoms carry a magnetic moment, and models in which both Co and Ni are

magnetic. This is in complete analogy to the system $\text{Th}(\text{Fe},\text{Co})_5$, where a similar distinction could not be made [24]. We assumed therefore equal moments on all transition metal atoms.

From our previous investigation [24] ThCo_5 is known to be a ferromagnet with its moment parallel to the c-axis. Ferromagnetic order was also found in $\text{ThCo}_{4.5}\text{Ni}_{0.5}$. In $\text{ThCo}_{3.5}\text{Ni}_{1.5}$ ($x = 0.7$) and in one sample of ThCo_4Ni ($x = 0.8$) however, the ferromagnetic order has disappeared and is replaced by ferrimagnetic order, the 2(c) and 3(g) sites carrying antiparallel moments. This applies to 4.2 K only; at room temperature no long range order magnetic scattering was observed in these samples.

In $\text{ThCo}_{2.5}\text{Ni}_{2.5}$ ($x = 0.5$) the intensity of magnetic scattering is of the order of the accuracy determined by counting statistics. This is reflected by the magnitude of the moment calculated in the ferrimagnetic model: $\mu = 0.3 \pm 0.3 \mu_B$ at 4.2 K. For all compounds investigated the moment is oriented parallel to the c-axis. In table 5 the results of the refinements are presented. These include information on the site occupancies n_i by quoting n for Co_i . It is seen that Co is found preferentially on the 3(g) site, and Ni on the 2(c) site. Values for ThCo_5 are taken from ref. 24; the R-factors quoted are calculated on the basis of integrated intensities.

When comparing the cell constants found by X-ray diffraction, reproduced in fig. 20, with those calculated from neutron diffraction diagrams one must bear in mind that the wavelength of the neutron is known less accurately than that of X-rays. However, since the quantity measured is $\sin\theta = \lambda/2d$ the c/a ratio can be determined accurately from the neutron diffraction data. These c/a values, shown in fig. 21, will be discussed below.

5.5. Discussion

The present study shows that in zero field not all $\text{Th}(\text{Co},\text{Ni})_5$ compounds are ferromagnets: ferrimagnetism, in which the 2(c) and 3(g) sites carry antiparallel moments sets in at or just below $x = 0.8$. It follows from the magnetic measurements that the application of a strong magnetic field disrupts the ferrimagnetic coupling, imposing ferromagnetic order. It is this feature, together with the strong anisotropy that enabled Atoji et al. [18] to find the direction of the magnetic moment.

It is a striking observation that the Curie-temperature, the lattice constants and the compressibility show a pronounced discontinuity at one and

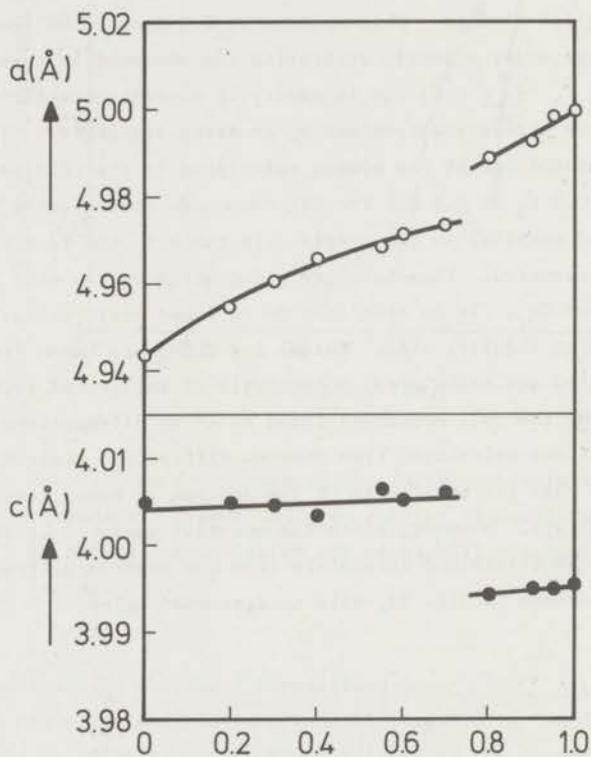
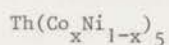


Fig. 20. Composition dependence of the lattice constants of a number of $\text{ThCo}_{5x}\text{Ni}_{5-5x}$ compounds as determined by X-ray diffraction at room temperature.

Table 5. Results of neutron diffraction investigation of compounds



| x | T(K) | a (Å) | c (Å) | c/a | n (Co ₁) | μ (μ _B) | R (%) |
|------|------|-----------|-----------|----------|----------------------|---------------------|-------|
| 1.0 | 300 | 4.9990(4) | 4.0015(3) | .8005(1) | 2.00(-) | 1.16(3) | 5 |
| | 4.2 | 4.9850(6) | 3.9899(6) | .8004(1) | 2.00(-) | 1.10(4) | 10 |
| 0.9 | 300 | 4.9943(4) | 3.9983(3) | .8806(1) | 1.734(6) | 0.52(4) | 3 |
| | 4.2 | 4.9788(5) | 3.9894(8) | .8013(1) | 1.713(8) | 0.74(5) | 9 |
| 0.8* | 300 | 4.9973(5) | 4.0008(5) | .8006(1) | 1.380(12) | - | 4 |
| | 4.2 | 4.9644(5) | 3.9994(5) | .8056(1) | 1.390(8) | ±1.07(9) | 7 |
| 0.7 | 300 | 4.9844(4) | 4.0037(3) | .8032(1) | 1.161(7) | - | 5 |
| | 4.2 | 4.9696(5) | 3.9949(4) | .8039(2) | 1.147(7) | ±0.79(13) | 5 |
| 0.5 | 300 | 4.9686(4) | 4.0094(3) | .8069(1) | 0.699(8) | - | 5 |
| | 4.2 | 4.9571(5) | 4.0004(4) | .8070(1) | 0.670(10) | - | 7 |

*) Diagrams at 300 and 4.2 K pertain to different samples; the ferrimagnetic sample examined at 4.2 K was prepared on a different occasion.

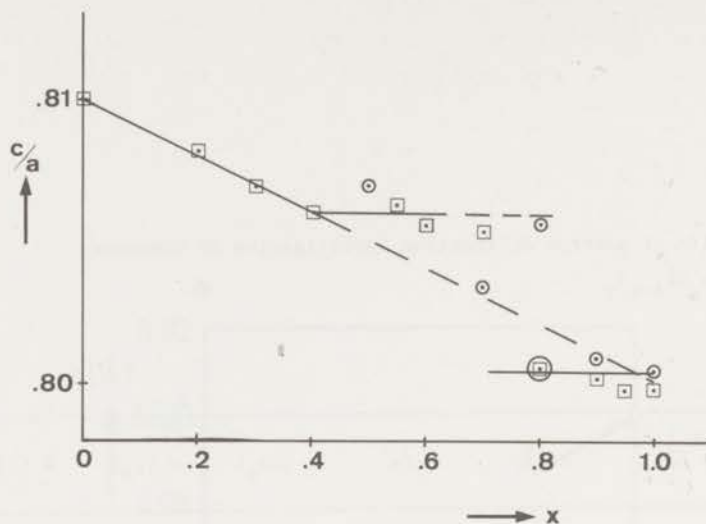


Fig. 21. Values of c/a for $\text{Th}(\text{Co}_x \text{Ni}_{1-x})_5$.

squares: results of X-ray diffraction at room temperature, taken from ref. 25.

circles: results of neutron diffraction, average of room temperature and 4.2 K, except for ThCo_4Ni where two values are given.

the same concentration [25]. It is not very probable that a direct explanation is found in the differences in site occupancies for the g and c sites, since the site occupancies vary smoothly near $x = 0.8$ and Co and Ni are found on both sites. Also, magnetostriction cannot be the cause of these discontinuities, since there is no marked change in the lattice constants upon going through T_c . A possible common origin to these phenomena may be found in electronic effects.

In ref. 31 it is explained how crystal structure deformations (at constant volume) may occur in simple metals. A band-structure dependent term is introduced in the cohesive energy which contains among other functions the pseudo-potential $v(q)$ of the atoms and a response function $\chi(q)$ of the conduction electrons.

First, if the magnitude of a reciprocal lattice vector g_1 is close to the value q_0 for which the pseudo-potential is zero, energy can be gained by an increase in the band gap at g_1 , thereby increasing the density of

states just below g_1 and lowering the total energy ($[31]$, p. 269 ff, in particular p. 272). This is effectuated by a deformation of the unit cell at constant volume such that $|q_0 - g_1|$ increases.

Second, the rapid variation of the response function $\chi(q)$ near $q = 2 k_F$ is thought to be responsible for the observed c/a values in hexagonal divalent metals $[31]$ and for the changes in c/a in CuAl_2 alloys $[32]$. If a reciprocal vector g_2 is close to $2 k_F$ energy can be gained by a change in c/a such that g_2 is drawn into the Fermi sphere.

Also, if the Fermi surface contains two parallel regions at a distance \vec{q}_1 energy can be gained. Now $\chi(q)$ has a deep minimum at $q_1 = 2k_F$, and it is energetically favourable for a reciprocal lattice vector to span the Fermi surface: $g = 2 k_F$. A famous example is found in anti-ferromagnetic Cr.

VI. INVESTIGATIONS OF R_2M_{17} COMPOUNDS

6.1 On the interpretation of Mössbauer-effect and diffraction measurements on rare earth iron compounds of the type R_2Fe_{17} +)

6.1.1 Introduction

When rare earth elements, yttrium or thorium, here designated by R, are combined with the proper amount of a 3d transition metal M, an intermetallic compound of composition R_2M_{17} is formed that can crystallize in three different crystal structures. These are closely related and derived from the well-known $CaCu_5$ structure by substitution of one pair of M for every third R in the RM_5 crystal.



The three structures encountered differ in the way of selecting "every third R". First of all, the substitutions may be completely at random. On the average the RM_5 space group $P6/mmm$ is conserved, each R site now having a probability of 1/3 of being occupied by an M pair.

In addition there are two systematic substitution schemes that may be considered analogous to hexagonal or cubic close packing in a monatomic crystal. The analogue of ccp consists of a rhombohedral substitution scheme leading to a tripling of the RM_5 c-axis and the space group $R\bar{3}m$ [33]. In the analogue of hcp the substitution in the third layer does not choose the rhombohedral site but duplicates the first layer. The c-axis is doubled with respect to RM_5 and the space group is $P6_3/mmc$ [34].

+)

J.B.A.A. Elemans, Kamerlingh Onnes Laboratory, Leiden, the Netherlands
P.C.M. Gubbens, Interuniversitair Reactor Instituut, Delft, the Netherlands
K.H.J. Buschow, Philips Research Laboratories, Eindhoven, the Netherlands.

to appear in: J. Less-Common Metals.

The free energies of the three forms are probably nearly equal. For instance, Gd_2Fe_{17} is reported to crystallize in either of the three, depending on the heat treatment [35]; the heavy rare earth compounds tend to hexagonal ordering whereas the light rare earth usually prefer rhombohedral structure, but many may crystallize in mixtures of rhombohedral and hexagonal phases.

It has been suggested that additional, disordered substitutions may occur in the hexagonal structure type, leading to off-stoichiometric compositions. Evidence for this is found in various diffraction experiments [35 - 39] and further support may be derived from Mössbauer experiments (see below). However, it will be shown in section 6.1.3 that the composition (in thermal equilibrium) of the hexagonal R_2M_{17} compounds is not richer in M than allowed by the stoichiometry.

6.1.2 Evidence for off-stoichiometry

In order to understand the single crystal diffraction result we shall consider the crystal structure in more detail. In fig. 22, derived from a similar figure in ref. 36, the R atoms (black dots) and substituted M pairs (white dots), are shown in the RM_5 a-c plane. In (a) the RM_5 frame is shown, in (b) the random substitution scheme; (c) presents the rhombohedral order in which the A, B and C chains are equivalent, (d) the ideal hexagonal scheme in which A is equivalent to B, but C carries no substitutions; in (e) the observed atomic distribution with additional random substitutions on the C chain, and some unsubstituted R on the A and B chains [36].

The disorder observed has been interpreted in terms of disordered substitutions. It will be shown that this must lead to an excess in M content.

We consider, for the moment, only one layer of atoms, e.g. as in the lower middle layer of fig. 22d, and more specifically the two R atoms (designated R_1 and R_2 since they are crystallographically inequivalent) and one M pair per unit cell. The ordered configuration may then be described as an R atom (R_1) at the intersection of the layer with chain C, and one (R_2) at the intersection with A, the M pair being located at the intersection with B, as shown in fig. 23.

Not shown in this figure is a single M atom (not taking part in the

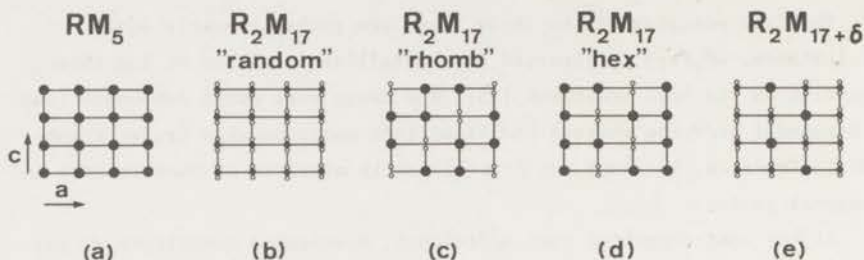


Fig. 22 Schematic representation of the $CaCu_5$ structure (a), the R_2M_{17} structure with a random distribution of M-pairs (b), the rhombohedral type (c), the ideal Th_2Ni_{17} -type (d), and the type proposed for Lu_2Fe_{17} in ref. [4], (4).

- R
- Fe-pairs
- ⊗ Statistical distribution between one R and one Fe-pair.

substitution scheme) which is located in the ideal RM_5 structure at the centre of gravity of the triangle ABC, but which is displaced towards the M pair in the hexagonal R_2M_{17} structure. This leads to a constraint on the substitutions: if a triangle would be occupied by 3 R atoms it would not accommodate the central M atom, and therefore this configuration is considered highly improbable.

From the observed mass distribution (fig. 22e) it is inferred that no disordered M pairs are found on the R_2 sites. Then, in addition to the normal configuration (RMR) for the triangle ABC, the disordered configurations (RRM) and (RMM) may be found. Of these, the configuration (RRM) would maintain the stoichiometry; however, as is illustrated in the middle part of fig. 23, when an interchange of R_1 and M occurs it is necessary to introduce configurations (RMM) as well, in order to avoid (RRR). Therefore, when disorder is introduced in this manner the composition of the crystal is necessarily richer in M than R_2M_{17} .

Many of the R_2Fe_{17} compounds were investigated by means of the ^{57}Fe Mössbauer effect [40]. In general the observed spectra could be resolved in sub-spectra, associated with the different Fe sites. It proved fairly easy to recognize the sub-spectra due to the Fe-pair, since these two atoms are extremely close together and give rise to the highest hyperfine

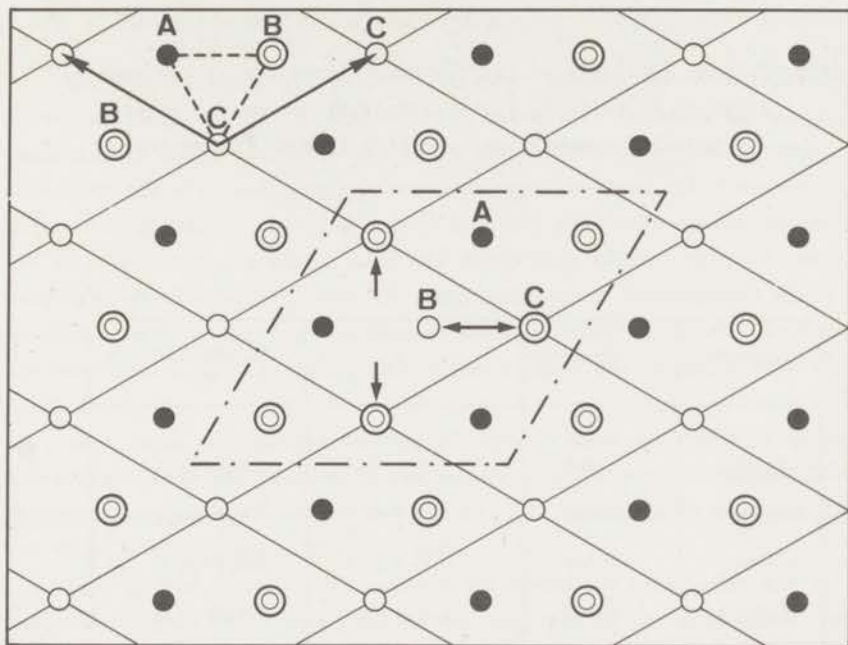


Fig. 23. Layer of R_2M_{17} structure illustrating the effect of disorder. Symbols used: \odot M pair; \circ R_1 ; \bullet R_2 . Upon interchange of an M pair and an R_1 (marked \leftrightarrow) one way of avoiding unfavourable configurations is by introducing additional M pairs at the sites marked \rightarrow .

field. The outermost lines of the sub-spectrum of the pair are also the outermost lines of the complete spectrum.

The ratio of the intensity of the pair sub-spectrum to that of the remaining spectra should be equal to 2 : 15; experimentally, however, significant deviations of this ratio are observed for hexagonal compounds, as listed in table 6. Such deviations indicate either an off-stoichiometry or a Debye-Waller factor different from the other ion sites.

Table 6. Partial intensity of the Mössbauer lines due to the substituted Fe pairs I_M (total intensity normalized to 17) and possible composition resulting from this intensity.

| Compound | Symmetry | I_M | "Composition" |
|---------------|----------|---------------|-----------------|
| Ce_2Fe_{17} | rhomb. | 1.9 ± 0.2 | $Ce_2Fe_{16.4}$ |
| Pr_2Fe_{17} | rhomb. | 2.1 ± 0.1 | $Pr_2Fe_{17.6}$ |
| Nd_2Fe_{17} | rhomb. | 2.0 ± 0.1 | Nd_2Fe_{17} |
| Gd_2Fe_{17} | rhomb. | 2.1 ± 0.1 | $Gd_2Fe_{17.6}$ |
| Gd_2Fe_{17} | hex. | 2.3 ± 0.1 | $Gd_2Fe_{18.8}$ |
| Tb_2Fe_{17} | hex. | 2.4 ± 0.1 | $Tb_2Fe_{19.4}$ |
| Dy_2Fe_{17} | hex. | 2.4 ± 0.1 | $Dy_2Fe_{19.4}$ |
| Ho_2Fe_{17} | hex. | 2.3 ± 0.1 | $Ho_2Fe_{18.8}$ |
| Er_2Fe_{17} | hex. | 2.3 ± 0.1 | $Er_2Fe_{18.8}$ |
| Tm_2Fe_{17} | hex. | 2.6 ± 0.1 | $Tm_2Fe_{20.6}$ |
| Y_2Fe_{17} | hex. | 2.3 ± 0.1 | $Y_2Fe_{19.4}$ |

6.1.3 Evidence for stoichiometric composition: metallographic examination.

The samples subjected to metallographic examination were prepared by arc melting from 99.9% pure starting materials, followed by vacuum annealing in Al_2O_3 crucibles sealed in evacuated quartz tubes. Long annealing times at moderate temperatures were required for compounds with a low peritectic melting point; e.g. for the Ce-Fe system annealing was at 900°C for six weeks. For the heavy rare earth compounds, which have high melting points, shorter times and higher temperatures could be used. After annealing the samples were quenched in water. Surfaces for examination were polished with diamond paste and etched with a 1-2% nital solution.

As a check on composition several samples were subjected to quantitative chemical analysis, with the result that changes in composition during preparation were less than 0.2 at. %. Results will be discussed for CeFe_x , TmFe_x , HoFe_x , YNi_x and ThNi_x .

In fig. 24a, b and c micrographs are shown for CeFe_x with $x = 8, 8.5, 9$. In fig. 24(a) dark regions are enclosed in the main phase. By means of X-ray diffraction they were identified as being due to the CeFe_2 phase. Samples with $x \approx 8.5$ were single phase, as shown in fig. 24(b). At higher Fe concentrations elemental Fe is present as a second phase (fig. 24(c)), indicating that the compound richest in Fe has a composition close to $\text{Ce}_2\text{Fe}_{17}$. The lamellar structure of the main phase is attributed to the coexistence of the hexagonal and rhombohedral modifications. In fig. 25a, b and c analogous results for HoFe_x are presented. All the HoFe_x samples shown in the figure were annealed and quenched from 1150°C . If the annealing was performed at much lower temperatures (800°C) essentially the same results were obtained. The small amounts of foreign phases present in the samples presented in fig. 25 a and c were identified by X-ray diffraction as $\text{Ho}_6\text{Fe}_{23}$ and elemental Fe, respectively. From the results shown in the figures it can be concluded that the compound richest in Fe in the Ho-Fe system has a composition close to $\text{Ho}_2\text{Fe}_{17}$. Similar results were also obtained for TmFe_x samples.

In fig. 26a the microstructure of an as-cast sample of the composition $\text{TmFe}_{9.5}$ is shown. As can be seen in fig. 26b, annealing of this sample does not lead to absorption of the elemental iron into the main phase but mainly results in a different distribution of the two phases in the sample. A microstructure without elemental Fe was obtained for a sample of the composition $\text{TmFe}_{8.5}$ (fig. 26c).

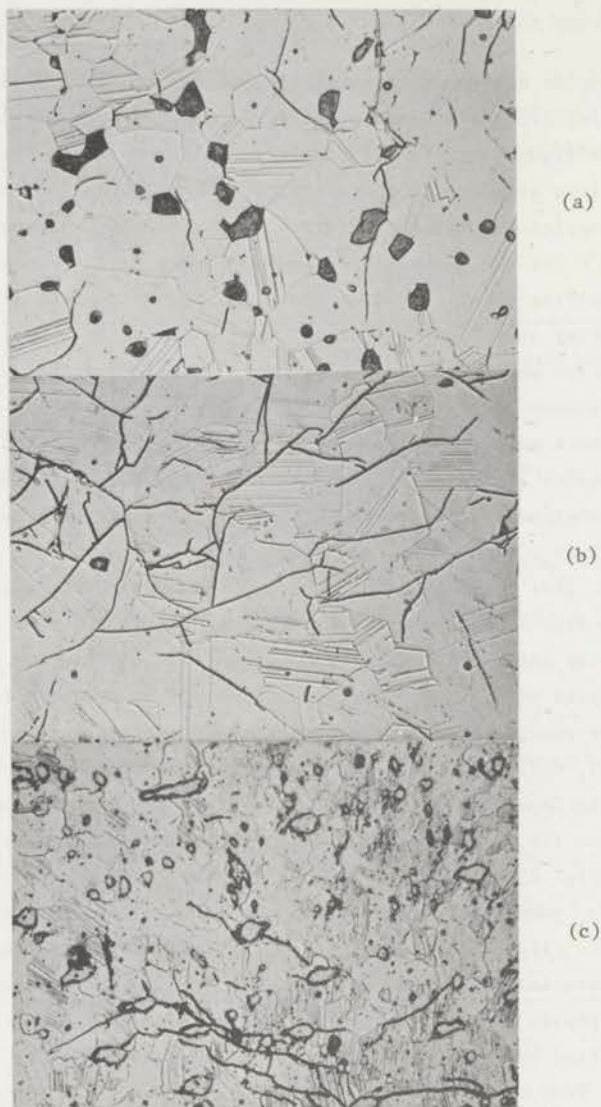


Fig. 24. Microstructure of various Ce-Fe samples after annealing for 6 weeks at 900 °C; a: $\text{Ce}_2\text{Fe}_{16}$; b: $\text{Ce}_2\text{Fe}_{17}$; c: $\text{Ce}_2\text{Fe}_{18}$. Magnification 320 x.

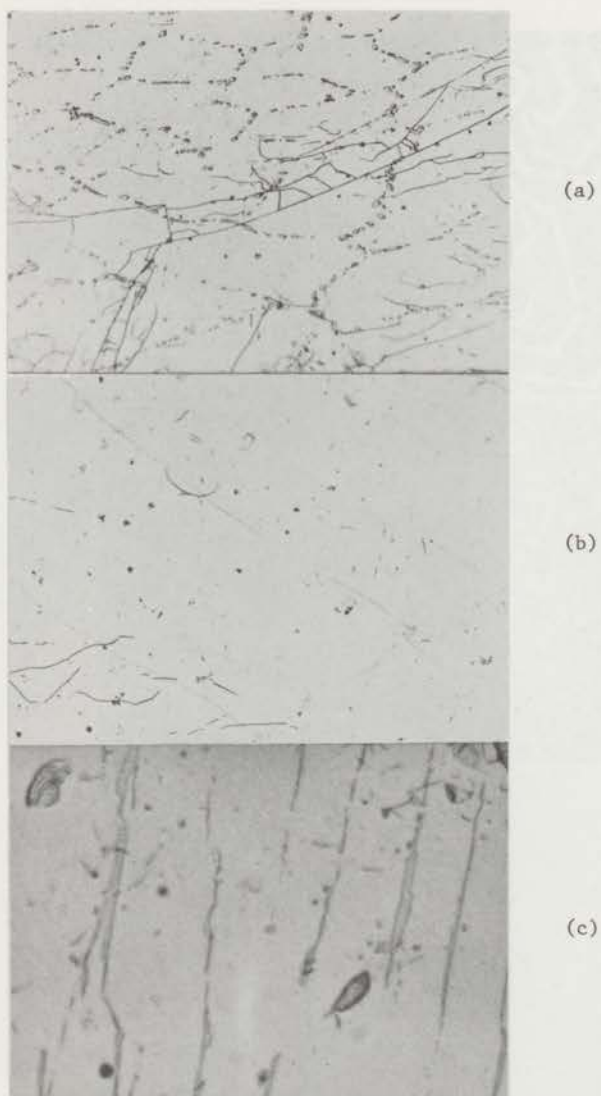


Fig. 25. Microstructure of various Ho-Fe samples after annealing at 1150 °C for 200 h and subsequent quenching in water; a: $\text{Ho}_2\text{Fe}_{19}$; b: $\text{Ho}_2\text{Fe}_{17}$; c: $\text{Ho}_2\text{Fe}_{16}$. Magnification 320 x.

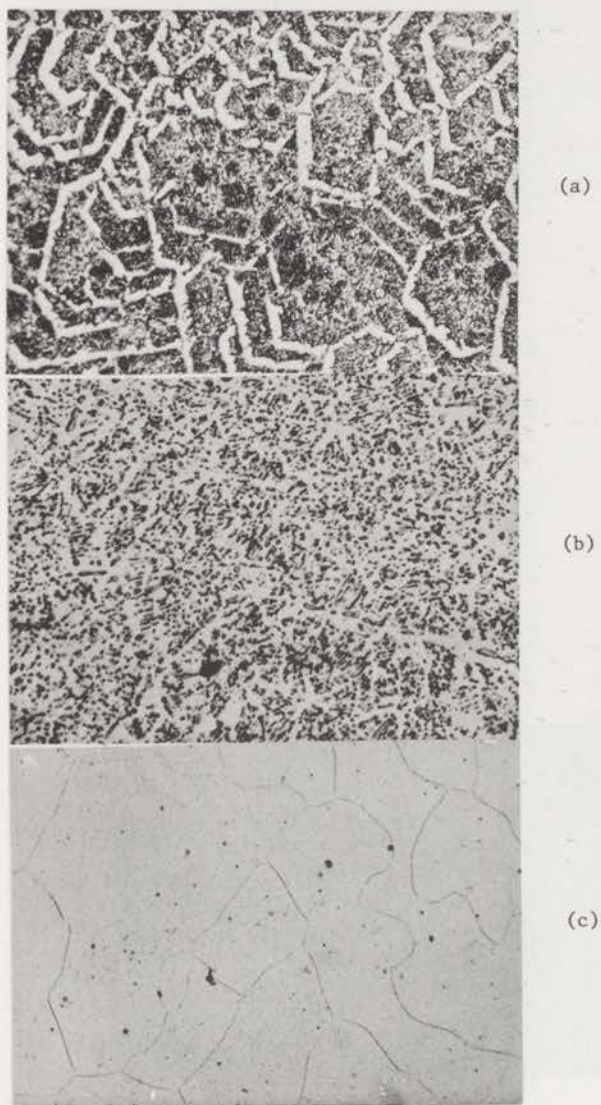


Fig. 26. Microstructure of some Tm-Fe samples; a: Tm_2Fe_{19} , as-cast; b: Tm_2Fe_{19} annealed for 3 weeks at $850^\circ C$, then 25 h at $1150^\circ C$ and subsequently quenched in water; c: Tm_2Fe_{17} annealed for 60 h at $1150^\circ C$ and subsequently quenched in water. Magnification 320 x.

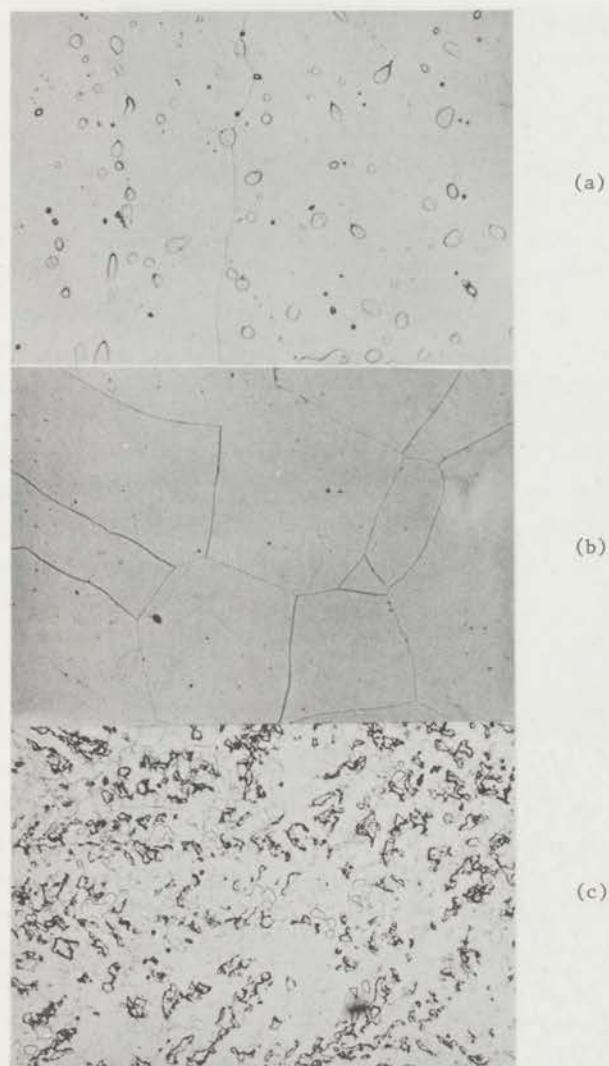


Fig. 27. Microstructure of some Y-Ni compounds after annealing at 1150 °C for 200 h and subsequent quenching in water; a: Y_2Ni_{17} ; b: Y_2Ni_{15} ; c: $Y_2Ni_{14.4}$. Magnification 320 x.

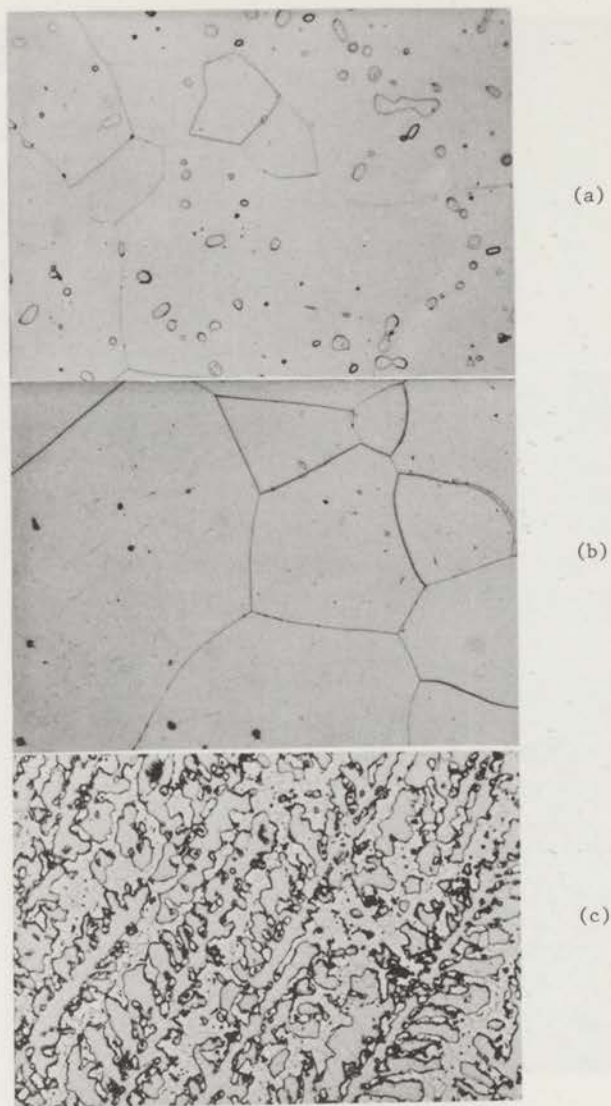


Fig. 28. Microstructure of Th-Ni compounds after annealing at 1150 °C for 200 h and subsequent quenching in water; a: $\text{Th}_2\text{Ni}_{17}$; b: $\text{Th}_2\text{Ni}_{15}$; c: $\text{Th}_2\text{Ni}_{13}$. Magnification 320 x.

In the case of ThNi_x and YNi_x single phases were found at about $x = 7.5$, i.e. $\text{Th}_2\text{Ni}_{15}$ and Y_2Ni_{15} . Results for the Yttrium compound are shown in fig. 27a, b and c. At $x = 8.5$ elemental Ni is present as a second phase, as demonstrated in fig. 27a. In fig. 27b the single phase at $x = 7.5$ is shown, whereas on further decrease of the Ni content beyond $x = 7.3$ a two-phase system again obtains, cf. fig. 27c. This is in agreement with the results of a metallographic examination of a sample with composition Y_2Ni_{17} , annealed at 970°C for 14 days, by Jaakola et al. [41]. This sample was estimated to contain 6-10% of free Ni.

In fig. 28a, b and c results for ThNi_x are shown. In fig. 28a elemental Ni is clearly present at $x = 8.5$. Figure 28b shows the single phase at $x = 7.5$; in fig. 28c some ThNi_5 is seen to be present at $x = 6.5$.

We are led to the conclusion that in the case of the Fe compounds the proper composition is close to R_2Fe_{17} , irrespective of hexagonal or rhombohedral type of structure, and that in the case of the Ni-compounds the tendency is towards Ni deficiency, resulting in an equilibrium composition close to R_2Ni_{15} , at least for Th and Y.

6.1.4 Alternative interpretation of the results of diffraction experiments.

We shall now proceed to show that, instead of disordered substitutions, a faulty stacking of planes can also explain the observed average distribution of atoms. If we consider again a triangle, numbered A, B, C as in section 6.1.2, with atom configuration $(\text{R}_2, \text{M}, \text{R}_1)$ in the selected layer, then the configuration is $(\text{M}, \text{R}_2, \text{R}_1)$ in the adjacent layer. In the perfect structure the C chain contains R_1 only, whereas R_2 and M zigzag over the chains A and B (see fig. 22d).

Now we introduce disorder through a stacking fault such that one or more zigzags are on the A and C chains, chain B now carrying no substitutions, as in fig. 29a. This introduces, on the average, some R_1 at the M sites on the A chain (and the same amount at R_2 sites, which is not noticed). On every second site of the C chain some M is introduced. If on the other hand the faulty zigzag is on chains B and C, no substitutions being found on A, R_1 is introduced on the M sites of the B chain, and M on the remaining sites of the C chain.

It remains to be noticed that the A and B chains are crystallographically equivalent, so that the probability is equal for both disorder

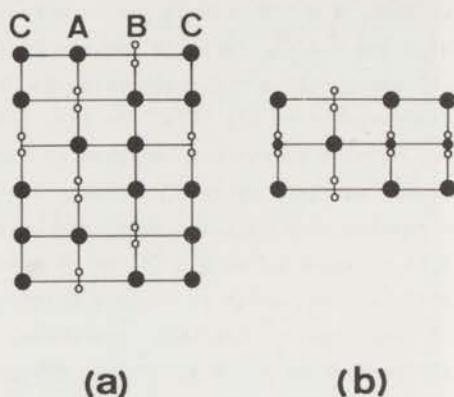


Fig. 29. Section through R_2M_{17} structure as in fig. 22 illustrating the effect of stacking faults. A stacking of layers as in (a) leads to an observed distribution of atoms as in (b).

processes. If the fault probability is high enough, the regions in which a "wrong" zigzag configuration takes place will be small enough for coherency to be conserved. The probability for either type of arrangement may then crudely be estimated as the apparent concentration of R_1 on the sites of the M pairs. If, however, this probability is very small, the results will be described by twinning through rotation over $\pm 60^\circ$ about the c -axis. Though the number of actual stacking faults is low, the overall effect will be very pronounced. Moreover, the "wrong" sections are not necessarily of equal size. If the "wrong" regions are of macroscopic size they will not be noticed in a powder diffraction diagram. The diffraction results obtained for Tm_2Fe_{17} [39], Y_2Fe_{17} [42] and Y_2Co_{17} [42] show clear disorder effects. When interpreted in this way, this means that the disorder is on a microscopic scale.

6.1.5 Discussion

The metallographic examination described in section 6.1.3 was intended to investigate whether under equilibrium conditions serious deviations from the stoichiometric composition R_2M_{17} occur. We did not perform a

scrutinous study regarding the presence and the extent of homogeneity regions at elevated temperatures close to the melting point of the compounds. However, by inspection of the two-phase micrographs shown in section 6.1.3 it can be deduced from the amount of second phases present that these regions are relatively small, even at 1150 °C. Indication that homogeneity regions are actually present at high temperatures is obtained from X-ray studies performed on samples annealed at low and at high temperatures, since it has been reported that at high temperatures the lattice dimensions increase in the c-direction and decrease in the a direction [43]. This leaves the possibility that close to the melting point of the compounds the homogeneity regions are rather extended and that strongly off-stoichiometric M-rich compositions may be obtained under non-equilibrium conditions, e.g. by quenching from the melt. For the single crystals examined by X-ray and neutron diffraction off-stoichiometric compositions may very well have occurred, since they were found in large cavities inside the solidified melt, or were grown by zone-melting techniques. In both cases deviations from the average composition are possible.

For the compound Tm_2Fe_{17} Mössbauer effect, neutron powder diffraction and metallography were performed on the same sample. Though disorder effects are clearly present in the diffraction diagrams, it is concluded on the basis of metallographic data that the composition is Tm_2Fe_{17} . This rules out the possibility of atomic disorder as described in section 6.1.2. On the other hand, stacking faults as described in section 6.1.4 are rather likely to occur. As can be seen in fig. 29a, these are equivalent to a locally rhombohedral stacking. For the Fe compounds the occurrence of the rhombohedral structure type is well known for the larger rare earths. For rare earths of medium size (Ce, Gd, Tb, Y) both forms often occur together, giving rise to two-phase microstructures (cf. fig. 24 a-c). It is likely that the additional energy associated with the occurrence of a stacking fault is small; once a fault is formed during crystallization it will not be removed by an annealing process since a large amount of energy is required to rearrange complete layers.

The alternative interpretation of the diffraction data given in section 6.1.4 does not explain why the Ni compounds are Ni-deficient (as observed by metallography). It gives, however, a hint in which direction one may have to look in order to bring the diffraction data in

Table 7. Position parameters for $\text{Tm}_2\text{Fe}_{17}$ at 300 K, R = 13%.
Standard deviations in units of the last decimal are given in parenthesis.

| | x | y | z |
|-----------|---------|----------|----------|
| Tm1 2(b) | 0 | 0 | 1/4 |
| Tm2 2(d) | 1/3 | 2/3 | 3/4 |
| Fe1 6(g) | 1/2 | 0 | 0 |
| Fe2 12(j) | .323(1) | -.037(1) | 1/4 |
| Fe3 12(k) | .164(1) | .328(2) | -.013(1) |
| Fe4 4(f) | 1/3 | 2/3 | .109(1) |

Table 8. Cell constants as a function of temperature

| | 300 K | 231 K | 80 K | 4.2 K |
|-------------------|----------|----------|----------|----------|
| a, Å | 8.417(1) | 8.338(6) | 8.403(1) | 8.412(1) |
| c, Å | 8.298(1) | 8.276(7) | 8.322(1) | 8.330(1) |
| V, Å ³ | 509.1(2) | 498(1) | 509.7(2) | 510.7(1) |

Table 9. Magnetic moments as a function of temperature.

| | 300 K | 231 K | 80 K | 4.2 K |
|---------------------|-------|---------|---------|---------|
| μ (Tm), μ_B | - | 0.0(3) | 4.2(2) | 6.4(2) |
| μ (Fe), μ_B | - | -1.5(3) | -2.2(1) | -2.2(1) |

agreement with the actual composition. Moreover, the above analysis gives no clue to a new interpretation of the Mössbauer effect observed. The pairs of Fe atoms have their axis along the c direction and give rise to a larger unit cell dimension in this direction than would be required otherwise. This might impose a relatively large stiffness to the thermal vibration of the Fe pairs in this direction. It is not impossible therefore that these Fe pairs have a relatively small Debye-Waller factor and hence a larger Mössbauer fraction. Indications for a lower Debye-Waller factor could not be obtained, however, from the diffraction experiments on these compounds [36,38].

6.2 The magnetic structure of Tm_2Fe_{17} . ^{†)}

Recent magnetization and Mössbauer effect measurements [44] showed that in Tm_2Fe_{17} a change in the magnetic structure occurs at $72K = T_0$. At this temperature a pronounced maximum in the magnetization and an increase in the Fe hyperfine field are observed. It was suggested that this compound might exhibit a complex type of magnetic order between T_0 and the Curie temperature $T_c = 275K$. In this section we report on the results of a neutron diffraction investigation of this compound.

The sample was prepared by arc melting of Tm, purity 99.9%, with Fe, purity 99.9%. Powder diagrams were recorded at the High Flux Reactor at Petten using $\lambda = 2.57 \text{ \AA}$ and the usual 30' collimation. The angular range $0.012 < \sin\theta/\lambda < 0.362 \text{ \AA}^{-1}$ was scanned at room temperature, 231 K, 80 K and 4.2 K. In the subsequent analysis the scattering lengths were taken to be 0.720 and $0.951 \cdot 10^{-12} \text{ cm}$ for Tm and Fe, respectively. The Freeman and Watson [26] form factor for Fe^{2+} was used; the Tm^{3+} form factor was evaluated according to Blume, Freeman and Watson [45]. For the refinements Rietveld's profile method [6] was applied.

At room temperature long range magnetic order was not noticed. The crystal structure is known to be of the hexagonal Th_2Ni_{17} type, space group $P6_3/mmc$. Refinement of the structure parameters resulted in an R-factor

^{†)} J.B.A.A. Elemans, Kamerlingh Onnes Laboratory, Leiden, the Netherlands
K.H.J. Buschow, Philips Research Laboratories, Eindhoven, the Netherlands.
Appeared in phys. stat. sol. (a) 24, K125 (1974)

based on intensities of 13%. It was possible to reduce the R-factor to 7% by allowing for disorder as proposed by Givord et al. [37] for $\text{Lu}_2\text{Fe}_{17}$. In doing so the composition $\text{Tm}_2\text{Fe}_{19.5}$ resulted, which does not agree with the homogeneity range of this compound, as determined by metallographic examination. However, we used the disordered model as a means of improving the values for the magnetic intensities at lower temperatures, taking advantage of the fact that nuclear and magnetic scattering are additive.

The structural parameters for the 13% refinement are given in table 7. No temperature dependence was found. The cell constants are given in table 8. Note that the thermal expansion coefficient is slightly negative in the ferrimagnetic region.

Magnetic scattering was observed superimposed on the nuclear intensities at 231, 80 and 4.2 K. The magnetic structure was found to be collinear, the Tm and Fe sublattices being antiparallel. At 4.2 K the moments are along the c-axis; at 80 and 231 K they are in the a-b plane. In table 9 the magnitudes of the moments are given; it is seen that the Fe moment has reached its full value already at 80 K whereas the Tm moment rises only slowly to $6.4 \mu_B/\text{atom}$ at 4.2 K, as compared to a free ion value of $7.6 \mu_B$.

At none of the temperatures considered evidence was found for a more complex type of magnetic order. The present results show that the difference in magnetization and hyperfine field above and below T_0 should be interpreted in terms of a change in magnetic anisotropy. Apparently the increase in hyperfine field at the Fe nucleus is not due to an increase in the transferred field induced by the Tm moment.

Isostructural Y_2Fe_{17} and Y_2Co_{17} are known to have easy plane anisotropy [46, 42]. Recent model calculations [13] on R_2Co_{17} (R = rare earth) compounds indicate that for Tm the preferred direction induced by the crystal field is parallel to the c-axis. The analysis is very likely applicable to $\text{Tm}_2\text{Fe}_{17}$ as well. In going from higher temperatures, where the Tm moment is very low, to temperatures where the Tm moment is appreciable, one may expect a change from easy plane to easy axis anisotropy, in agreement with the present observation.

VII. MAGNETIC ORDER IN ThFe_3 AND Th_2Fe_7

7.1 Introduction

In a very early stage of the investigation neutron diffraction data were collected for ThFe_3 and Th_2Fe_7 . This was not so much because of intrinsic interest in the structures of these compounds: it was suspected that they might be present as impurities in the ThFe_5 sample under investigation, and therefore it was important to know where their diffracted intensities would coincide with those of the main phase (cf. chapter III).

The diagrams, obtained in the usual manner, did not look very promising for analysis. Especially Th_2Fe_7 is not very well crystallized, as is evident from the peak shape of the (107) reflection: it is approximated by a lorentzian rather than by a gaussian function. Moreover, the 00l reflections were all observed up to $l = 6$, although the space group, $P6_3/mmc$, does not allow hhl reflections with odd l .

In the meantime a Mössbauer investigation of RFe_3 compounds was carried out at the Interuniversitair Reactor Instituut (I.R.I.), Delft. Here it was found that the Mössbauer spectrum of ThFe_3 could not be interpreted along the lines of thought that proved appropriate for the analysis of the lanthanide compounds [47]. Moreover, the magnetization curve of this compound as a function of temperature in a weak magnetic field was found to be remarkable [48]: from 4.2 K to roughly 200 K and above about 300 K to $T_c = 425$ K the spontaneous magnetization follows a Brillouin type function. In the intermediate temperature region there appears to be no net magnetization. In a neutron depolarization experiment carried out at I.R.I. it was confirmed that the spontaneous magnetization in the absence of an external field is zero in the intermediate temperature range, and that the transitions between the two states are very sharp [47]. Interest in the old diagrams was thus revived and an analysis was carried out. The results are described in the next two sections.

Table 10. Atomic positions for ThFe_3 , taken from ref. 49. The space group is $R\bar{3}m$; $a = 5.18(2) \text{ \AA}$, $c = 25.2(3) \text{ \AA}$.

| | | | | | |
|-----------------|-------|---|-----------|---------------|----------------------------------|
| Th ₁ | 3(a) | 0 | 0 | 0 | |
| Th ₂ | 6(c) | 0 | 0 | z | $z = 0.1414(9)$ |
| Fe ₁ | 3(b) | 0 | 0 | $\frac{1}{2}$ | |
| Fe ₂ | 6(c) | 0 | 0 | z | $z = 0.331(4)$ |
| Fe ₃ | 18(h) | x | \bar{x} | z | $x = 0.526(5)$ $z = 0.079(2)$ |

Table 11. Results for ThFe_3 at 4.2 K

| | x | y | z | ferri μ_x | ferro μ_z | μ^{tot} |
|--------------------|-----------|------------|---------------|------------------|------------------|--------------------|
| Th ₁ | 0 | 0 | 0 | | | |
| Th ₂ | 0 | 0 | 0.1397(2) | | | |
| Fe ₁ | 0 | 0 | $\frac{1}{2}$ | -1.06(5) | 1.58(6) | 1.90(5) |
| Fe ₂ | 0 | 0 | 0.3322(2) | +1.06 | 1.58 | 1.90 |
| Fe ₃ | 0.4984(7) | -0.4984(7) | 0.0800(2) | +1.06 | 1.58 | 1.90 |
| cell, \AA | 5.2058(3) | | 25.095(2) | | | |
| R, % | 4 | | | | | |

Table 12. Results for ThFe_3 at 300 K

| | x | y | z | ferri μ_x | ferro μ_z | μ^{tot} |
|--------------------|-----------|------------|---------------|------------------|------------------|--------------------|
| Th ₁ | 0 | 0 | 0 | | | |
| Th ₂ | 0 | 0 | 0.1392(3) | | | |
| Fe ₁ | 0 | 0 | $\frac{1}{2}$ | -0.80(6) | 1.49(7) | 1.69(7) |
| Fe ₂ | 0 | 0 | 0.3318(3) | +0.80 | 1.49 | 1.69 |
| Fe ₃ | 0.4982(7) | -0.4982(7) | 0.0795(2) | +0.80 | 1.49 | 1.69 |
| cell, \AA | 5.2150(4) | | 25.142(3) | | | |
| R, % | 5 | | | | | |

7.2 ThFe₃

7.2.1 Ferromagnetic temperature regions.

The crystal structure of ThFe₃ is known from a single crystal X-ray investigation [49]. The space group is $R\bar{3}m$ and the atomic positions are those of table 10.

All reflections observed at room temperature and at 4.2 K follow the rhombohedral reflection condition - $h+k+l = 3n$, indicating that the crystal and magnetic unit cells are identical.

The diagram at 4.2 K was analyzed first. In view of the ferromagnetic behaviour of the compound and of the fact that the (003) reflection is clearly observed, as a first guess equal parallel moments in the ab-plane were assumed. This model provided a poor agreement with the experimental data, which clearly could not be improved by the addition of a c-component. On the basis of the discrepancies between the calculated and observed intensities of several reflections it was concluded that Fe₁ and Fe₂ should have antiparallel components in the ab-plane, whereas no conclusion was reached with respect to Fe₃ on the basis of the structure factors considered.

Upon refinement the model with Fe₃ parallel to Fe₁, antiparallel to Fe₂, proved most definitely wrong. The model with Fe₃ parallel to Fe₂, antiparallel to Fe₁, was comparable in quality to the ferromagnetic model, but now the differences between observed and calculated intensities were indicative of a ferromagnetic component in addition to the ferrimagnetic one assumed in the model.

The measurements allow a ferromagnetic component parallel as well as perpendicular to the c-axis. Different magnitudes must be assumed in each case in order to explain the observed intensities. If the ferromagnetic component is assumed to be in the ab-plane the value of $2.6 \mu_B/\text{Fe}$ is found, whereas $1.6 \mu_B/\text{Fe}$ results in the case of a c-component. In view of the bulk magnetization measurements [17] the first value is far too high, and therefore the second case is adopted. The final results for this model are given in table 11.

The same model also yields a satisfactory fit to the room temperature data, as shown by table 12, and is mathematically stable in the sense that independent refinements of the magnitudes of the components for the three Fe-positions does not lead to significant numerical changes.

The structure found consists of layers for which the ferrimagnetic components are stacked in the sequence -+++, layers of Fe₁ and Fe₂ always being separated by an Fe₃ layer (cf. fig. 30).

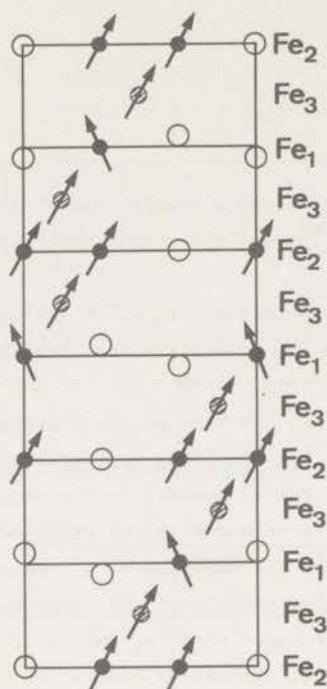


Fig. 30. Magnetic structure of ferromagnetic ThFe_3 .

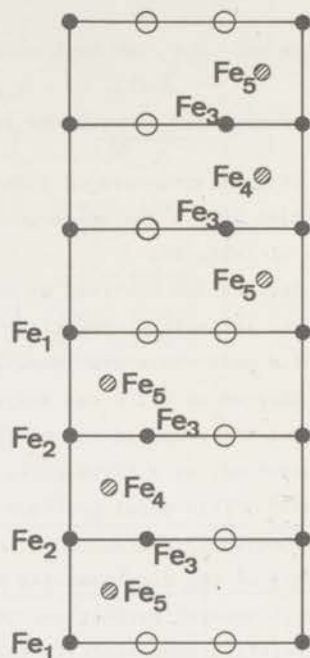


Fig. 31. Crystal structure of Th_2Fe_7 showing inequivalent Fe positions.

Table 13. Atomic positions for Th_2Fe_7 , taken from ref. 20.

The space group in $P6_3/mmc$; $a = 5.193(6) \text{ \AA}$, $c = 24.785(9) \text{ \AA}$.

| | | x | y | z |
|-----------------|-------|--------|--------|-------|
| Th ₁ | 4(f) | 1/3 | 2/3 | 0.030 |
| Th ₂ | 4(f) | 1/3 | 2/3 | 0.167 |
| Fe ₁ | 2(a) | 0 | 0 | 0 |
| Fe ₂ | 4(e) | 0 | 0 | 0.167 |
| Fe ₃ | 4(f) | 2/3 | 1/3 | 0.167 |
| Fe ₄ | 6(h) | -0.167 | +0.167 | 1/4 |
| Fe ₅ | 12(k) | -0.167 | +0.167 | 0.083 |

7.2.2 *Intermediate temperature range*

The solution obtained for the ferromagnetic temperature range poses a problem for the structure to be expected between 200 and 300 K. Since the number of magnetic moments per primitive unit cell is odd it is not possible to make them vectorially add to zero in a uniaxial configuration. Moreover, even if one would assume that Fe_1 loses its moment it would be necessary to break the parallel coupling in the Fe_2 or Fe_3 layers.

A natural way of obtaining a zero moment would be by doubling of the unit cell, such that neighbouring unit cells carry antiparallel moments.

In an attempt to determine the magnetic structure a diagram was taken at 250 K. No evidence for additional reflections, caused by an enlarged unit cell, was found; however, it was also clear from the general appearance of the diagram that the sample had badly deteriorated with time, so that the evidence must be considered inconclusive. The structure in the intermediate range therefore remains unsolved.

7.3 Th_2Fe_7

This compound was described for the first time in ref. 20, cf. chapter II. In one and the same sample usually both the hexagonal and rhombohedral forms are observed, but the hexagonal modification, space group $P6_3/mmc$, appears to be the stable one. This structure, as determined from X-ray powder diffraction [20], is shown in fig. 31 and the atomic coordinates are given in table 13.

In the sample investigated no traces of the rhombohedral form were found. Yet, as pointed out in section 7.1, the sample is not very well crystallized, and one may therefore not expect to achieve good agreement between observation and calculation. Indeed, in actual refinements the misfit of the nuclear scattering is estimated to be about 20%, as compared to a usual value of 5-10%. Nevertheless an attempt was made to solve the magnetic structure.

Models can be tested on the relative intensities of the low-order 001 reflections, in which the component in the ab -plane is visible. Observation of scattering in the reflections (001) and (003) indicates that one or more of the Fe positions must have an antiferromagnetic component such that moments in layers separated by $\frac{1}{2}c$ are antiparallel.

It will now be shown that this requirement cannot be met by one unambiguous magnetic space group compatible with the crystal space group. The symmetry elements to be considered are the screw axis, the mirror plane and the centre of symmetry, and the problem is to find all possible transformations for moments in the ab -plane, as only these may scatter in (001) reflections. Special attention must be given to atoms for which the point symmetry includes one of the symmetry elements under consideration, viz. Fe_1 at the inversion centre and Fe_4 in the mirror plane.

For Fe_1 the centre cannot be an anticomplexe or the moment of Fe_1 must be zero. The screw axis and mirror plane connecting the layers of Fe_1 can be proper symmetry elements, connecting antiparallel ab -components, or anti-elements, connecting parallel moments. The symmetries possible for Fe_1 are therefore 2_1 , i , m for antiparallel moments, and $2_1'$, i , m' , parallel moments.

Similarly, for Fe_4 the mirror plane must be an antimirror m' in order to accommodate a moment in the ab -plane. Parallel moments at z and $\frac{1}{2} + z$ are then described by $2_1'$, i , m' and antiparallel moments by 2_1 , i' , m' .

It is seen that one symmetry is shared by the two atomic positions, viz. $2_1'$, i , m' , connecting layers with parallel moments. However, this means that they will not scatter in (hhl) reflections with odd l . If therefore this symmetry would hold for Fe_1 and Fe_4 the other atoms must be scattering in these reflections, and must by necessity have a different symmetry.

The other possibilities were 2_1 , i , m and 2_1 , i' , m' , both antiferromagnetic. For layers at z , $\frac{1}{2}-z(m)$, $\frac{1}{2}+z(2_1)$ and $-z(i)$ these would correspond to moment sequences of ++++ and +-+- respectively. The third possibility for antiferromagnetism, ++--, does not lead to scattering in (hhl), odd l , since layers separated by $\frac{1}{2}c$ are parallel.

It was hoped that, despite the imperfect knowledge of the crystal structure, the magnetic structure could be solved on the basis of a simple combination of symmetries. At first the centre of symmetry was assumed to be present for all atoms, corresponding to ++ for Fe_4 and ++++ for all other Fe positions. Moreover, Fe_2 and Fe_3 are always assumed to be parallel since they lie in the same layer. Models then differ in the relative orientation of Fe_1 , $Fe_2 + Fe_3$ and Fe_5 . For all combinations the calculated intensity ratio of 001 and 003, observed as roughly 2/3, is clearly wrong: in each case one of the two reflections is calculated to be not observed. These models were therefore rejected, and it was thought that parallel stacking for Fe_5 in addition to Fe_4 would improve the agreement between

observed and calculated scattering. Indeed, refinement of models based on this assumption showed improvement but still no satisfactory agreement.

Clearly the assumption of a centrosymmetric structure is untenable. One set of non-centrosymmetric models was investigated, viz. the stacking sequence $++--$. When this was found not to lead to further improvement it was decided to discontinue the investigation, since it would be an enormous task to carry out a systematic analysis of all possible models. In view of the quality of the sample the expected result will not justify the effort.

7.4 Discussion

The results of this chapter are rather disappointing: the structure found for ferromagnetic ThFe_3 does not lead to an understanding of the anti-ferromagnetic structure. Experimental evidence for the structure of anti-ferromagnetic ThFe_3 was not obtained, probably due to oxidation of the sample with time.

In the case of Th_2Fe_7 the magnetic structure could not be solved at all, due to imperfection of the sample. Beyond doubt this must be attributed to stacking faults. Irregularities at a large scale in the substitutions would cause differences between the intensities of the regular structure and those of the actual structure. This may very well be the cause of the high R factor in the nuclear scattering. It is not expected that better samples will be obtained in the immediate future, and unsatisfying though the results are they are the maximum attainable at present.

VIII. SUMMARY AND CONCLUSIONS.

8.1 Introduction

After the piecemeal presentation of the experimental data in chapters III through VII, where many details required attention, we now return to the initial question of this investigation and re-examine the results obtained.

As was stated in section 2.4, the first experiments aimed at the determination of the magnetic structure of ThFe_5 , which could not be derived unambiguously from Mössbauer data [19]. The further work can be divided into two parts, each in a different way related to the first problem, viz. the work on pseudo-binary compounds and the investigations on Th-Fe compounds. In the following sections the results will be collected and examined with respect to their internal consistency and their compatibility with the experiments of other workers.

The discussion will be divided into three sections: the crystal structure of the ThM_5 compounds, the magnetic structures of the ThM_5 compounds, and the magnetic order in Th-Fe compounds.

8.2 Crystal structure of the ThM_5 pseudo-binary compounds.

8.2.1 Symmetry and atomic coordinates.

For all the compounds investigated structural data have been reported by other investigators before the beginning of the present investigation. In some cases single crystal X-ray data are available, but single crystals of ThFe_5 have not yet been prepared because of its peritectic melting point. Since powder X-ray data have limited accuracy special attention was given to the crystal structure of the pseudo-binary compounds and ThFe_5 itself.

Deviations from the ideal CaCu_5 type structure are most easily recognized in the series $\text{Th}(\text{Fe},\text{Ni})_5$ since all scattering lengths involved are nearly equal. As described in chapter IV, evidence for a lowering of the symmetry and for displacements of atoms from their ideal positions is not convincing, despite the discrepancies between the observed intensities and the values calculated for the ideal structure. Also in the $\text{Th}(\text{Fe},\text{Co})_5$ series symmetries lower than $P6/mmm$ were considered with negative results (cf. chapter III). Therefore on the basis of the present data the ideal structure is accepted. If deviations do occur they must be discovered by the analysis of samples of better quality.

8.2.2 Site occupancies in the pseudo-binary systems.

Relative site occupancies can be determined in those cases where the scattering lengths of the two kinds of M atoms present differ appreciably, i.e. in the Co-containing compounds. The results for $\text{Th}(\text{Fe},\text{Co})_5$ and $\text{Th}(\text{Ni},\text{Co})_5$ are collected in table 14, where the site occupancies for the two kinds of M atoms at the two atomic positions are given. It must of course be remembered that, though there are four entries in the table for each compound, there is only one variable, since there are three relations between the entries.

In fig. 32 the site occupancies $n(\text{M}_1')$ are shown as a function of x . It is seen that to a good approximation the data points for the two systems lie on a single curve.

In the case of $\text{Th}(\text{Fe}_{1-x}\text{Co}_x)_5$ the results can be correlated with the cell constants, taken from ref. 19 and reproduced in fig. 33.

It is seen that on the Fe-rich side the c -axis is fairly constant, and that the a -axis shows a linear x -dependence. In the same concentration range the Co introduced goes mainly into the 2(c) site, as is evident from table 14 and fig. 32. For the intermediate concentrations the additional Co is substituted in about equal amounts on the two sites; in this region both a and c vary with x . This substitution scheme is different from the one proposed in ref. 19, but it supports the interpretation by Rothwarf et al. of their measurement of the anisotropy constant K_1 in $\text{Th}(\text{Co},\text{Fe})_5$ [50]. They found that the value of K_1 is constant for compositions between ThCo_5 and ThCo_4Fe , but that a further increase in Fe concentration causes the value of K_1 to decrease. They concluded that the anisotropy

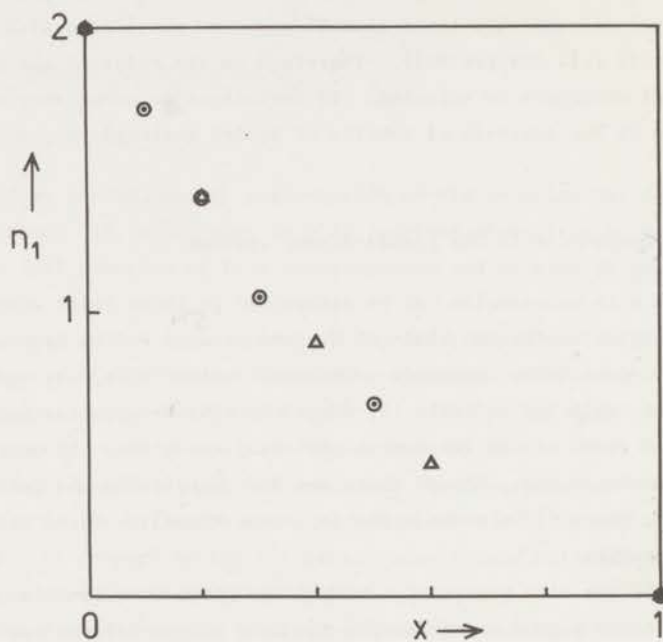


Fig. 32. Site occupation $n_1 = n(M'_1)$ in $\text{Th}(M'_{1-x}M''_x)_5$.

triangles $\text{Th}(\text{Fe}_{1-x}\text{Co}_x)_5$;

circles $\text{Th}(\text{Co}_{1-x}\text{Ni}_x)_5$.

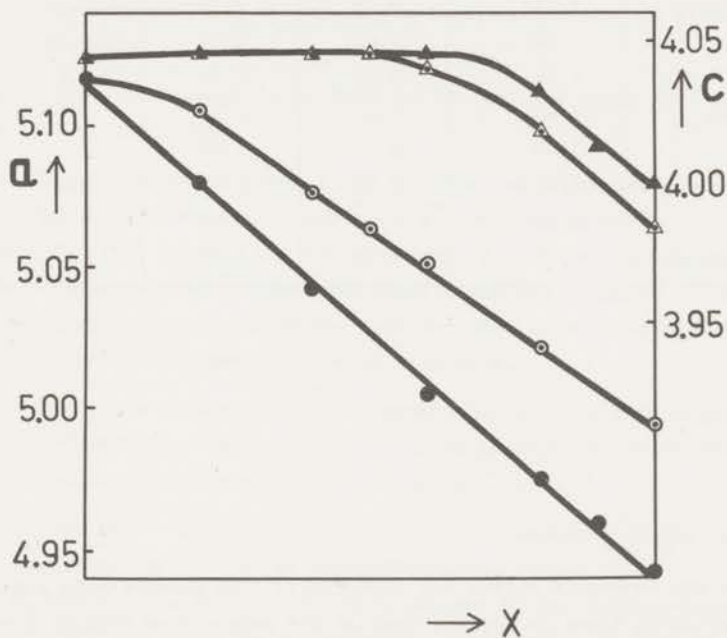


Fig. 33. Cell constants for $\text{Th}(\text{M}'_{1-x}\text{M}''_x)_5$, taken from ref. 19.

open symbols $\text{Th}(\text{Fe}_{1-x}\text{Co}_x)_5$;

closed symbols: $\text{Th}(\text{Fe}_{1-x}\text{Ni}_x)_5$;

circles: a-axis; triangles: c-axis

Table 14. Site occupancies in $\text{Th}(\text{M}'_{1-x}\text{M}''_x)_5$

| | $n(\text{M}'_1)$ | $n(\text{M}''_1)$ | $n(\text{M}'_2)$ | $n(\text{M}''_2)$ |
|------------------------------------|------------------|-------------------|------------------|-------------------|
| ThCo_5 | 2.00 | 0 | 3.00 | 0 |
| $\text{ThCo}_{4.5}\text{Ni}_{0.5}$ | 1.72 | 0.28 | 2.78 | 0.22 |
| ThCo_4Ni | 1.38 | 0.62 | 2.62 | 0.38 |
| $\text{ThCo}_{3.5}\text{Ni}_{1.5}$ | 1.15 | 0.85 | 2.35 | 0.65 |
| $\text{ThCo}_{2.5}\text{Ni}_{2.5}$ | 0.68 | 1.32 | 1.82 | 1.18 |
| ThFe_5 | 2.00 | 0 | 3.00 | 0 |
| ThFe_4Co | 1.40 | 0.60 | 2.60 | 0.40 |
| ThFe_3Co_2 | 0.90 | 1.10 | 2.10 | 0.90 |
| ThFe_2Co_3 | 0.47 | 1.53 | 1.53 | 1.47 |

is mainly due to the Co on the (c) site (Co_1). The present data strengthen their conclusion since it appears that at the composition ThCo_4Fe a considerable Fe_1 concentration starts to develop.

Site occupancies are not known for $\text{Th}(\text{Fe},\text{Ni})_5$ but from the data available a hypothesis can be formulated. The site occupancies in $\text{Th}(\text{Fe}_{1-x}\text{Co}_x)_5$ and $\text{Th}(\text{Co}_{1-x}\text{Ni}_x)_5$ behave essentially similar as a function of x . If we could assume the same function to be valid for $\text{Th}(\text{Fe},\text{Ni})_5$ it would still be undecided whether we should write $\text{Th}(\text{Fe}_{1-x}\text{Ni}_x)_5$ or $\text{Th}(\text{Ni}_{1-x}\text{Fe}_x)_5$ in order to conform to the concentration dependence shown in fig. 32. Here the cell constants provide the necessary additional information: it is seen in fig. 33 that the same qualitative behaviour in the cell constants is found for $\text{Th}(\text{Fe}_{1-x}\text{Co}_x)_5$ and $\text{Th}(\text{Fe}_{1-x}\text{Ni}_x)_5$: the constant part for c and the decrease for a and c are very similar. Moreover, the x-dependence of the c-axis sets in at about the same value of x. This might indicate a very similar behaviour of site occupancies as well. This hypothesis will be used in the next section for a reinterpretation of magnetic order in $\text{Th}(\text{Fe},\text{Ni})_5$.

8.3 Magnetic order in ThM₅ compounds.

8.3.1 Summary of previous results.

In chapter III the following results were obtained for Th(Fe,Co)₅, cf. fig. 14.

- a) for compositions ThCo₅ to ThFe₂Co₃ the magnetic moment is parallel to the c-axis.
- b) in ThFe₃Co₂ the moment is oriented at an angle of about 30° with respect to the c-axis.
- c) in ThFe₄Co the moment lies in the ab-plane and shows two components, viz. $\vec{k} = 0$ (ferromagnetic) and $\vec{k} = \frac{1}{2} \vec{c}^*$ (antiferromagnetic). The phase relation between the two components is, of course, unknown. If the moments of all transition metal atoms are required to have equal magnitudes the components must be taken to be perpendicular to one another, which means a canted structure.
- d) in ThFe₅ the antiferromagnetic component has increased in magnitude. The ferromagnetic component appears to be parallel to the c-axis. This conclusion is based on the following:
 1. in the (001) reflection the difference is measured of the sublattice magnetization of the two crystallographic sites:
 $\vec{F}_M(001) = 2 \vec{\mu}(M_1) - 3 \vec{\mu}(M_2)$; because of the angular dependence of the scattering the ab-component is measured. In view of the standard deviation of the background count at the relevant 2θ - value the reflection should be observable if $|F_{ab}(001)| \gtrsim 0.7 \mu_B$, but in fact this reflection is not observed.
 2. upon refinement of an arbitrary moment direction by simultaneous variation of the c- and ab-component it was found that the magnitude of the ab-component did not follow from the experimental data: successive cycles of the refinement diverged and the ab-component tended to increase to a very large ($> 10 \mu_B/\text{at}$) value. At the same time the c-component was well-defined at a value of $1.8 \mu_B/\text{atom}$.
 3. when the moment is constrained to be in the ab-plane an estimated misfit of $R_{\text{mag}} = 16\%$ results as compared to $R_{\text{mag}} = 9\%$ for a ferromagnetic moment parallel to the c-axis. Moreover, the value found for the ferromagnetic component has the very large value of $2.3 \mu_B/\text{atom}$.

When the reflections (200) and (102) are excluded from the calculation (probably being affected by scattering from a secondary phase) the result for the c -component does not change; for the ab -component R_{mag} drops also to 9% and the magnitude of the component becomes $2.1 \mu_B/\text{atom}$, still too high. The conclusion based on these considerations is straight-forward.

In chapter IV the investigation of the series $\text{Th}(\text{Fe},\text{Ni})_5$ was described, cf. fig. 16. At the Fe-rich side ($\text{ThFe}_5 - \text{ThFe}_4\text{Ni}$) an antiferromagnetic component as in $\text{Th}(\text{Fe},\text{Co})_5$ was found. For intermediate concentrations ($\text{ThNiFe}_4 - \text{ThNi}_3\text{Fe}_2$) the (001) reflection was clearly observed. Contrary to the case of ThCoFe_4 this could not be explained on the basis of an average ferromagnetic component per transition metal atom. Moreover, it was found that the moments on the two crystallographic sites could not be determined independently, whereas an appreciable difference might be the cause of the observed value of the (001) reflection. As described in chapter IV antiparallel components were assumed for the two sites, in addition to a ferromagnetic c -component. We shall return to this in section 8.3.2.

Chapter V gives the results obtained for $\text{Th}(\text{Co},\text{Ni})_5$. Ferromagnetic order prevails for the composition range $\text{ThCo}_5 - \text{ThNiCo}_4$; at or just beyond this last composition the magnetic order changes to ferrimagnetic, and the cell constants show a marked discontinuity (fig. 20). The moments are always oriented parallel to the c -axis. Since the c -components are always well-defined we do not question these results as we do those of chapter IV.

8.3.2 Reinterpretation of the diffracted intensities in $\text{Th}(\text{Fe},\text{Ni})_5$

In section 8.2 it was put forward as a hypothesis that the site occupancies in $\text{Th}(\text{Fe},\text{Ni})_5$ closely resemble those in $\text{Th}(\text{Fe},\text{Co})_5$ and $\text{Th}(\text{Co},\text{Ni})_5$. Also it follows from the magnetization measurements mentioned in chapter IV that the spontaneous magnetization per unit cell can be described as the sum of the contributions of Fe and Ni, Fe carrying $1.9 \mu_B$ and Ni carrying $0.4 \mu_B$ if sufficient Fe is present to induce the Ni-moment. We shall now show that this leads to a different interpretation of the scattered intensity by calculating the structure factor for the (001) reflection for a model in which site occupancies are taken from fig. 32 and the moments are parallel in the ab -plane.

The values so obtained are collected in table 15. It is seen that there is good agreement for ThFe_4Ni . For the two other compounds the agreement is less satisfactory but can be improved by adjusting the relative site occupancies or the magnitudes of the moments. Adjusted values for the site occupancies $n(\text{Fe}_1)$ for the three compounds are 1.26, 0.38 and 0; these would indicate that Ni shows a stronger preference for the 2(c) site than Co when replacing Fe in ThFe_5 .

It must be emphasized that this model cannot be treated by least squares refinement since it is not possible to refine the magnitudes of the moments on the two sites independently, or equivalently, to refine site occupancies at constant magnitude of the moments. However, though it is not possible to prove or disprove the model given above the data of table 15 show that it is not necessary to assume a ferrimagnetic component in order to explain the intensity of the (001) reflection, and we must accept the possibility of ferromagnetic order with moments in the ab-plane.

Table 15. The structure factor for the (001) reflection in $\text{Th}(\text{Fe},\text{Ni})_5$. The magnetic moments assumed are $1.88 \mu_B$ for Fe and $0.4 \mu_B$ for Ni.

| | $n(\text{Fe}_1)$ | F_{calc} | $ F_{\text{obs}} , 4.2 \text{ K}$ |
|----------------------------|------------------|-------------------|-----------------------------------|
| ThFe_4Ni | 1.39 | -2.2 | 2.6(2) |
| ThFe_3Ni_2 | 0.90 | -2.1 | 3.7(2) |
| ThFe_2Ni_3 | 0.47 | -2.0 | 3.6(2) |

8.3.3 The canted structure of ThFe_5 .

As described in chapter III, several reflections are observed in ThFe_5 that can be described on the basis of a unit cell doubled in the c-direction. The intensity of these reflections is a function of temperature, and, in the pseudo-binary compounds, of the Fe-concentration. The concentration dependence appears to be roughly the same for $\text{Th}(\text{Fe},\text{Co})_5$ and $\text{Th}(\text{Fe},\text{Ni})_5$, which would indicate that the presence of the $\vec{k} = \frac{1}{2} \vec{c}^*$ component is not an electron concentration effect. It is probably impossible

to say whether one of the two crystallographic sites in particular is responsible for the canting: the component vanishes near a composition where on the average one atom per sublattice and per unit cell has been replaced by Co or Ni.

Quite another interpretation for the antiferromagnetic reflections in relation to the Fe concentration cannot be totally excluded: it cannot be stated with absolute certainty that these reflections are not due to impurities. In all samples investigated some ThO_2 is clearly present, and in the Co-rich samples some CoO is found. One would therefore not be surprised to find an Fe oxide present in the Fe-rich samples. In favour of an impurity effect could be the observation of a similar reflection in the diagram of ThFe_3 at 250 K, recorded about a year later than the other diagrams. However, for $\text{Th}_2\text{Fe}_{17}$, which has the highest Fe-concentration of all compounds investigated in our work, the reflection is absent.

In favour of a real effect, due to the main phase, is the temperature dependence observed for the $(00\frac{1}{2})$ reflection in ThFe_5 . Above room temperature its structure factor is found to decrease linearly with temperature, vanishing at $120 \pm 5^\circ\text{C}$ (note that $T_c = 680\text{ K}$). This implies a linear decrease of the magnitude of the component of the moment responsible for that reflection. Such a temperature dependence is not usually associated with the vanishing of long range magnetic order, and moreover no Fe-oxide is known to the author that shows magnetic scattering at the relevant two-theta value or has its magnetic ordering temperature at about 400 K. Finally, previously to the sample described in chapter III diffraction intensities had been recorded for a sample of ThFe_5 that was rather rich in impurities. This was not reflected in the intensity of the $00\frac{1}{2}$ reflection relative to other reflections of ThFe_5 . Therefore, though a proof is not given there is strong evidence that indeed the antiferromagnetic reflections must be attributed to ThFe_5 itself and not to impurities.

The second problem associated with the structure found concerns the direction of the ferromagnetic component of the magnetic moments. The Mössbauer experiments of ref. 19 have been repeated at I.R.I. and lead to a discrepancy with the present results: the Mössbauer spectrum of ThFe_5 indicates that the moments lie in the ab-plane $|51|$ whereas the diffraction results indicate a canting of about 30° with respect to the c-axis. In view of the Mössbauer results a model was constructed that has ab-components only whilst the structure factor for the (001) reflection is zero. This, of course, is done by adjusting the ferromagnetic components

for the two crystallographic sites to $\mu_2 = 2/3 \mu_1$. The antiferromagnetic moment must then be divided over the two sites such that the magnitudes of the total moment per atom is equal for the two sites. The results obtained by refinement of this model must then be compared to the older results.

Excluding the reflections (200) and (102) from the refinement, imposing the constraint μ_2 (ferro) = $2/3 \mu_1$ (ferro) and allocating the antiferromagnetic component to $\vec{\mu}_2$ yields an R_{mag} of 9%, which is as good as the value obtained before (cf. section 8.3.1, paragraph d sub 3), but the resulting values for the magnetic moments are not acceptable: $\vec{\mu}_1$, with a ferromagnetic component, has a calculated value of $3.1 \mu_B$, and $\vec{\mu}_2$ has a ferromagnetic component of $2.1 \mu_B$ and an antiferromagnetic component of $1.2 \mu_B$, total moment $2.4 \mu_B$. When the constraint on the ferromagnetic component is removed the values for the two sites tend to become equal and assume the value of $2.1 \mu_B$, without showing a further decrease in R factor. Moreover, the not observed reflection (001) now, of course, is calculated at an observable level.

Yet, when in ThCoFe_4 the moment is found in the ab-plane and when it is possible to interpret the structures for $\text{Th}(\text{Fe},\text{Ni})_5$ compounds on the basis of moments in the ab-plane it is difficult to accept that it should be different for ThFe_5 . Moreover, the Mössbauer results also indicate moments in the ab-plane. Thus we are led to the conclusion that the diffraction result for ThFe_5 is in fact incorrect. The cause of the erroneous result is not clear: too much intensity can be attributed to an unknown impurity; too little intensity may be caused by e.g. preferred orientation in the sample or by disorder; a wrong distribution of intensities may be due to impurity contributions to some reflections or by disorder in the sample.

8.4 Magnetic structures of the Th-Fe compounds.

Magnetic structures were determined for the compounds $\text{Th}_2\text{Fe}_{17}$, ThFe_5 and ThFe_3 . No conclusion was reached for Th_2Fe_7 , other than that antiferromagnetic components must be present in this compound. The only straightforward result is that obtained for $\text{Th}_2\text{Fe}_{17}$, which is clearly a ferromagnet with its moment in the ab-plane. The magnitude of the moment is $2.5(1) \mu_B/\text{Fe}$, as compared to $2.2 \mu_B/\text{Fe}$ found from bulk magnetization measurements.

The value found is high but differs only three standard deviations from the bulk magnetization value. The difference may be partly accounted for by the observation that when the moments are refined independently the moment of the substituted pair tends to increase to $2.7 \mu_B$ /atom, the other Fe atoms carrying $2.2 \mu_B$.

In ThFe_5 canting is found; if equal magnitudes for all Fe moments are assumed the stacking sequence follows as $++--$ for the antiferromagnetic component (cf. fig. 14). If this condition is not imposed a layer sequence of $+0-0$ is also possible (0 indicating no canted component).

In ThFe_3 canting is observed with a stacking sequence of $-+++$, and a ferromagnetic component parallel to the c -axis is found. However, since the diffraction result of ThFe_5 also indicated a ferromagnetic c -component the result for ThFe_3 may be considered questionable as well. It must be recalled, though, that for ThFe_5 the solution adopted in chapter III did not correspond to a least squares minimum, whereas the solution for ThFe_3 is a local least squares minimum: when all components are refined independently their values do not show significant shifts from the values found when the moments are refined with identical components for all sites.

Whereas in $R_2\text{Fe}_{17}$ compounds with non-magnetic R helical magnetic structures have been observed [14], [21], in the present system of Th-Fe compounds $\text{Th}_2\text{Fe}_{17}$ appears to be the only true ferromagnet. The complex structures found for the other compounds show that a non-collinear arrangement is very well possible in compounds with Fe that do not have the extremely short Fe-Fe distances found for the substituted pair in R_2M_{17} compounds.

One would like to be able to put forward a mechanism explaining the observed structures. One might speculate about the relative magnitudes of $d-d$ and $d-s$ exchange. In pure Fe the latter is considered to be one order of magnitude smaller than the former. It is difficult to say anything about relative orders of magnitude in the present compounds, since nothing at all is known about the band structure.

L I S T O F R E F E R E N C E S

- [1] Marshall, W. and S.W. Lovesey, Theory of Thermal Neutron Scattering, Oxford, 1971.
- [2] International Tables for Xray Crystallography, Birmingham, 1969.
- [3a] Bacon, G.E., Neutron Diffraction, 2nd edition, Oxford, 1962.
- [3b] Onderzoek vaste stof en vloeistof met behulp van neutronen, Cursusdictaat RCN cursus 8-11 mei 1973.
- [4] Caglioti, G., A. Paoletti and F.P. Ricci, Choice of collimators for a crystal spectrometer for neutron diffraction, Nucl. Instr. 3, 223 (1958).
- [5] Loopstra, B.O., Neutron powder diffractometry using a wavelength of 2.6 Å, Nucl. Instr. Meth. 44, 181 (1966).
- [6] Rietveld, H.M., A profile refinement method for nuclear and magnetic structures, J. Appl. Cryst. 2, 65 (1969).
- [7] Taylor, K.N.R., Adv. Phys. 20, 551 (1971).
- [8] Wallace, W.E., Rare Earth Intermetallics, Academic Press, New York and London, 1973.
- [9] Buschow, K.H.J., J. Less-Common Metals 16, 45 (1968).
- [10] Freeman, A.J., in: Magnetic properties of Rare Earth Metals, ed. R.J. Elliott, Plenum Press, London and New York, 1972.
- [11] Friedel, J., in: The physics of metals I, electrons, ed. J.M. Ziman, Cambridge University Press, 1969.
- [12] Duff, K.J. and T.P. Das, Phys. Rev. B 3, 192 and 2294, (1971).
- [13] Greedan, J.E. and V.U.S. Rao, J. Sol. State Chem. 6, 387 (1973).
- [14] Lemaire, R., D. Paccard, R. Pauthenet and J. Schweizer, J. Appl. Phys. 39, 1092 (1968).

- [15] Givord, D., F. Givord and R. Lemaire, *J. de Physique*, 32, C1-668 (1971).
- [16] Thomson, J.R., *J. Less-Common Metals* 10, 432 (1966).
- [17] Buschow, K.H.J., *J. Appl. Phys.* 42, 3433 (1971).
- [18] Atoji, M., I. Atoji, C. Do-Dinh and W.E. Wallace, *J. Appl. Phys.* 44, 5096 (1973).
- [19] Diepen, A.M. van, K.H.J. Buschow and J.S. van Wieringen, *J. Appl. Phys.* 43, 645 (1973).
- [20] Buschow, K.H.J. and A.S. van der Goot, *J. Less-Common Metals* 23, 399 (1971).
- [21] Givord, D., R. Lemaire, W.J. James, J.M. Moreau and J.S. Shah, *IEEE Trans. Magnetics* 7, 657 (1971).
- [22] Buschow, K.H.J. and A.S. van der Goot, *J. Less-Common Metals* 14, 323 (1968).
- [23] Laforest, J. and J.S. Shah, *IEEE Trans. Magnetics* 9, 217 (1973).
- [24] Elemans, J.B.A.A. and K.H.J. Buschow, *phys. stat. sol. (a)* 24, 393 (1974).
- [25] Buschow, K.H.J., M. Brouha and J.B.A.A. Elemans, to appear in *phys. stat. sol. (a)*, 30 (1975).
- [26] Watson, R.E. and A.J. Freeman, *Acta Cryst.* 14, 27 (1961).
- [27] Kuijpers, F.A. and B.O. Loopstra, *J. Physique* 32, C1-657 (1971).
- [28] Elemans, J.B.A.A., K.H.J. Buschow, H.W. Zandbergen and J.P. de Jong, to appear in *phys. stat. sol. (a)*, 30 (1975).
- [29] Buschow, K.H.J., M. Brouha and A.G. Rijnbeek, *Solid State Comm.* 16, 31 (1974).
- [30] Gignoux, D. and R. Lemaire, *Solid State Comm.* 14, 877 (1974).
- [31] Heine, V. and D. Weaire, in: *Solid State Physics* 24, 249 (1970).

- [32] Havinga, E.E., *J. Less-Common Metals*, 27, 187 (1972).
- [33] Marakov, E.S. and S.I. Vinogradov, *Kristallografia* 1, 634 (1956).
- [34] Florio, J.V., N.C. Baenziger and R.E. Rundle, *Acta Cryst.* 9, 367 (1956).
- [35] Givord, F. and R. Lemaire, *J. Less-Common Metals* 21, 463 (1970).
- [36] Givord, D., F. Givord, R. Lemaire, W.J. James and J.S. Shah, *J. Less-Common Metals* 29, 389 (1972).
- [37] Givord, D., R. Lemaire, J.M. Moreau and E. Roudaut, *J. Less-Common Metals* 29, 361 (1972).
- [38] Johnson, Q. and G.S. Smith, *Acta Cryst.* 23, 327 (1967).
- [39] Elemans, J.B.A.A. and K.H.J. Buschow, *phys. stat. sol. (a)* 24, K 125 (1974).
- [40] Gubbens, P.C.M., J.J. van Loef and K.H.J. Buschow, *J. de Physique*, 35, C6-617 (1974).
- [41] Jaakola, S., S. Parviainen and H. Stenholm, *Z. Physik B* 20, 109 (1975).
- [42] Elemans, J.B.A.A. and K.H.J. Buschow, unpublished data.
- [43] Goot, A.S. van der and K.H.J. Buschow, *J. Less-Common Metals*, 21, 151 (1970).
Buschow, K.H.J. and A.S. van der Goot, *phys. stat. sol.* 35, 515 (1969).
- [44] Gubbens, P.C.M. and K.H.J. Buschow, *J. Appl. Phys.* 44, 3739 (1973).
- [45] Blume, M., A.J. Freeman and R.E. Watson, *J. Chem. Phys.*, 37, 1245 (1962).
- [46] Ray, A.E. and K.J. Strnat, *Proc. 7th Rare Earth Conf.*, Moscow, Sept. 1972.
- [47] Kraan, A.M. van der, private communication.
- [48] Buschow, K.H.J., private communication.

- [49] Smith, J.F. and D.A. Hansen, *Acta Cryst.* 19, 1019 (1965).
- [50] F. Rothwarf, H.A. Lempold, J. Greedan, W.E. Wallace and D.K. Das, *Int. J. Mag.* 4, 267 (1973).
- [51] Kraan, A.M. van der, private communication.

SAMENVATTING

Na een exposé van de gebruikte experimentele techniek (neutronen-diffractie aan poederpreparaten) en een overzicht van het onderzoeksveld volgt de analyse van de magnetische ordening en, voor zover daarvoor relevant, van de kristalstructuren in intermetallische verbindingen van Th en ijzer en pseudo-binaire verbindingen met de samenstelling ThM_5 , waarin $M = (\text{Fe}, \text{Co}), (\text{Fe}, \text{Ni})$ of (Co, Ni) .

Door de aanwezigheid van verontreinigingen (meest oxiden) worden de experimentele gegevens dikwijls vertekend en bovendien blijkt men geconfronteerd te worden met een inherent gebrek aan informatie. De gegevens zijn daardoor niet geheel eenduidig te interpreteren, maar door onderlinge vergelijking kan men toch tot resultaten komen.

De voldoende conclusies worden getrokken:

a) $\text{Th}(\text{Fe}, \text{Co})_5$: ThCo_5 is een ferromagneet met de momenten parallel aan de c-as. Wanneer ongeveer 3 Co atomen per cel door Fe atomen zijn vervangen, beginnen de momenten naar het a-b vlak te draaien. In ThCoFe_4 , en waarschijnlijk ook in ThFe_5 , liggen de momenten in het basisvlak maar zijn niet langer parallel: er is een antiferromagnetische component, waarvoor de c-as verdubbeld moet worden en die tot een gekantelde structuur leidt.

b) $\text{Th}(\text{Fe}, \text{Ni})_5$: de ordening in ThNiFe_4 is gelijk aan die in ThCoFe_4 ; bij hogere Ni concentraties verdwijnt de kanteling en is de ordening waarschijnlijk ferromagnetisch, met de momenten in het basisvlak.

c) $\text{Th}(\text{Co}, \text{Ni})_5$: voor samenstellingen tussen ThCo_5 en ThCo_4Ni wordt ferromagnetische ordening gevonden; voor Ni-rijkere preparaten is de ordening ferrimagnetisch. De twee kristallografische posities dragen hier antiparallelle momenten. De richting van de momenten is altijd langs de c-as.

d) $\text{Th}_2\text{Fe}_{17}$ is een ferromagneet met momenten in het basisvlak.

e) in het ferromagnetische temperatuurgebied vertoont ThFe_3 een gekantelde structuur, tenzij men zou toelaten dat sommige Fe atomen geen moment dragen. Er zijn onvoldoende experimentele gegevens om de structuur op te lossen in het temperatuurgebied waar geen spontane magnetisatie gevonden wordt.

f) In Th_2Fe_7 moet men op grond van de waargenomen reflecties tot een gekantelde structuur besluiten. Het bleek echter niet mogelijk de structuur te bepalen. Dit moet waarschijnlijk worden toegeschreven aan een hoge mate van wanorde in de kristalstructuur.

NAWOORD

Nu het onderzoek wordt afgesloten, wil ik graag diegenen bedanken die eraan meegewerkt hebben.

Het Reactor Centrum Nederland, en met name de werkgroep Vaste Stof Fysika (huidige leider J. Bergsma) heeft mij gastvrijheid verleend en de faciliteiten, nodig voor het onderzoek, ter beschikking gesteld. De technische realisering van het proefschrift is sterk vergemakkelijkt door de geboden mogelijkheid, het tegelijkertijd als extern rapport (RCN-75-230) te laten verschijnen.

B.O. Loopstra heeft mij ingeleid in het gebied van de structuuranalyse m.b.v. diffractietechnieken en zich voortdurend in het onderzoek geïnteresseerd getoond.

J. Strang heeft ontelbare diagrammen gemeten.

W. van der Gaauw, G.J. Lagendijk en F. de Jong hebben de tekeningen gemaakt.

G.E. Möls en M. Beukers-de Ridder hebben de publikaties verzorgd en E.Y. Vermeulen-van Leeuwen heeft het proefschrift vorm gegeven.

De Reprografische Dienst heeft al het drukwerk uitgevoerd.

K.H.J. Buschow (Philips Nat. Lab.) heeft de preparaten geleverd en vele discussies met mij gevoerd. De resultaten van de onderzoekingen zijn dan ook door ons gezamenlijk gepubliceerd.

Dit onderzoek zou niet mogelijk geweest zijn zonder de grote mate van vrijheid, die de promotor J. van den Handel mij gegeven heeft bij de vormgeving van het onderzoek.

Dit proefschrift zou misschien niet voltooid zijn zonder de ruggesteun van R.J. Barton, die hiervoor zijn direct persoonlijk belang opzij heeft gezet.

CURRICULUM VITAE

J.B.A.A. Elemans werd in 1943 te Leiden geboren.

Na het eindexamen Gymnasium β , afgelegd in 1961, afgelegd aan het St. Agnes lyceum te Leiden, en na een verblijf van een jaar in de Verenigde Staten, ving zij in 1962 de natuurkundestudie in Leiden aan. Het kandidaatsexamen a' volgde in 1967.

Na het kandidaatsexamen werd zij opgenomen in de werkgroep van J. van den Handel, en eind 1968 naar het Reactor Centrum Nederland uitgezonden.

Het aldaar verrichte onderzoek heeft bijgedragen tot het doctoraal examen experimentele natuurkunde met bijvak klassieke mechanica, dat werd afgelegd in 1970.

Een deel van het na 1970 uitgevoerde onderzoek heeft geleid tot het hier aangeboden proefschrift.

